

Downloaded from SHAREOK. Persistent Handle URL: https://hdl.handle.net/11244/1846



This dissertation has been microfilmed exactly as received

65–7263

HELANDER, Donald Peter, 1931–
THE EFFECT OF PORE CONFIGURATION, PRESSURE, AND TEMPERATURE ON ROCK RESISTIVITY.

The University of Oklahoma, Ph.D., 1965
Engineering, general

University Microfilms, Inc., Ann Arbor, Michigan

THE UNIVERSITY OF OKLAHOMA

GRADUATE COLLEGE

THE EFFECT OF PORE CONFIGURATION, PRESSURE, AND TEMPERATURE ON ROCK RESISTIVITY

A DISSERTATION

SUBMITTED TO THE GRADUATE FACULTY

in partial fulfillment of the requirements for the

degree of

DOCTOR OF PHILOSOPHY

BY

DONALD P. HELANDER

Norman, Oklahoma

1965

THE EFFECT OF PORE CONFIGURATION, PRESSURE, AND TEMPERATURE ON ROCK RESISTIVITY

APPROVED BY

J. W. Campbell

Arthur Burkhart

Bernard O. Heston

Arthur W. McCray

John A. E. Norton

DISSERTATION COMMITTEE

ACKNOWLEDGMENT

The author wishes to express his appreciation to the many people who helped make this work possible. Without their patience, understanding, and moral support, the task would have been very difficult indeed.

Special thanks are extended to Dr. John M. Campbell, under whose astute guidance this work was done. His comments and suggestions have materially enhanced this manuscript.

I also wish to acknowledge the help of the Socony-Mobil Company for both their financial assistance and the loan of the resistivity cell and additional equipment used in this work, and The Ford Foundation for its financial aid.

The assistance of Dowell, Inc., in helping to find and provide a suitable cementing material and the Pan American Research Laboratory for obtaining the pore size distribution data is gratefully acknowledged.

Finally, I would like to express my gratitude to The University of Tulsa for their encouragement of this work, their financial assistance and the use of their laboratory facilities. It is only hoped that in some small way, this endeavor will repay them for the confidence and trust they placed in me.

TABLE OF CONTENTS

	Page
ACKNOWLEDGMENT	iii
LIST OF TABLES	vi
LIST OF FIGURES	vii
ABSTRACT	x
Chapter	
I. INTRODUCTION	1
II. LITERATURE REVIEW	7
III. SYNTHETIC CORE DESIGN AND CONSOLIDATION	21
Unconsolidated Pack Design	22
Unconsolidated Pack Preparation	27
Consolidating Material	30
Consolidating Procedure	32
Sample Identification	35
Core Evaluation	36
IV. EXPERIMENTAL APPARATUS AND PROCEDURE	40
Pressure Equipment	40
Temperature Equipment	47
Electrical Measuring System	48
Saline Water	50
Saturating Procedure	50
Auxiliary Core Measurements	51
Experimental Approach	53
V. EXPERIMENTAL RESULTS AND ANALYSIS	55
Basic Core Data	55
Pressure Data	59
Surface Area Relationship	65
Influence of Sample Character	70
Comparison of Similar Cores	73
Evaluation of Cementation Factor	75

Page

Relationship of Surface Area with Pore Structure Change 77
Double Layer Concept. 82
Double Layer Influence at Static Conditions . . 84
Double Layer Influence Associated with Compression. 90
Summary of Pressure Effects 94
Temperature Data. 96

VI. CONCLUSIONS 105

REFERENCES 107

APPENDIX A

BASIC CORE INFORMATION 111

APPENDIX B

EXPERIMENTAL DATA. 134

APPENDIX C

CALCULATED DATA ON NATURAL CORES 164

LIST OF TABLES

Table		Page
1.	Previous Studies of Rock Resistivity under the Influence of Pressure.	16
2.	Data Relative to Production of Unconsolidated Packs.	26
3.	Tabulated Data on the Synthetic Cores.	38
4.	Tabulated Properties of the Synthetic Cores Studied.	56
5.	Comparison of Sample and Pore Size Distribution Plug Porosities	76
6.	Surface Area Calculations on Synthetic Cores . . .	127
7.	Resistivity Changes Due to Pressure.	135
8.	Compressibility Data	143
9.	Change in m ($F = \phi^{-m}$) with Net Pressure.	147
10.	Change in m ($\Delta m = m^{P} - m^{1200}$) with Net Pressure	155
11.	Resistivity Changes Due to Temperature	156
12.	"Approximate" Pore Volume Change Due to Temperature	160
13.	Pore Size Distribution Data.	165
14.	Surface Area Calculations on Natural Rocks	166

LIST OF FIGURES

Figure		Page
1.	Formation Factor Versus Formation Porosity.	10
2.	Formation Factor Variations in Shaly Sands Due to Varying the Resistivity of the Saturating Solution.	10
3.	Formation Resistivity Factor Versus Porosity for Constant Tortuosity (T) and Various Constriction Factors (C).	14
4.	Computed Possible Minimum Voids in Bed of Two to Four Component Sizes If Initial Voids in Bed of Uniformly Sized Material Are 40 Percent. .	23
5.	Packing Equipment	29
6.	Epoxy Flooding Equipment.	33
7.	Method of Large Core Sectioning	35
8.	Schematic Diagram of Pressure Control System. . . .	41
9.	High Temperature and Pressure Resistivity Cell. . .	42
10.	Schematic of Resistivity Measuring System	49
11.	Schematic Diagram of Saturating System.	52
12.	Relative Formation Resistivity Factor Versus Pressure.	61
13.	Pore Volume Compressibility Versus Net Pressure . .	62
14.	Relative Formation Resistivity Factor Versus Pore Compressibility.	63
15.	Change Occurring in Relative Resistivity Ratio above 400 Psi.	66
16.	The Effect of Overburden Pressure on Rock Resistivity	71

Figure Page

17. Relative Formation Resistivity Factor Versus Net Pressure. 74

18. Change in m ($F = \phi^{-m}$) with Net Pressure on Synthetic Cores 78

19. Change in m ($\Delta m = m^{P} - m^{1200}$) with Net Pressure . 79

20. Descriptive Illustration of Greater Number of Constrictions Associated with Smaller Grains. . 81

21. Electrical Double Layer Concept 84

22. Cross Section of Pore Including Double Layer. . . 85

23. Cross Section of Pore Indicating Two Different Resistivity Paths 85

24. Sketch Showing Relative Importance of Double Layer Path with Respect to Total Pore Size. . . 86

25. The Change in m ($F = \phi^{-m}$) with Net Pressure on Natural Cores. 93

26. Resistivity Changes Due to Temperature. 97

27. Cumulative % Pore Volume Change Occurring to 240° F. Versus Temperature 104

28. Klinkenberg Permeability. 112

29. Mercury Injection Capillary Pressure Data - Core 35 113

30. Mercury Injection Pore Size Distribution - Core 35 114

31. Mercury Injection Capillary Pressure Data - Core 48 115

32. Mercury Injection Pore Size Distribution - Core 48 116

33. Mercury Injection Capillary Pressure Data - Core 65 117

34. Mercury Injection Pore Size Distribution - Core 65 118

Figure Page

35. Mercury Injection Capillary Pressure Data - Core 48-3 119

36. Mercury Injection Pore Size Distribution - Core 48-3 120

37. Mercury Injection Capillary Pressure Data - Core 65-3 121

38. Mercury Injection Pore Size Distribution - Core 65-3 122

39. Mercury Injection Capillary Pressure Data - Core 200. 123

40. Mercury Injection Pore Size Distribution - Core 200. 124

41. Mercury Injection Capillary Pressure Data - Core 65-S 125

42. Mercury Injection Pore Size Distribution - Core 65-S 126

43. Water Formation Volume Factor Versus Pressure and Temperature 163

ABSTRACT

Resistivity measurements were made on six synthetic bead cores and one synthetic sand core at varying conditions of pressure and temperature. Properties of the cores were "controlled" to provide a reasonably constant porosity in conjunction with varying pore sizes. The influence of overburden pressure was evaluated up to 10,000 psi. and the influence of temperature separately studied up to 320° F.

The resistivity increase accompanying a pressure increase was found to be a function of the theoretically calculated surface area of the core. The mechanisms influencing this resistivity increase, other than porosity, were qualitatively described and their relationship with surface area defined. The analysis indicates that an equation of the form

$$\frac{F^P}{F} = f \text{ (Surface Area)}$$

will provide a suitable approach for predicting the effect of pressure on the formation resistivity factor.

A definite trend in the rate of change of the relative formation resistivity factor was noticed as an apparent function of the matrix character. This supports the contention that rock resistivity changes under pressure should be

separately evaluated for specific group types such as sandstones, carbonates and shales.

The temperature portion of the study indicates that the initial rate of change in the relative formation resistivity factor is a function of the surface area of the core, although the total change appears to be a function of the matrix material. Packing, also, appears to be an influencing factor in these synthetic cores, presumably due to the fact that they are not at their minimum packing arrangement.

THE EFFECT OF PORE CONFIGURATION, PRESSURE, AND TEMPERATURE ON ROCK RESISTIVITY

CHAPTER I

INTRODUCTION

Application of a formation resistivity factor-porosity relationship is one of the fundamental concepts of quantitative log analysis. This relationship has been studied both experimentally and theoretically by numerous investigators with the primary attention being focused on the behavior of this relationship at some static condition. Up to the present time, however, few studies have been devoted to the effect associated with this relationship due to varying conditions of pressure and temperature. And, of these studies, fewer yet have attempted a quantitative analysis of their results. This study was, therefore, initiated in order to provide a deeper insight into the observed rock behavior associated particularly with formation resistivity under varying pressures and temperatures.

The necessity for requiring a knowledge of the behavior of the formation resistivity variation with temperature and pressure can be readily demonstrated. As will be

discussed in greater detail later, no one relationship has been found to express the formation resistivity factor-porosity relationship over the complete range of porosities encountered in natural rocks. Of these relationships, as quoted from Pirson,[30] "Only two, both of which are empirical, have survived the test of usefulness." Since they are empirical, however, each requires a knowledge of the inherent proportionality constants necessary to relate the formation resistivity factor with porosity. One of these relationships is the familiar Archie equation.[4]

$$F = \phi^{-m} \qquad (1)$$

where: F = formation resistivity factor

ϕ = porosity

m = proportionality constant generally referred to as the "cementation" factor.

Practical application of this equation in any particular area is then accomplished by evaluating the cementation factor using laboratory measured values of the formation resistivity factor and porosity. This surface measured value of cementation factor is then used in conjunction with either of the two remaining parameters for determining the other at subsurface conditions. A problem is encountered when employing this technique, however, since experimental observation indicates that the change in formation resistivity factor with pressure and temperature is more rapid than can be accounted

for solely on the basis of porosity change. In fact, as pointed out by Hilchie,[20] errors in the range of 80% might possibly be encountered when using a laboratory evaluated cementation factor with subsurface resistivity data for porosity determinations.

There are two primary reasons why the formation resistivity of subsurface samples are measured at atmospheric pressure and ambient temperature in the laboratory. The first is that resistivity measurements at increased pressure and temperature conditions are rather difficult and time consuming. Secondly, until recently, wells were relatively shallow and the effects of pressure and temperature did not appear to be so critical. This is probably true, to some extent, since a greater change in the formation resistivity factor is noted with an increase in pressure and temperature and lower porosity rocks, all three of which are generally associated with deeper wells. The trend toward deeper wells necessitates a consideration of the effects of pressure and temperature on rock resistivity behavior.

Another important reason necessitating a knowledge of formation resistivity behavior with pressure changes is due to the stress distortion occurring in the formation surrounding the wellbore. This wellbore stress distortion has been theoretically discussed by Hubbert[21] and its influence on quantitative log analysis briefly considered by Glanville.[16] The analysis by Hubbert indicates that the horizontal stress

around the wellbore may be substantially relieved with respect to the stress actually existing in the formation. This distortion, however, may only exist a few hole diameters into the formation. This could be an important factor if a tool having a short depth of investigation, such as a microdevice, is used in obtaining the basic resistivity data for a porosity determination. A tool having a deeper depth of investigation would probably see the formation in more or less its original state, and this problem would be obviated. However, at this time, micro and sonic devices, which have relatively shallow depths of investigation, are considered basic porosity tools. Here again, the trend toward deeper wells will tend to amplify the problem.

These problems could obviously be relieved if all the formation samples, from which formation resistivity factor-porosity data was required, would be studied at elevated pressure and temperature. This analysis, however, will probably never become routine due to the difficulty and time required in performing this type of measurement. The most practical approach would be to continue the practice of performing the formation resistivity measurements at atmospheric pressure and ambient temperature, and then, in conjunction with additional data, such as pore size distribution or surface area information, correct the surface measured resistivity values to existing formation conditions. At the present time, however, the correlations available, such as

those by Hilchie (one based on percent clay content and the other one percent pore volume having a pore size below 0.5 microns), were developed on rather limited amount of data and, therefore, statistically speaking, are not generally applicable.

A second approach would be to study under elevated pressure and temperature only those samples which would probably exhibit a fairly significant change in formation resistivity factor at these increased conditions. Even to do this, it is necessary to have a reliable indicator available to distinguish those samples where the variation in formation resistivity at elevated pressure and temperature conditions is significant.

The establishment of a reliable correlation requires a thorough knowledge of rock behavior accompanying the application of increased pressures and temperatures. This behavior is not only confined to that exhibited by the solid framework or matrix of the rock, but also that behavior associated with the change in the conducting path within this framework, as will be pointed out in this study. The behavior of any one particular natural rock, since it is a function of a great many different although interrelated factors, provides a very diverse, complex model from which to garner definitive information. The data which are collected from this type of study with natural rocks can be utilized for detecting trends or, if enough have been

evaluated, to promote general relationships which may or may not be applicable. However, confidence in the applicability of these relationships observed in natural and complex systems can only be established by an understanding of the mechanisms inducing the observed behavior and the relationship of these mechanisms to specific parameters associated with the rock.

Based on the trends observed by Hilchie in his work on natural rock, it was decided to further investigate the relationship of formation resistivity variation with pore size. Synthetic porous systems were chosen for this study in order to circumvent the complexity associated with natural rock systems. Utilization of synthetic cores greatly reduces the number of influencing parameters and those remaining can, for the most part, be controlled. From this study, then, a more definite understanding of the operative mechanisms and their interrelationship with "controlled" parameters is possible.

CHAPTER II

LITERATURE REVIEW

The concept of formation resistivity factor, F, has been the subject of much scientific endeavor during the past three quarters of a century. However, the term formation resistivity factor is a rather recent definition of the initial relationship of interest, namely the ratio of the resistivity of a solution containing non-conductive solids to the resistivity of that solution. This can be stated in equation form as:

$$F = \frac{Ro}{Rw} \qquad (2)$$

where: F = formation resistivity factor

Ro = resistivity of a non-conducting medium, 100% saturated with a conducting solution, ohm-meters

Rw = resistivity of the conducting solution, ohm-meters

Initial studies of this relationship were generally associated with unconsolidated arrangements of various types of solid particles. Probably the first such study was by Maxwell[24] who theoretically related this resistivity ratio (formation resistivity factor) with porosity for a dispersed

sphere system. Numerous other relationships have subsequently been theoretically and experimentally developed in this area of unconsolidated systems. Notable among these were proposed by Rayleigh,[32] Fricke,[14] Salwinski,[34] and Dakhnov.[8]

The relationships proposed for unconsolidated systems do not necessarily conform to the relationships existing in natural rocks, except in possibly special cases. This is due to the greater complexity of a naturally consolidated porous media. Since natural rock systems essentially preclude a mathematical treatment for the development of a definitive relationship between the formation resistivity factor and porosity, the only avenue of approach has been the empirical analysis of experimental data.

Two such empirical relationships have been proposed and have received wide acceptance. One such relationship is that proposed by Archie[4] as defined in Chapter I. The second is a more generalized form of Archie's equation as determined experimentally by Winsauer, et al.[37] This relationship can be stated as follows:

$$F = \frac{Ro}{Rw} = C\,\phi^{-m'} \qquad (3)$$

The constants C and m' are obtained from the best straight line through the formation resistivity factor-porosity data as plotted on logarithmic graph paper. A large number of sample points are desirable for determining these constants although for general application Winsauer, et al.[37] proposed

the values of 0.62 and 2.15 for m' and C, respectively. For completeness, a restatement of Archie's equation will be included again.

$$F = \frac{Ro}{Rw} = \phi^{-m} \qquad (1)$$

The cementation factor, m, has been found to vary over a wide range of values from 1.3 to approximately 2.5. The effect of the varying cementation factor values in the Archie relationship is graphically illustrated in Figure 1. As can be seen from this relationship, the greater the cementation factor, the higher the formation resistivity factor for a particular porosity. An increase in cementation factor also is associated with an increase in rock consolidation or cementation.

The reason for the observed variation in cementation factor has been attributed to a number of different factors. A listing of these would include the following:

(1) Degree of cementation[43, 19]

(2) Shape, sorting and packing of the particulate system[6, 43]

(3) Type of pore system - intergranular, intercrystalline, vuggy, etc.[37, 7, 5]

(4) Tortuosity of the pore system[37, 44, 42, 28, 35]

(5) Constrictions existing in porous system[28, 35]

(6) Presence of "Conductive Solids"[10, 29, 38]

(7) Compaction due to overburden pressure[11, 12, 16, 18, 20, 27, 33, 39, 40]

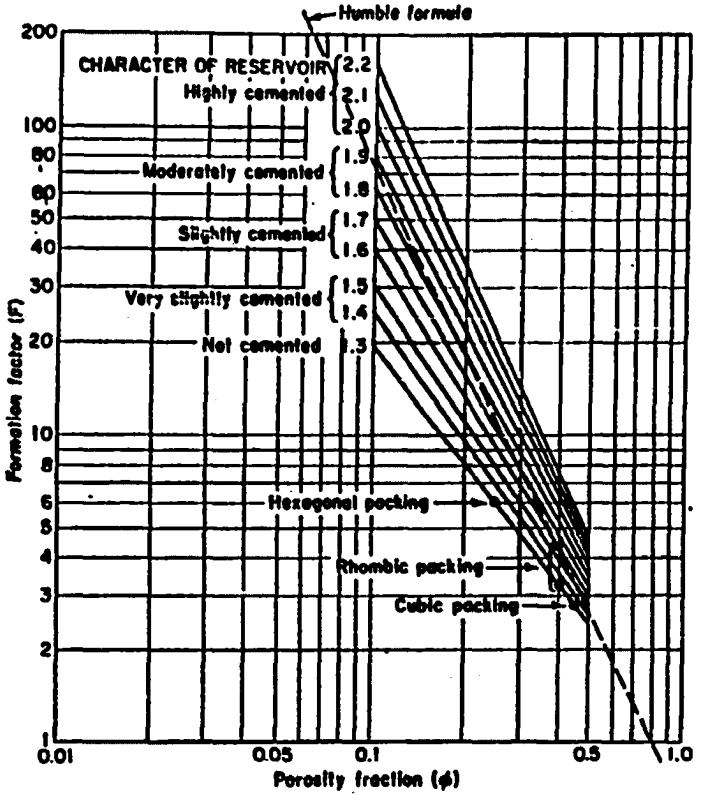

FIG. 1.--FORMATION FACTOR VS. FORMATION POROSITY (FROM PIRSON[30])

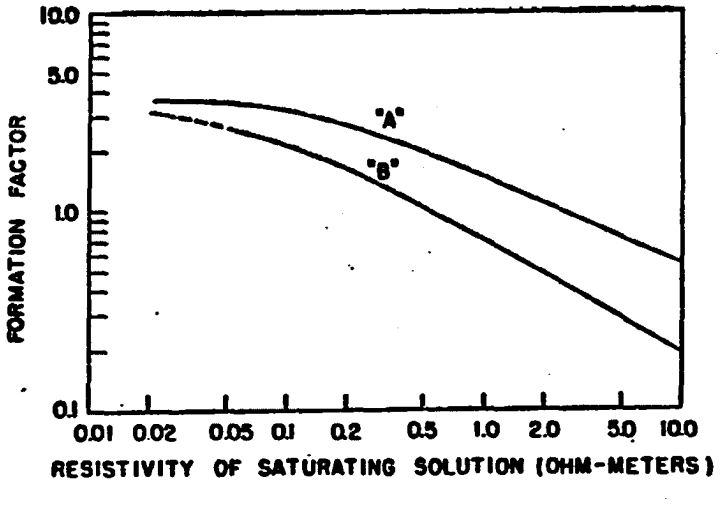

FIG. 2.--FORMATION FACTOR VARIATIONS IN SHALY SANDS DUE TO VARYING THE RESISTIVITY OF THE SATURATING SOLUTION (FROM WYLLIE[42])

(8) Thermal expansion[20]

The complexity of natural rocks is aptly indicated by the general listing above. As implied by these factors, no one concept or factor adequately describes the relative behavior of the formation resistivity factor with porosity. This, of course, can be ascribed to the fact that no one parameter can adequately describe pore geometry primarily because it is a function of a number of interrelated factors. These interrelated factors produce an essentially unlimited number of possible pore geometries. The outcome of this is a variation of pore geometries in an essentially unlimited number of possibilities. Any physical explanation of the observed variation in cementation factor for natural rocks must, therefore, be tied to a number of different factors and their subsequent interrelationships.

The cementation factor is often related to tortuosity. This term has significant merit, however, since it does attempt to define the pore passages in the medium. This tortuosity coefficient as defined by Pirson[30] is "a conceptual dimensionless number representing the departure of a porous system from being made up by a bundle of straight-bore capilliares." It is, therefore, a measure of the tortuous path available for current flow with respect to the direct path available in a conductive solution. Using this concept alone to explain the effect of pore geometry upon

the cementation factor implies that the differing resistance noted for rocks having the same porosity is due to changes in tortuousity. Hence, all formation factors could be accounted for merely by changing the value of tortuosity.

The limitations associated with trying to ascribe the higher formation resistivity factors solely to tortuosity have been recognized. Two important theoretical contributions provide a greater insight into the influence of pore geometry. These studies by Owen[28] and Towle[35] utilized synthetic pore models which could be considered mathematically. Although the systems were greatly oversimplified, a significant concept evolved - pore constriction. This is essentially the effect of the variations in cross-sectional area of the conducting path on resistivity. A porous system employing both the concepts of tortuosity and pore constriction are, as stated by Owen[28] "as being more nearly analagous to conditions within a natural porous body than is a uniform diameter tube system which requires high tortuosity values to explain large formation factors."

The particular utility of these interrelated concepts of tortuosity and pore constriction is not immediately apparent except for the fact that a more logical explanation of pore geometry effects on formation resistivity is available. As pointed out by Owen, an infinite number of combinations of

tortuosity and constriction factors can be chosen to give a particular porosity. Figure 3 has been included to indicate how the formation resistivity factor increases with an increase in constriction factor at a constant value of tortuosity. The usefulness of this concept cannot be fully appreciated, however, until a logical explanation of the variation of formation resistivity under pressure is attempted.

The application of these two concepts (tortuosity and pore constriction) essentially incorporate all the factors affecting pore geometry. Therefore, the effect on formation resistivity ascribed to (1) degree of cementation, (2) shape, sorting and packing of the particulate system and (3) type of pore system can be accounted for by these two parameters.

The effect of "conductive solids" on the cementation factor have been noted by Patnode and Wylie,[29] de Witte,[10] and Winsauer and McCardell.[38] The term conductive solids is essentially a misnomer since the effect is actually due to double layer conductivity associated with the highly charged clay surfaces. The resultant effect of this conductivity is to reduce the cementation factor as the conductivity of the saturating solution decreases. This effect can be essentially negated by increasing the conductivity of the

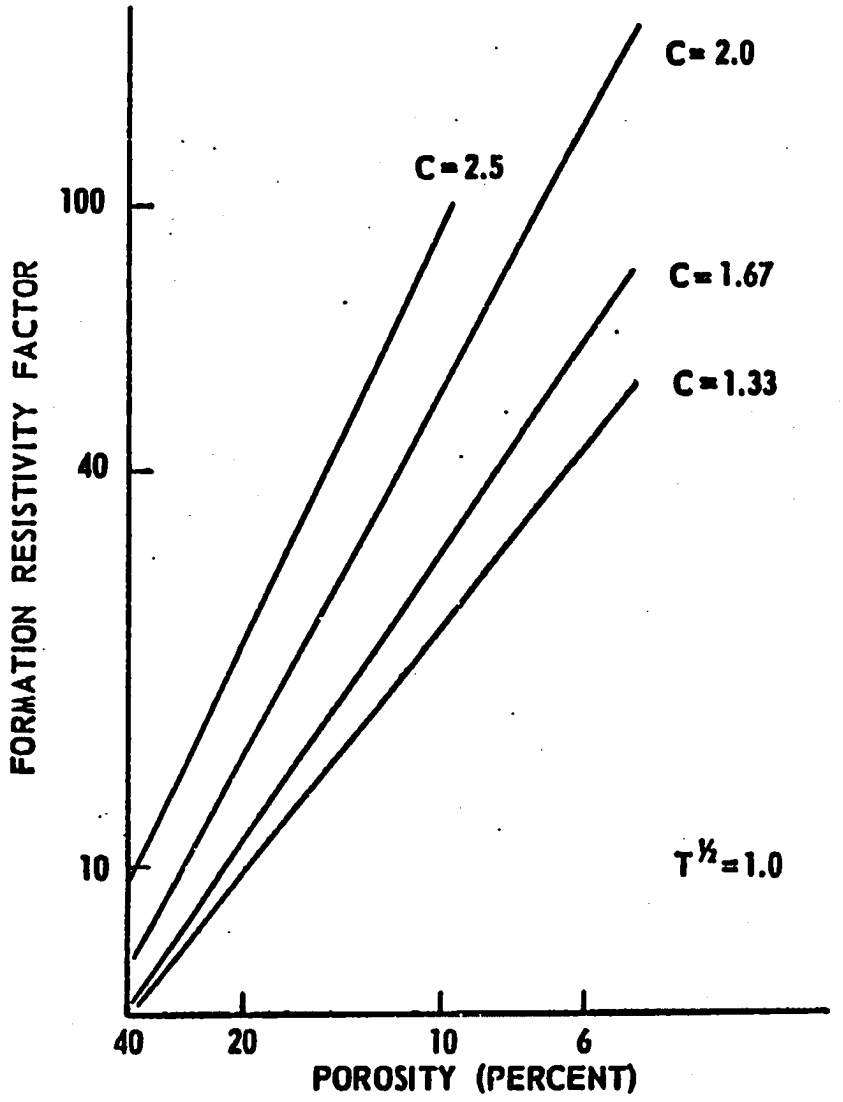

FIG. 3.--FORMATION RESISTIVITY FACTOR VERSUS POROSITY FOR CONSTANT TORTUOSITY (T) AND VARIOUS CONSTRICTION FACTORS (C) (AFTER OWEN[28])

saturating solution. If this conductivity becomes high enough, a constant value of formation resistivity factor will be attained with the resultant value of the cementation factor now being assumed to reflect the true tortuosity and constriction factor of the formation. Figure 2 graphically illustrates the influence of the "conductive solids" on static formation resistivity factor measurements.

Up to this point, consideration has been given to the factors affecting the formation resistivity factor-porosity relationship at a static condition of pressure and temperature. In other words, we have been referring to the effect of the geologic factors as applied to a particular state at which the core exists. However pressure and temperature, have also been found to affect this formation resistivity factor-porosity relationship. Changes have been observed in the formation resistivity factor when changing the pressure state from atmospheric conditions to a higher external pressure condition. It has also been found that this change in resistivity cannot be accounted for simply by considering the pore volume change alone.

For the most part, the studies related to the effects of pressure have been of a qualitative nature with only two investigators attempting quantitative interpretations of their data. This can be attributed to the limited number of samples

studied, the variation in technique making it difficult to relate the results of the various studies and a lack of understanding of the operative mechanisms associated with the effect of pressure. The tabulated information in Table 1 indicates the limited data in this area.

TABLE 1

PREVIOUS STUDIES OF ROCK RESISTIVITY UNDER THE INFLUENCE OF PRESSURE

Investigator	No. of Samples and Type	Net External Pressure Range Studied
Fatt[12]	20 Sandstones	0-5000 Psi.
Wyble[39,40]	3 Sandstones	0-5000 Psi.
Glanville[16]	2 Sandstones	0-5000 Psi.
	3 Carbonates	0-5000 Psi.
Redmond[33]	4 Sandstones	0-20,000 Psi.
Glumov and Dobrynin[18]	1 Sandstone	0-350 Atmospheres
	1 Limestone	0-350 "
Orlov and Gimaev[27]	2 Carbonates	0-400 Atmospheres
Dobrynin[11]	2 Sandstones	0-5000 Psi.
Hilchie[20]	3 Sandstones	0-10,000 Psi.
	1 Shale	"
	1 Limestone	"
	1 Artificial (Alundum)	"

Some of the significant differences observed with respect to technique, should be noted. It has been shown by Hilchie and others that the time necessary for equilibrium conditions to be attained ranges anywhere from one to over 100 hours. In fact, even after 100 hours, equilibrium was not attained on the carbonates studied by Orlov and Gimaev. The experimental measurements of Glumov and Dobrynin were made 15-20 minutes after each pressure increase, making it unlikely that the samples had reached equilibrium.

Another area of concern is that associated with the type of core mounting used. In the studies of both Fatt and Dobrynin, the samples were mounted in Lucite which has structural strength and will tend to minimize some of the applied force to the core. This is probably not too important at high pressures, but its influence could become critical at low pressures. The manner in which the external pressure is applied to the core is also important. The technique employed by Wyble, Redmond, and Glumov and Dobrynin, involved the application of only a radial stress on the cores. It is believed that rocks existing in the natural state are subjected to stresses somewhere between the normally used three equal stresses and that of a large vertical stress and small horizontal stresses. Withstanding these differences, all investigators who have contributed in this area agree that the effect of pressure on the formation resistivity can be quite large.

Dobrynin presented the first relationship in which the relative formation resistivity factor ratio was related to the overburden pressure, porosity and compressibility. Hilchie, however, was not able to verify this correlation. He felt this was due to the reliance of Dobrynin's correlation on the low pressure data (which is subject to question due to the use of Lucite mountings) and the idealization of the pressure-compressibility relationship.

Hilchie developed two relationships that characterized his data. The first relates the relative formation resistivity factor with the percent shale contained in the shaly sands:

$$\frac{F^P}{F} = 1.053 + 0.147 \log C + 12.5 \times 10^{-6} (P-1000) \quad (4)$$

where: $\frac{F^P}{F}$ = Relative formation resistivity factor; ratio of formation resistivity factor at pressure P to the formation resistivity factor at atmospheric pressure.

C = Percent clay in the sand

P = Net pressure in psi.

The second relates the relative formation resistivity factor with the pore volume less than 0.5 microns existing in the sample.

$$\frac{F^P}{F} = 0.868 + 0.225 \log (PV<.5) + A (P-1000) 10^6 \quad (5)$$

where: $PV<0.5$ = the percent of the pore volume having pores with a radii less than 0.5 microns.

A = lithology constant of 12.5 for sands and 21 for limestones.

The general applicability of these two empirical equations is subject to conjecture because of the limited number of samples used. The results of this study, however, tend to lend credence to them, since the correlating parameters of $PV<0.5$ clay content would seem to be indicative of the effectiveness of the operative mechanisms, discussed later in this study.

The effects of temperature on the formation resistivity have been evaluated only by Hilchie to date. He found that as the temperature increased (net pressure constant) the formation resistivity factor went through a minimum after which it increased. The magnitude of this minimum and the temperature at which it occurred, as well as the magnitude of the increase after the minimum occurred, varied with the samples studied. He presented a method for predicting the effect of temperature, if the percent pore volume consisting of pores less than 0.5 microns, and the minimum temperature, were known. This prediction method can be represented as follows:

$$\frac{F^T}{F} = G + \left[\left(\frac{T}{100}\right)^{\frac{1}{2}} + \left(\frac{T}{100} - \alpha\right)^2\right]^{\frac{1}{2}} A \qquad (6)$$

where: $\frac{F^T}{F}$ = relative formation resistivity factor at temperature T

T = temperature in ^oF.

α = a variable which locates the minimum with respect to temperature

A = empirical value determining the magnitude of the minimum

G = empirical constant that normalizes each curve at the initial temperature

This relationship was not designed to be used as a working correlation. Its purpose was simply to illustrate the effect of the known parameters. Further work in this area is required in order to properly evaluate this effect.

The combined effects of temperature and pressure were also studied by Hilchie. In general it was found that the additive results of the separate pressure and temperature data were equal to the combined pressure and temperature data at low and moderate temperatures. This would imply that pressure and temperature may be considered as independent variables in this range.

CHAPTER III

SYNTHETIC CORE DESIGN AND CONSOLIDATION

The use of synthetic cores in evaluating the effect of pore geometry on the formation resistivity factor under varying conditions of pressure and temperature imposes a number of requirements on the samples to be used. The desired aim of the study itself dictates that the pore size of the artificial media be "controlled" at least to the extent that the separate cores produced will provide different pore size distributions. The core should also:

1. Behave as a consolidated rock under high pressures and temperatures.
2. Have essentially the same porosity in all the separate cores.
3. Have other properties such as permeability and compressibility similar to that of natural rocks.
4. Provide a non-conductive matrix.
5. Be inert to the effect of salt water.
6. Be essentially homogeneous.
7. Contain the same specific volume of cementing material in each sample.

Unconsolidated Pack Design

Furnas[15] has developed a method for computing the proportion of particles of various sizes needed to produce a minimum porosity. He found it to be generally true that minimum voids were obtained as the ratio between the particle sizes increased and as the number of sizes increased. Although these formulas are not rigorous, they have been corroborated for spheres in work reported by Wylie and Gregory.[43] Even though a samll discrepancy exists between the experimental and theoretical results, it was felt that this theoretical analysis provided a reasonable basis for determining the grain sizes to be used. Furnas has presented graphical solutions of his theory whereby the size ratio and volume proportion of the different beads to be used can be quickly determined for any minimum, unconsolidated pack porosity desired. One of these solutions is presented in Figure 4. Since spherical beads were used, it was assumed that the initial voids in a pack of uniformly sized material would be 40%.

Based on this approach, it can be seen that, if two different sizes of beads are uniformly mixed together in volume percents, of 71.5 for the larger bead and 28.5 for the smaller bead and, at the same time, the ratio of the smaller to the larger size is 0.2, then the unconsolidated pack

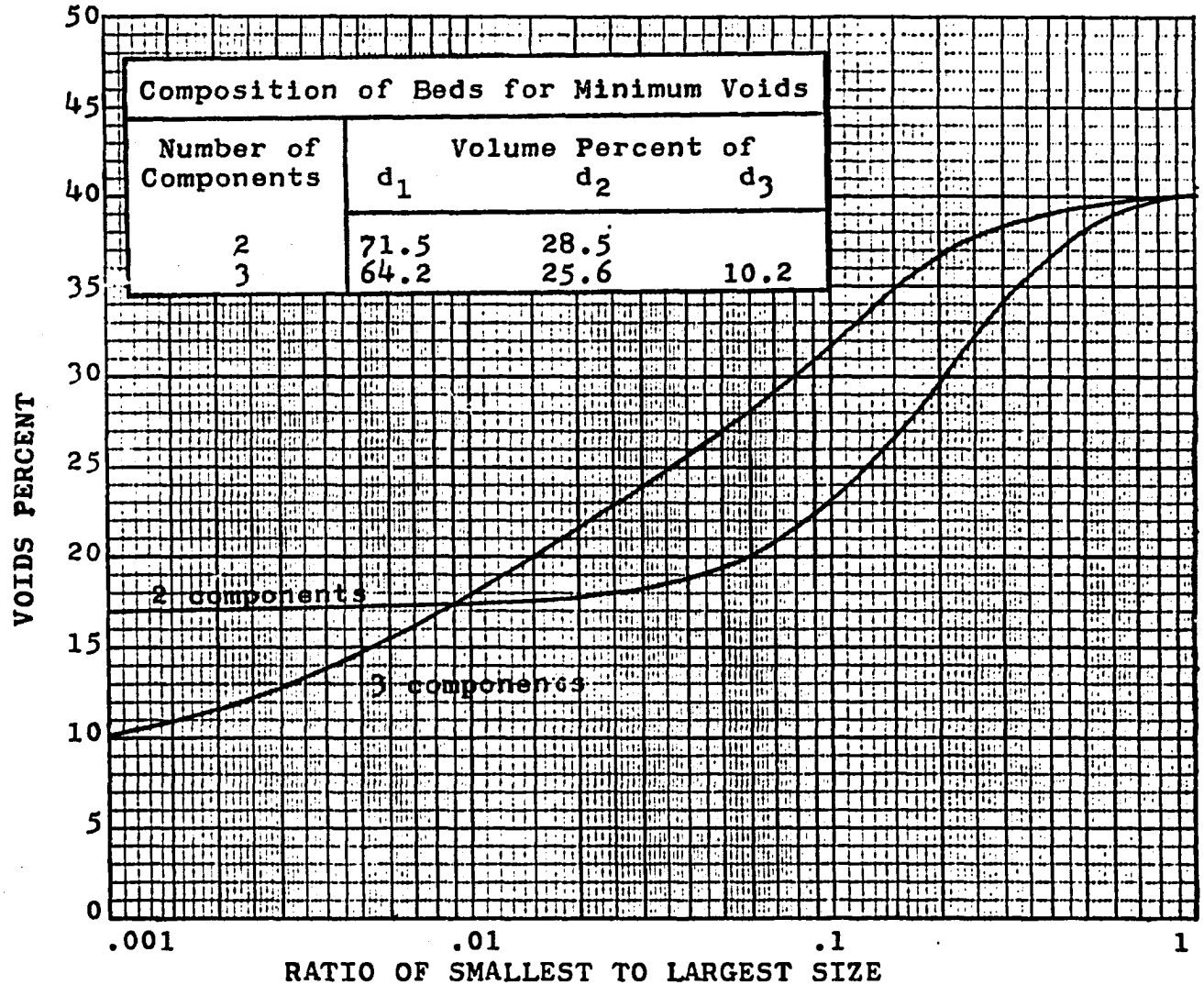

FIG. 4.--COMPUTED POSSIBLE MINIMUM VOIDS IN BED OF TWO TO FOUR COMPONENT SIZES IF INITIAL VOIDS IN BED OF UNIFORMLY SIZED MATERIAL ARE 40 PERCENT (FROM FURNAS[15])

should have a porosity of 30%. By using combinations of different bead sizes, each combination having the same size ratio of 0.2 and mixed uniformly in the volume percents dictated by the theory, unconsolidated packs can be produced having the same porosity but differing pore sizes. These concepts of Furnas therefore provided the guidelines for the bead combinations used.

The choice of bead sizes also requires other considerations to be made. These include (a) similarity to natural sandstones, (b) desirability of small pores, and (c) practical bead sizes. An understanding of grain size distributions in natural sands is necessary in choosing bead sizes. One such indicator is the screen analysis of 23 various sands presented in Muskat.[26] Using this tabulation, it can be seen that the sands consist of grains having a mesh size greater than 40. All the sands analyzed also contain some percentage of grains having a mesh size over 270. Based on this information, it was felt that no mesh sizes less than 30 to 40 should be used, especially if small pore sizes are desired. Additionally, at least a portion of the beads should be 200 mesh or greater.

A set of six different bead combinations and one sand combination were chosen. The basic data relative to the

production of the unconsolidated packs for these combinations is presented in Table 2. The first three combinations were the initial mixtures used. Based on the data from these, the other combinations were made. Combination 4 was chosen primarily as a limiting case for small pores while combinations 5 and 6 were intended to fill the intermediate area in the data. Finally, combination 7, which uses the same mesh sizes as combination 3, was made out of sand grains rather than beads.

The beads used in making the synthetic cores were purchased from the Microbead Division of the Cataphote Corporation and are manufactured from high grade optical crown glass, soda lime type, with a silica content not less than 68 percent. This composition is of a type to resist wear and fracture. The beads are annealed in their spherical shape to equalize internal stresses. The sized beads contain not more than five percent irregularly shaped particles and are, therefore, essentially free of sharp angular beads. They are also reasonably free of particles showing surface scoring and foreign matter. Since 90% of the beads were also guaranteed to be in the size range ordered, no additional sieving was done before making the desired volumetric combinations.

TABLE 2

DATA RELATIVE TO PRODUCTION OF UNCONSOLIDATED PACKS

Combination	Large Mesh Size	Diameter in Inches	% Vol.	Intermediate Mesh Size	Diameter in Inches	% Vol.	Small Mesh Size	Diameter in Inches	% Vol.	Ratio of Smallest to Largest Size	Predicted Unconsolidated Porosity
1	35	.0165	71.5	-	-	-	200	.0029	28.5	.176	28.5
2	48	.0117	71.5	-	-	-	270	.0021	28.5	.179	28.5
3	65	.0083	71.5	-	-	-	325	.0017	28.5	.205	30.0
4	200	.0029	71.5	-	-	-	325	.0017	28.5	.586	38.5
5	48	.0117	64.2	270	.0021	25.6	325	.0017	10.2	.145	34.5
6	65	.0083	64.2	270	.0021	25.6	325	.0017	10.2	.205	36.5
7 (sand)	65	.0083	71.5	-	-	-	325	.0017	28.5	.205	30.0

Unconsolidated Pack Preparation

The ability to produce essentially tightly prepared, homogeneous, unconsolidated packs was one of the most important features in obtaining the desired synthetic cores. In order to accomplish this, it was necessary to have a standardized mechanical technique for preparing the unconsolidated packs. Since core samples having a diameter of 1.5 inches and a length of two inches were desired for use in the resistivity cell, it was decided to make the packs in glass tubing having an inside diameter of 1.5 inches. There were a number of advantages for using glass tubing which included:

(a) smooth cores having the exact diameter desired could be obtained,

(b) any length of pack desired could be made,

(c) the rigid tube and centered axis reduced the difficulty in packing,

(d) the progress of flooding the pack with the cementing material could be easily followed,

(e) the glass could be easily removed from the core.

Packing of the beads in the tube was accomplished by utilizing a technique described by Wygal.[41] In this method, a "particle distributor" was used. It could be prepared simply and quickly, and appeared to produce uniform reproducible packs. The purpose of the distributor was to maintain the upper layers of beads in the pack in a continuous state

of agitation and to keep these layers perfectly level. Poorly distributed particles do not keep the surface active and, therefore, some of it may be buried in an unstable position. A diagram of the packing apparatus is shown in Figure 5.

The "particle distributor" was made from 1.5 inch I.D. plastic tubing. The 12 inch long tube was cut perpendicular to the axis five times and circular screens were epoxied into each cut. The screens were set one inch apart. The distributor was then connected to the glass tube to be packed by a rubber sleeve similar to that used for mounting the cores. A rubber stopper, in which a small glass tube was inserted, closed the lower end of the glass tube. A cloth screen was cemented to the stopper to prevent the beads from leaving the tube. A vacuum pump was connected to the stoppered end of the glass tube in order that a vacuum could be applied to the system during the packing process. The use of a vacuum was recommended by Wygal for the packing of particles smaller than 120 mesh.

The length of the glass tube used in this process is not restricted, and, therefore, any size of core desired can be made. However, in this study, a tube 10.5 inches long was used, thereby providing a core of approximately 9-9.5 inches. Allowing for end scrap, approximately three-two inch cores and a short section to be used for mercury injection were easily obtained. This tube was then attached by the rubber sleeve to the particle distributor, stoppered, the

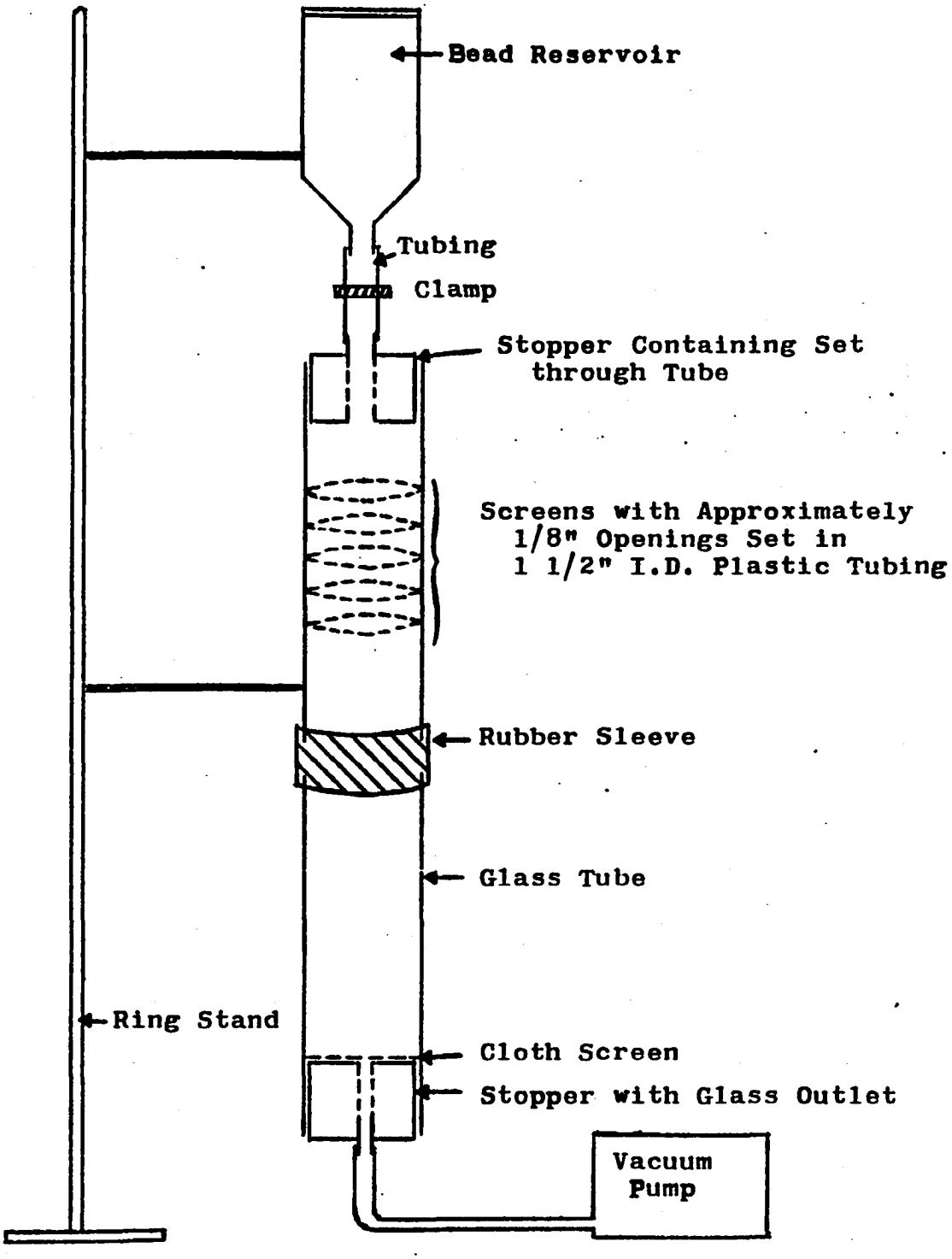

FIG. 5.--PACKING EQUIPMENT

vacuum pump attached and a vacuum pulled on the system. The clamp on the tubing above the particle distributor was closed at this time. The pre-mixed bead combination to be packed was then placed in the bead reservoir. The clamp above the "particle distributor" was then opened, allowing the beads to fall through the distributor and pack in the glass tube. The flow rate of the beads was controlled by adjusting the clamp. The primary objective was to control the flow rate while maintaining a continuous flow.

Consolidating Material

Finding a cementing material that met all the requirements was the greatest single problem in developing the desired artificial cores. In order to compare the behavior of any one synthetic core to another it was necessary to cement each unconsolidated pack with the same volume and type of cementing material. In this way the effect of the cementing material became a relative parameter. Secondly, a cementing material was needed which could be placed in the unconsolidated pack after it was produced. In addition, the cementing material had to essentially coat all of the grains in the same fashion, coat them uniformly and be reasonably reproducible in the nature of its coating. It also had to be reasonably flexibile in order that a brittle or incompressible core, similar to various ceramics or alundum, did

not result. Finally, it had to be able to withstand high temperatures and pressures, salt water effects and be electrically non-conductive.

These requirements were all met by an epoxy resin formulation made available by the Dowell Division of The Dow Chemical Company. It is similar to formulations used for consolidation of incompetent sand formations in oil wells. The important feature of this epoxy system is that solvents initially mixed with the resin and curing agent can be "sweated" out of the synthetic core once the epoxy has set. During the hardening process the resin preferentially coats the beads in the pack, thereby leaving the solvent in the center of the pores. The epoxy also tends to coat the beads with a unifcrm smooth coating.

This "sweating" process allows close control of the amount of cementing material which is deposited. The amount deposited is simply a function of the amount of solvent in the initial mixture. The amount of solvent used with the epoxy material is somewhat arbitrary. A 50-50 volumetric ratio of epoxy material and solvent was chosen for this study. Theoretically then, if one fills the entire pore space of the unconsolidated pack with the epoxy-solvent mixture, the pore volume of the unconsolidated pack should be reduced by 50 percent. At the same time, the pore geometry should still be

primarily governed by the bead shape since the epoxy preferentially and uniformly coats the beads.

The solutions for consolidating the cores were prepared from materials and procedures furnished by Mr. E. D. Mullen of Dowell. Since the resin and hardener must finally be mixed in a specified ratio by weight, specific gravity measurements were used to determine the final volumetric mixing proportions. This was found to be a ratio of 3.3 cc. of resin solution for every 1.0 cc. of hardener solution. This will give a final mixture of approximately 47.5 percent by volume epoxy resin and 52.5 percent by volume solvent.

Consolidating Procedure

The consolidating technique used for placing the cementing material in the unconsolidated pack was nothing more than a gravity type flooding approach. This technique is highly desirable since it is very simple and the resultant pack is stable. A diagram of this method is shown in Figure 6.

With this technique, it can be seen that in order to convert from the packing system to the flooding system only a few things had to be done. First, the glass tube containing the unconsolidated pack was removed from the sleeve connecting

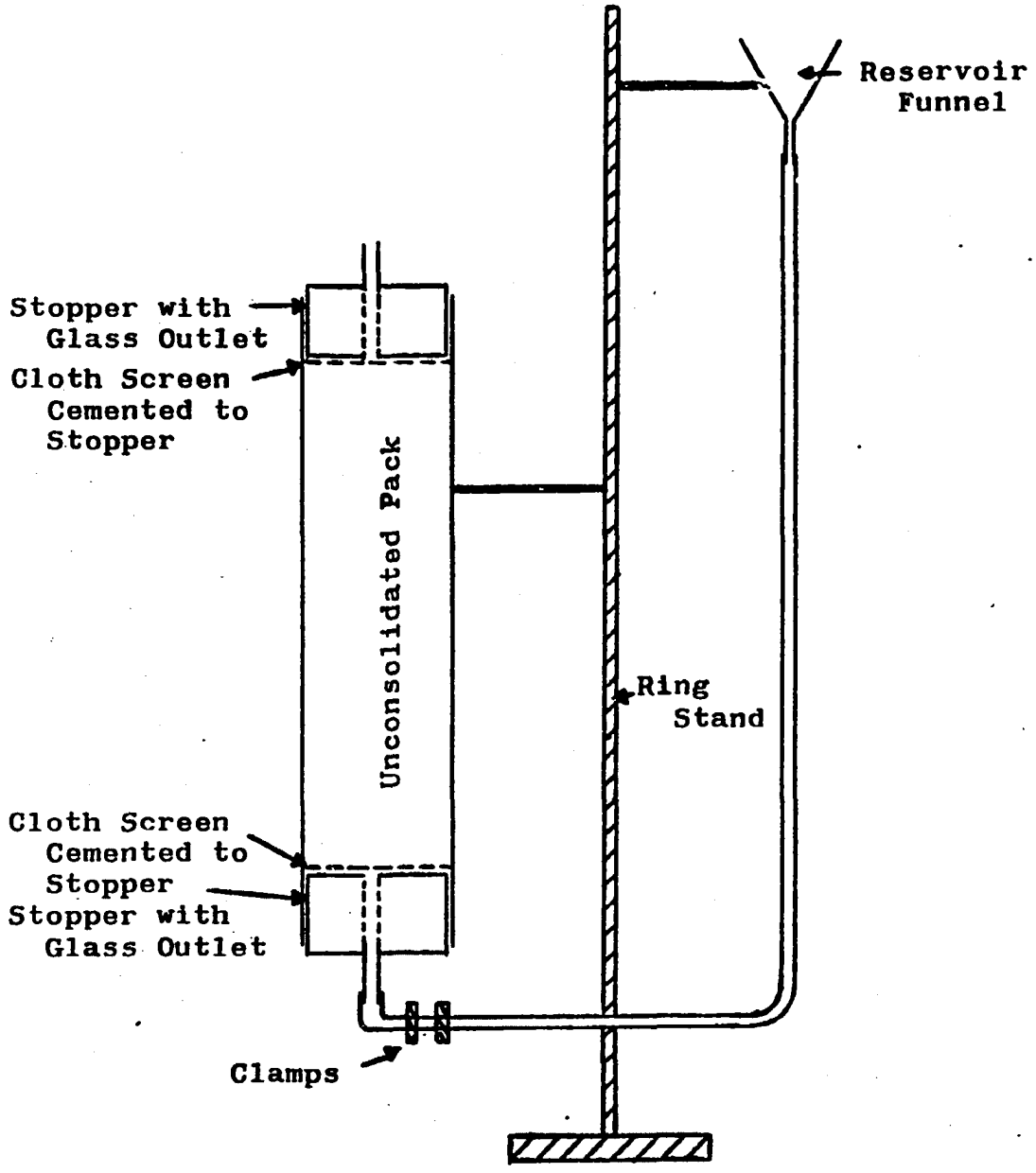

FIG. 6.--EPOXY FLOODING EQUIPMENT

it to the "particle distributor." A rubber stopper containing a glass tube and having a cloth screen cemented to it was placed tightly in the open end. The two stoppers were then wired together so they could not shift during the flooding process. In this way, the unconsolidated pack was firmly held in place. The tubing attached from the lower end to the vacuum pump was then connected to a funnel serving as the reservoir for the cementing material. One of the clamps on the flexible tubing was then closed and the tubing and reservoir filled with the cementing material. Once this portion of the system was full, the clamp was opened and the pack flooded with the cementing material. The air was displaced from the pack through the glass tubing in the upper stopper.

The flow properties of the epoxy resin mixture were nearly ideal for this gravity type of flood. The rate of progress of the flood front was not so slow that an excessive length of time was required and it was not so fast as to trap air to any extent. The flood progressed at a uniform rate. It should be mentioned that the epoxy-solvent mixture remains fluid for an extended period of time at room temperature.

Once the core had been completely flooded, the two clamps on the flexible tubing were closed and the tubing cut

between the clamps. The glass tube containing the flooded pack was then placed in an oven and cured. After an initial curing period, during which the epoxy hardened, the core was removed from the glass tube by breaking the glass and pealing it away from the core. It should be pointed out that the epoxy forms a good bond with the glass and will make it nearly impossible to remove the glass tube unless this bond is eliminated. This was overcome by applying a thin film of silicone on the inside of the tube prior to packing it with the beads. After the core has been removed from the glass tube, it is again placed in an oven and heated, thereby evaporating out the solvent. This produces a dry, clean core.

Sample Identification

The cured core, approximately 10 inches long, was then cut with a diamond saw into short samples in the following manner:

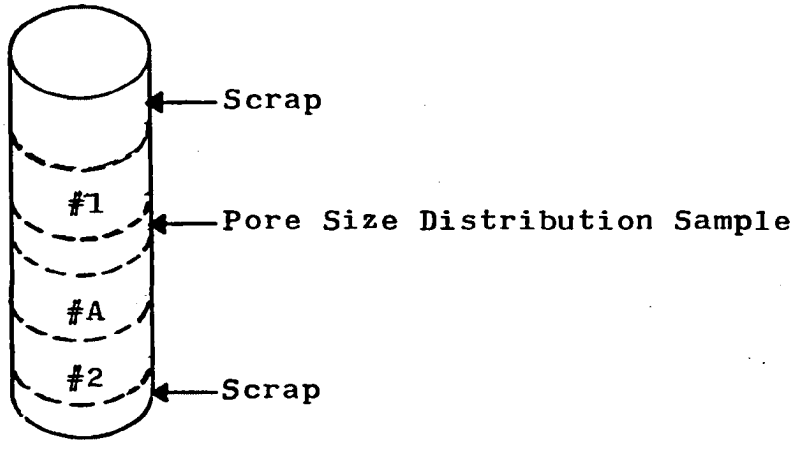

FIG. 7.--METHOD OF LARGE CORE SECTIONING

Three cores were obtained (#1, A, and 2) all of which were approximately two inches long. A shorter section was cut between samples #1 and #A to be used for mercury injection pore size distribution data. Samples #1 or #A were the desirable samples to use in the resistivity cell since they were cut adjacent to the sample used for the mercury injection data. Additional labelling was also necessary to distinguish the different synthetic cores from each other. The first identification number of each core is actually the mesh number of the largest bead size used in that core. If the core contained two bead components such as in combination two (Table 2), then it would be designated core number 48. If the A sample was studied, then it was referred to as 48-A. The only exception to this is when two components of sand were used and then an "S" indicator was used to define the sand sample, i.e. 65-S-A. For the cases where three bead sizes were used and, at the same time the largest mesh size was the same as in a two-component core, an additional identifier was used. As an example, consider combination number 6. The A sample would be labelled 65-3-A where the 3 indicates a three-component sample.

Core Evaluation

The short samples and the pore size distribution (PSD) plugs were all analyzed for porosity and since either the Number 1 or A sample was to be used for obtaining the

resistivity data, they were also analyzed for "Klinkenberg" air permeability. This information is shown in Table 3. It should be noted that the data for cores 48-3-1 and 2 is missing from the table. This is because they were damaged prior to making these measurements. Considering now the tabulated porosity values, it can be seen that in all cases core Number 2 deviates from the general trend exhibited by the others. This deviation is high in some cases and low in others which tends to eliminate any explanation as to the cause. A group consideration of the porosities of the other samples (#1, PSD and A) in each core indicate fairly good uniformity.

The average Klinkenberg air permeability as determined from cores 1 and A indicate a generally decreasing value as the bead sizes making up the core decrease. This, of course, is to be expected, since mixtures of smaller and smaller beads lead to smaller and smaller pores.

Based on the porosity and permeability measurements on samples 1 and A, along with the PSD sample, it is felt that the upper portion of the large cores display a reasonable uniformity. Since this portion of the core seems reasonably uniform, the assumption that the pore size distribution data obtained from the small sample is representative of sample 1 or A appears valid.

The high porosity range exhibited by the sand core resulted from the use of sand grains rather than beads in

TABLE 3

TABULATED DATA ON THE SYNTHETIC CORES

Core No.	Porosity, %	Klinkenberg k, md.	Avg. k, md.
35-1	12.82	149.0	
PSD. Sample	13.00		
35-A	13.32	107.5	128.2
35-2	12.07		
48-1	13.95	81.0	
PSD. Sample	13.90		
48-A	14.70	118.1	99.6
48-2	16.79		
65-1	14.90	60.1	
PSD. Sample	13.50		
65-A	16.40	99.0	79.6
65-2	12.00		
PSD. Sample	15.90		
48-3-A	16.70	55.5	55.5
65-3-1	12.35	24.0	
PSD. Sample	13.25		
65-3-A	13.69	46.0	35.0
65-3-2	16.61		
200-1	18.89	8.8	
PSD. Sample	16.67		
200-A	16.12	7.4	8.1
200-2	13.52	3.4	
65-S-1	22.81	25.0	
PSD. Sample	22.20		
65-S-A	21.35	25.5	25.2
65-S-2	20.06		

making the core. In this case, it is thought that the angularity and shape of the grains caused a large amount of bridging of the grains to occur.

CHAPTER IV

EXPERIMENTAL APPARATUS AND PROCEDURE

Pressure Equipment

The experimental equipment used in this study was the same as that used by Hilchie[20] with only a few modifications being incorporated. The only experimental change of any consequence was in the internal pressure system which was redesigned using a high pressure nitrogen supply to exert the internal pressure on the core rather than the handpump method used by Hilchie. This system was redesigned so that the pore volume changes occurring during the temperature change phase of the study might be estimated. A schematic diagram of both the internal and external pressure systems is shown in Figure 8.

The primary piece of equipment in this system is the high pressure autoclave in which the core was mounted and pressurized. The autoclave was designed by Hilchie to operate to a pressure of 15,000 psig. A schematic of this cell and internally mounted core is shown in Figure 9. The cell top is removable with the upper electrode being directly attached to the top. A hole through the electrode and cell top

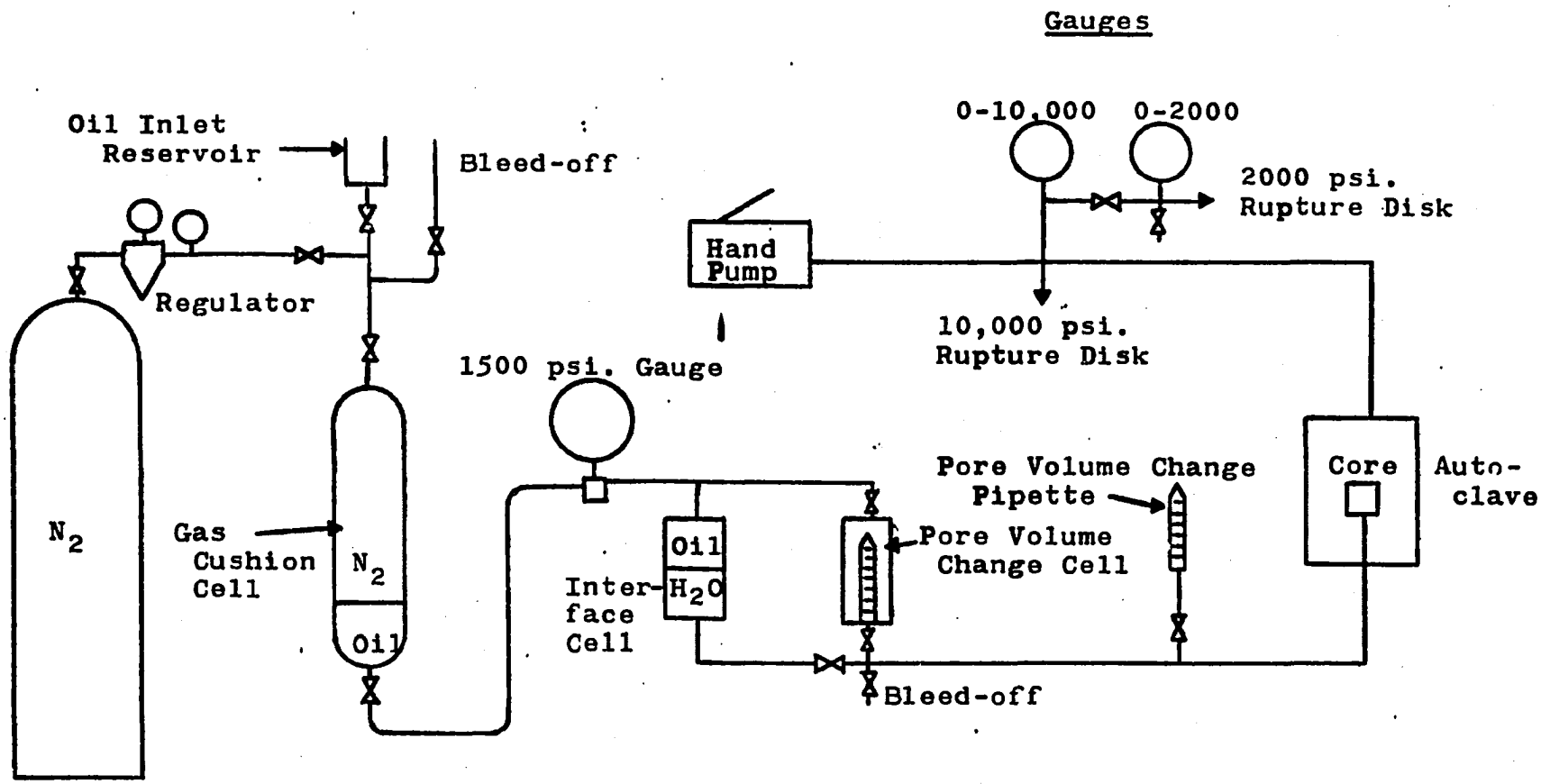

FIG. 8.--SCHEMATIC DIAGRAM OF PRESSURE CONTROL SYSTEM

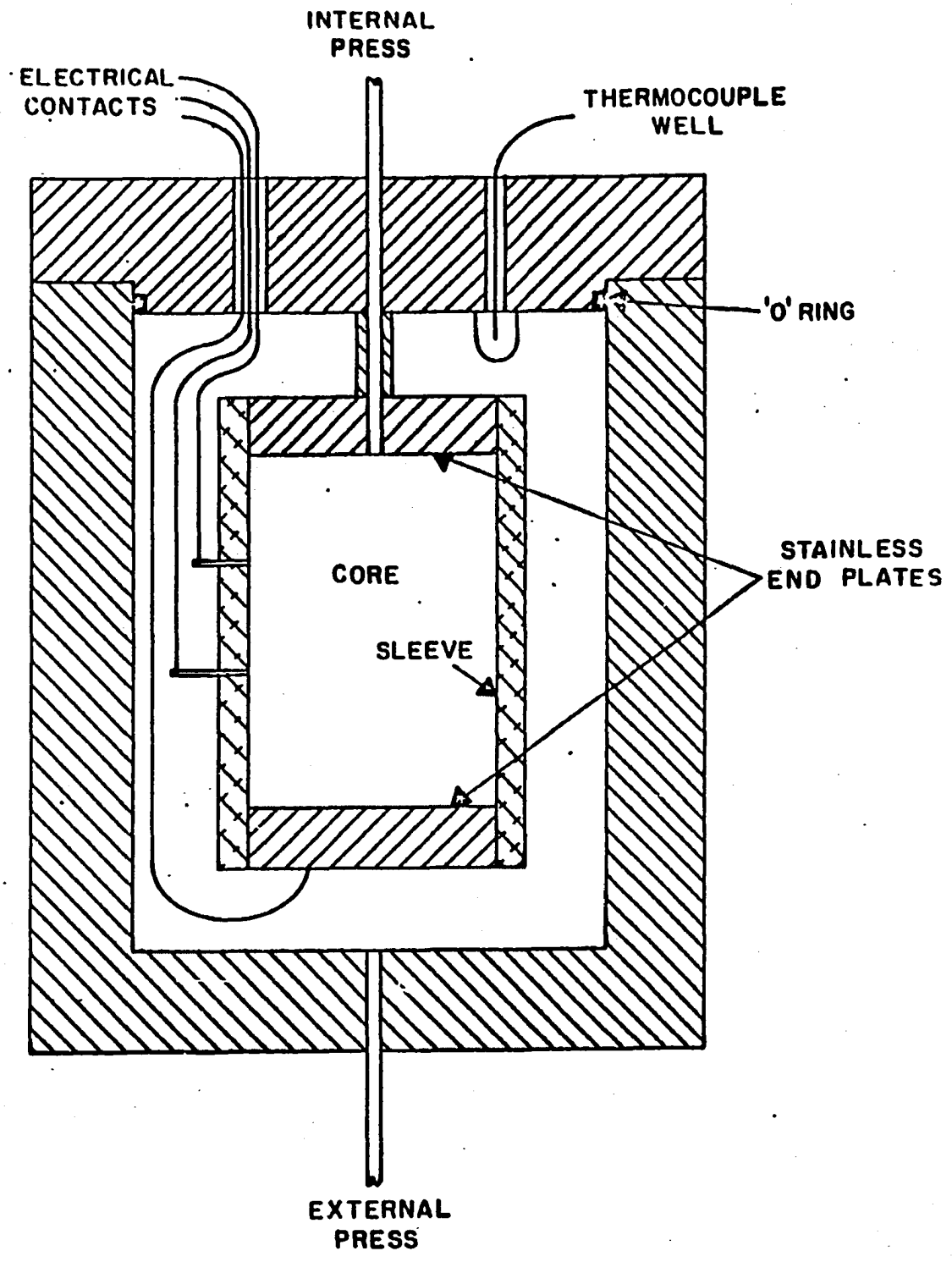

FIG. 9.--HIGH TEMPERATURE AND PRESSURE RESISTIVITY CELL (FROM HILCHIE[20])

connected the internal pressure system to the core.

The core was mounted in Hycar sleeves in both the pressure and temperature experiments. The potential measuring electrodes were placed parallel to the sleeve axis one inch apart. These electrodes were stainless steel (2/56) bolts in which the screw slots were silver soldered and then ground flat to approximately the original head thickness. Thin cadmium disks were placed between the core and the electrodes in order to provide a good electrical contact. The cadmium disks were fairly soft and malleable, thereby deforming to fit the core and filling up the voids between the core and the electrodes. This prevented the sleeve from extruding between the electrode and the core. Once the sleeve was mounted on the core and the cadmium disks were in place, the lower electrode was slipped into the sleeve and the hose clamp, holding the lower electrode in place, slightly tightened. Hose clamps were used to secure the sleeves tightly around the electrodes rather than the wire wound method which required soldering. The use of hose clamps allowed the mounting procedure to be done by one person. With the lower electrode in place, the whole assembly was then slipped onto the upper electrode. In this position, both hose clamps were securely tightened. The electrical connections were then made and their continuity checked before the top assembly was placed on the cell.

The external pressure system as shown in Figure 8

used a high pressure hand pump to pressurize the system. The pressure was transmitted to the annular portion of the autoclave with a high flash point transformer oil. The system also included two pressure gauges and a bleeder valve. A low pressure, 2000 psig., Foxboro gauge was used to measure the external pressure up to 2000 psig. and a 10,000 psig. Ashcroft gauge was used to measure the pressure from 2000 psig. to 10,000 psig. The gauges could be read to $\pm$ 5 psig. and $\pm$ 25 psig., respectively. Both gauges were calibrated with a dead weight tester. The maximum deviation over the complete pressure range of the Foxboro gauge was found to be less than $\pm$ 0.5%. The Ashcroft gauge was found to have an accuracy of $\pm$ 0.5% at 2000 psig. and $\pm$ 1.0% at 10,000 psig. The pressure measurements were therefore considered to be accurate within 1%. The bleed-off valve was used to regulate the internal pressure, primarily during the temperature phase of the study.

The internal pressure system, also shown in Figure 8, utilized three different fluids for operation. A high pressure nitrogen gas supply was used as the pressure source for applying an internal pressure. The gas pressure was transmitted to an oil system which in turn transmitted the pressure to the saline water. Oil was used to transmit the pressure to the saline water rather than the gas so that the water would not become contaminated by dissolved nitrogen. A fairly large "gas cushion" stainless steel cell approximately one-third full of oil was used as an interface cell for the nitrogen-oil. A sight gauge was used for the

oil-water interface cell.

During the pressure experiments (varying external pressure and atmospheric internal pressure) the entire internal pressure system was closed off from the cell except for the calibrated pipette used for measuring the pore volume change. The pipette had a volume of 0.2 ml. and pore volume changes of 0.0002 ml. could be read.

For the temperature phase of the study, this low pressure pore volume measuring system was closed off and a constant pressure of 1100 psig. was applied to the core. A 1500 psig. Crosby gauge was used to indicate this pressure. The gauge could be read to $\pm$ 5 psig. and was calibrated with a dead weight tester. The maximum deviation of this gauge over the pressure range from 1000 to 15000 psig. was $\pm$ 0.7%.

As mentioned previously, a high pressure pore volume change system was devised for measuring the pore volume change occurring during the temperature study. The system is similar to that used by Fatt[13] in measuring pore volume compressibilities of rocks while also under internal pressure. The system consisted of sealing a pipette into a bushing which is then screwed into the lower end of a sight gauge. A great deal of difficulty was encountered in obtaining a seal of this pipette in the bushing. Initially the pipette was sealed with an epoxy (not the same epoxy used in consolidating the cores) which, after three cores had been run, was found to have been leaking. This particular epoxy was slowly being

attacked by the salt water and, as a result, some of the water being expelled by the cores was collecting in the lower portion of the sight gauge and, therefore, not being measured in the pipette. The pipette was finally sealed securely in the bushing by initially cementing it in place with a mixture of litharge (PbO) and glycerol and then applying a second seal using the salt water resistant epoxy used for consolidating the cores.

When the internal pressure system was to be placed in operation, the high pressure pore volume measuring system was initially shut off by closing the valves above and below the sight gauge. A pressure of 1100 psig. was then applied by using the regulator on the high pressure nitrogen bottle. Once a pressure of 1100 psig. was attained in the system, the upper valve on the sight gauge was opened and the annular fluid around the pipette allowed to come to equilibrium with the system. Finally, the lower valve was opened and the entire system allowed to come to equilibrium. Once an equilibrium state was obtained, the valve above the gas cushion cell and the valve between the oil-water interface cell and core were closed. In this way, any volumetric change of the water in the internal system would be observed in the pipette. At the same time, the volumetric change being observed would actually displace the same amount of oil in the gas cushion cell. Since this volumetric change was so small in comparison to the volume of nitrogen in the cell, the system remained at

a constant pressure of 1100 psig. The bleed-off valve in the system was used to lower the water level in the pipette. A 0.2 ml. pipette was also used in this high pressure pore volume measuring system.

Temperature Equipment

Temperature control of the cell was achieved through the manual operation of two wire wound heaters cemented to the exterior of the cell. A 2500 watt, 220 volt, switch operated, heater was used for the primary increase in cell temperature. A 500 watt, 110 volt, Variac controlled, auxiliary heater was used primarily for fine temperature adjustments. For the initial temperature increase desired both heaters were used.

Temperature measurements were obtained with an iron-constantan thermocouple system. The equilibrium temperature recorded during the temperature phase of the study was measured with a thermocouple extending 1-1/2 inches below the cell top. A second thermocouple was placed below the cell as an aid in controlling the cell temperature. It was found by trial and error that when both heaters were on the desired temperature could be attained by shutting off the 2500 watt heater when the external thermocouple measured a temperature approximately 20° F. above the desired equilibrium temperature. At the same time, the 500 watt heater would be turned down low with the internal temperature then coasting to the

desired temperature.

Temperature measurements were performed with a Leeds and Northrup potentiometer and a Rubicon galvanometer. All potential measurements were made in comparison to a calibrated Eppley 103 standard cell. The thermocouples were calibrated against boiling point values of five different liquids covering the complete range of interest. The accuracy of the thermocouple measuring system was better than $\pm$ 0.5° F.

Electrical Measuring System

The resistivity measuring system was of the same design as that used by Hilchie and is diagramatically shown in Figure 10. The system is a convertible two to four electrode measuring system, although all resistivity measurements were made using the four electrode system. The four electrode system eliminates the contact resistances associated with the current electrodes which are also the potential electrodes of the two electrode system. Placement of the potential measuring electrodes away from the current electrodes allows the current density in the core to be essentially uniform.

The circuit consisted of a 0-110 volt Variac, 500 ohm potentiometer, milliammeter, and precision resistor all in series with the core. A variable voltage 60 cycle current was passed through this circuit. The vacuum tube voltmeter (VTVM) was adjusted for full scale meter deflection when

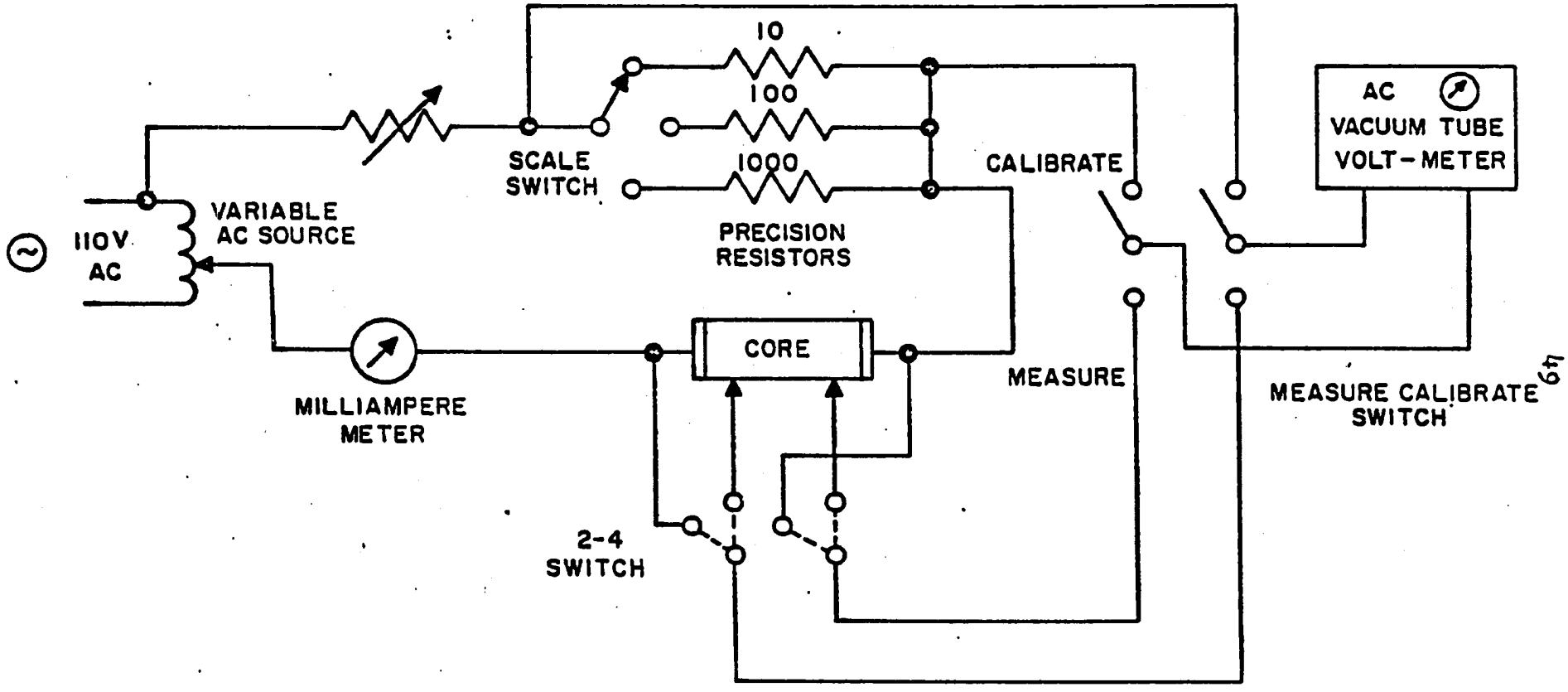

FIG. 10.--SCHEMATIC OF RESISTIVITY MEASURING SYSTEM (FROM HILCHIE[20])

placed across a precision resistor. When full scale deflection was obtained, the VTVM was placed across the core. With a constant current flow in the circuit, the resistance of the core was determined by simply multiplying the percent deflection of the VTVM by the resistance of the precision resistor. The precision resistors had an accuracy of $\pm$ 1%. Since a calibration was performed for each measurement, changes in lead resistance (due to changes of temperature in the cell) did not affect the measurements.

The VTVM used in this study was a Hewlet-Packard 400-H. The internal resistance of this VTVM is 0.5 megohms and, therefore, the current required for the instrument is extremely low and, for all practical purposes, did not disturb the current flow in the core.

Saline Water

The saline water used in saturating these cores was prepared from distilled water and 99.9 percent pure sodium chloride crystals. The resistivity of the water was measured in a Jersey resistivity cell as described by Lynn.[22] It was found to have a resistivity of 0.0778 ohmmeters at 72° F. or a salt concentration of approximately 97,000 PPM.

Saturating Procedure

It was found that the clean, dry, synthetic cores would imbibe the saline water at atmospheric conditions although the process was very slow. A saturating system was

built, as schematically shown in Figure 11. The core was saturated under vacuum and subsequently pressured to 500 psig. In operation, the clean dry core to be saturated was placed in the pressure cell and evacuated. Once a vacuum had been pulled on the core, the valve to the vacuum pump was closed and the valve below the sight gauge opened, allowing the saline water to enter the cell and core. After the system was full of water, a pressure of 500 psig. was applied overnight to the cell.

The saturated core was then removed from the saturating system and mounted in the autoclave. At this point the core was not subjected to resistivity measurements but only stressed up to an external pressure of 10,000 psig. After the core was pre-stressed, it was again placed in the pressure cell of the saturating equipment and the cell filled with saline water. A pressure of 500 psig. was then applied for a period of at least one hour after which it was allowed to slowly bleed off. The core was then removed and placed in a closed container filled with saline water. A period of at least twelve hours was allowed after the pressurizing process before any one of the cores was used in the resistivity cell in order that equilibrium conditions in the core would be assured.

Auxiliary Core Measurements

Core porosities were measured in a Boyles Law porosimeter designed to handle large cores of this size. All

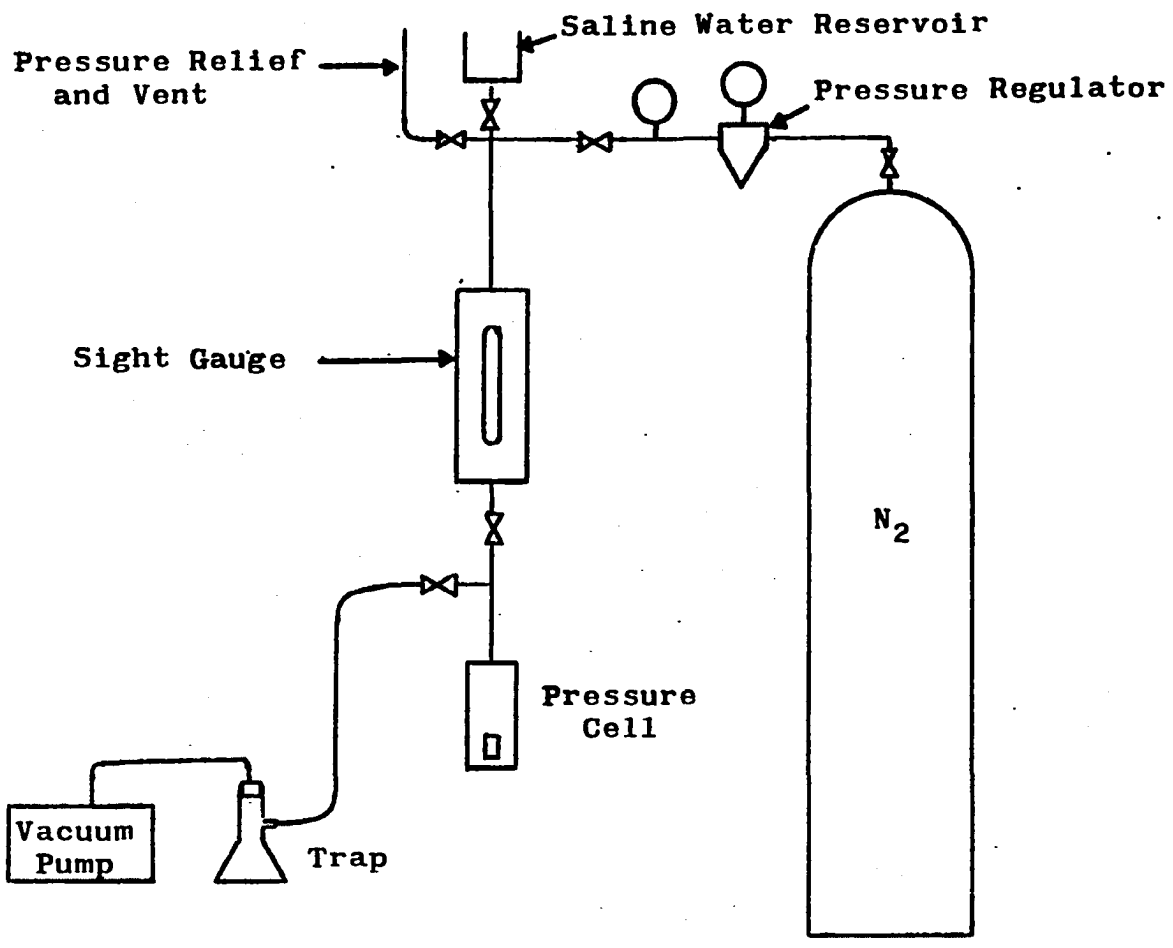

FIG. 11.--SCHEMATIC DIAGRAM OF SATURATING SYSTEM

permeability values referred to in this study are "Klinkenberg" air permeabilities and were measured in an air permeameter. For each core, at least five data points were obtained in order that a "Klinkenberg" type plot could be made.

The mercury injection pore size distribution data were determined by the Pan American Research Laboratory in Tulsa, Oklahoma. These measurements were made on small samples taken from the large core as indicated in Chapter III.

Experimental Approach

The experimental portion of the study consisted of two phases. In the first phase, the sample resistivity was measured at increasing increments of external pressure. The changes in pore volume, occurring during these pressure increases, were also recorded. The internal pressure of the core was atmospheric while the temperature remained essentially constant at room temperature. During this phase, the net pressure on the core was increased from 0 to 100, 200, 400, 800, 1200, 2000, 3000, 4000, 6000, 8000 and 10,000 psi. Initial net pressure increments of less importance between 0 and 100 psi. were also made. These steps were included due to the large initial compressibility of the synthetic cores. With the synthetic cores, the resistivity usually reached equilibrium within 30 minutes and the pore volume generally reached equilibrium between 30 minutes and one hour. This shorter length of time to reach equilibrium, as opposed to the time required by

Hilchie[20] when using natural cores, is probably due to the simpler pore geometry and the type of core material used.

The second experimental phase consisted of measuring the sample resistivity at increasing increments of temperature while at a constant net stress. The core was externally pressured to 2100 psig., while an internal pressure of 1100 psig. was being maintained. This net stress is the same as that used by Hilchie.[20] After an initial equilibrium was reached at a net stress of 1000 psi., the temperature was raised at increments of approximately 40° F. to a maximum of about 320° F.

An attempt was also made to obtain pore volume change data during these temperature runs but numerous problems were encountered and the data collected are not complete.

CHAPTER V

EXPERIMENTAL RESULTS AND ANALYSIS

Basic Core Data

Properties of the seven different cores studied are shown in Table 4. The porosities of the six bead cores all fall in a small range between 12.82 percent to 16.70 percent with the average being 14.82 percent. The ideal situation, of course, would have been to have cores with exactly the same porosity and different pore sizes. Of the two cores (either number 1 or A) which could have been used, these particular cores were chosen due to their similar porosity with respect to that of the sample used for the PSD measurements. The one exception to this is core number 48-A which was not the original sample chosen. Core number 48-1 was originally intended for use but was ruined in the resistivity cell. (The hose clamps were not tight enough and the core was damaged by the transformer oil.)

The tabulated air permeability values shown for these cores were obtained from Klinkenberg type permeability graphs. The Klinkenberg graphs for these cores are presented in Figure 28 in Appendix A.

TABLE 4

TABULATED PROPERTIES OF THE SYNTHETIC CORES STUDIED

Core No.	ϕ	k, md	Calculated Surface Area, cm^{-1}
35-1	12.82	149.0	10,987
48-A	14.70	118.1	7,693
65-1	14.90	60.1	9,565
48-3-A	16.70	55.5	16,011
65-3-A	13.69	46.0	11,214
200-2	13.52	3.4	22,206
200-A	16.12	7.4	26,484.8
65-S-A	21.35	25.5	24,373.7

Mercury injection data obtained from the small samples are presented in essentially three different forms. The original data as determined by Pan American Research Laboratory are presented as a mercury injection capillary pressure curve in which the mercury injection pressure is plotted versus the percent of pore volume saturated by mercury.

The capillary pressure data can be readily converted into pore size distribution data by using the capillary pressure expression in terms of surface forces.[30] This expression which represents the minimum capillary pressure required to inject a non-wetting fluid into a capillary tube of radius, r is given by

$$P_c = \frac{2\sigma \cos\theta}{r} \qquad (7)$$

where: P_c = capillary pressure, atm.

r = capillary tube radius, microns

σ = interfacial tension, dynes/cm

θ = contact angle

Purcell[31] assumed the contact angle for mercury was 140° and the interfacial tension of mercury was 480 dynes/cm. Using these values and converting capillary pressure into psia., the equation reduces to:

$$r = \frac{107}{P_c} \qquad (8)$$

The pore size distribution obtained using the above equation is presented as bar graphs in Appendix A. These

graphs show that in most cases the core will have one predominant pore size. This is not particularly true, however, with cores 35-1 or 65-S-A. Core number 35-1 has pores covering the complete range with even a larger number of small pores than most of the cores made of smaller beads. This core was made of the largest bead size used and theoretically should consist of the fewest small sized pores. This indicates that the larger pores, when completely filled with epoxy-solvent solution, were of such volume that a secondary porosity was formed consisting of small blow holes in the epoxy itself. Based on this, it appears that the pore size is not strictly controlled in this consolidating technique until bead sizes are at least 48 mesh.

Core number 65-S-A also has pore sizes covering the entire range with no particular predominant pore size. It also has a large number of small pores. Here again it is felt that this large number of small pores is due to the secondary type porosity formed by small blow holes in the epoxy filling the large pores formed by particle bridging. One thing that can be deduced from these data and the air permeability data is that the pores in this sand sample are poorly interconnected. One would expect that, with the large number of larger pores, as compared with the other cores, this sand core would have a high permeability. This is not the case, however, since the permeability is 25.5 md. As can be seen from Figure 28 in Appendix A, the slope of the

Klinkenberg plot is also much greater than those of the other cores. These factors, coupled with the fact that the m value (cementation factor) is quite high, leads to the conclusion that interconnection of the pores in the sand core is not nearly as good as it is in the bead cores.

The third method of presenting the mercury injection data is essentially an extension of the pore size distribution data. It consists of calculating a pseudo or theoretical surface area from the distribution data assuming that all the pores are straight tubes. This concept can be simply developed as follows:

$$\text{Surface Area} = 2\pi r L \tag{9}$$

$$\text{Pore Volume} = PV = \pi r^2 L \tag{10}$$

or:

$$L = \frac{PV}{\pi r^2} \tag{11}$$

Substituting 11 into 9 we find:

$$\text{Surface Area} = \frac{2(PV)}{r} \tag{12}$$

Naturally, the numerical values obtained are hypothetical in nature but they do provide a guideline for comparing cores. Essentially, what is being accomplished is placing a numerical value on the entire pore size distribution graph. The theoretically calculated surface areas for the cores studied are shown in Appendix A.

Pressure Data

The resistivity data obtained, for all the synthetic

cores studied, indicate a significant increase in resistivity with an increase in net pressure. These basic data are graphically presented in Figure 12 where the relative formation resistivity factor is plotted versus net pressure. The relative formation resistivity factor is the ratio of the formation resistivity factor at a net pressure (F^P) to the formation resistivity factor at atmospheric pressure (F).

A high initial pore volume change was also observed to occur, as indicated in the compressibility tables in Appendix A. The compressibility in these synthetic cores was initially greater than observed in natural cores but after the first 200-400 psi. of net pressure they displayed a substantially similar range of compressibilities as that displayed by natural rocks. The variation in compressibility with net pressure for these synthetic samples is shown in Figure 13. In general, all the cores show a similar compressibility-pressure curve with all the curves tending to lie in the same range as shown by the cross-hatched area.

The relationship between relative formation resistivity factor and compressibility is graphically shown in Figure 14. These data, which confirm that for natural cores, do not indicate any particular pattern of behavior. This is probably due to the fact that compressibility in itself is a macroscopic parameter that does not necessarily reflect the microscopic manner in which the media is being compressed. In other words, it indicates that the media is being reduced

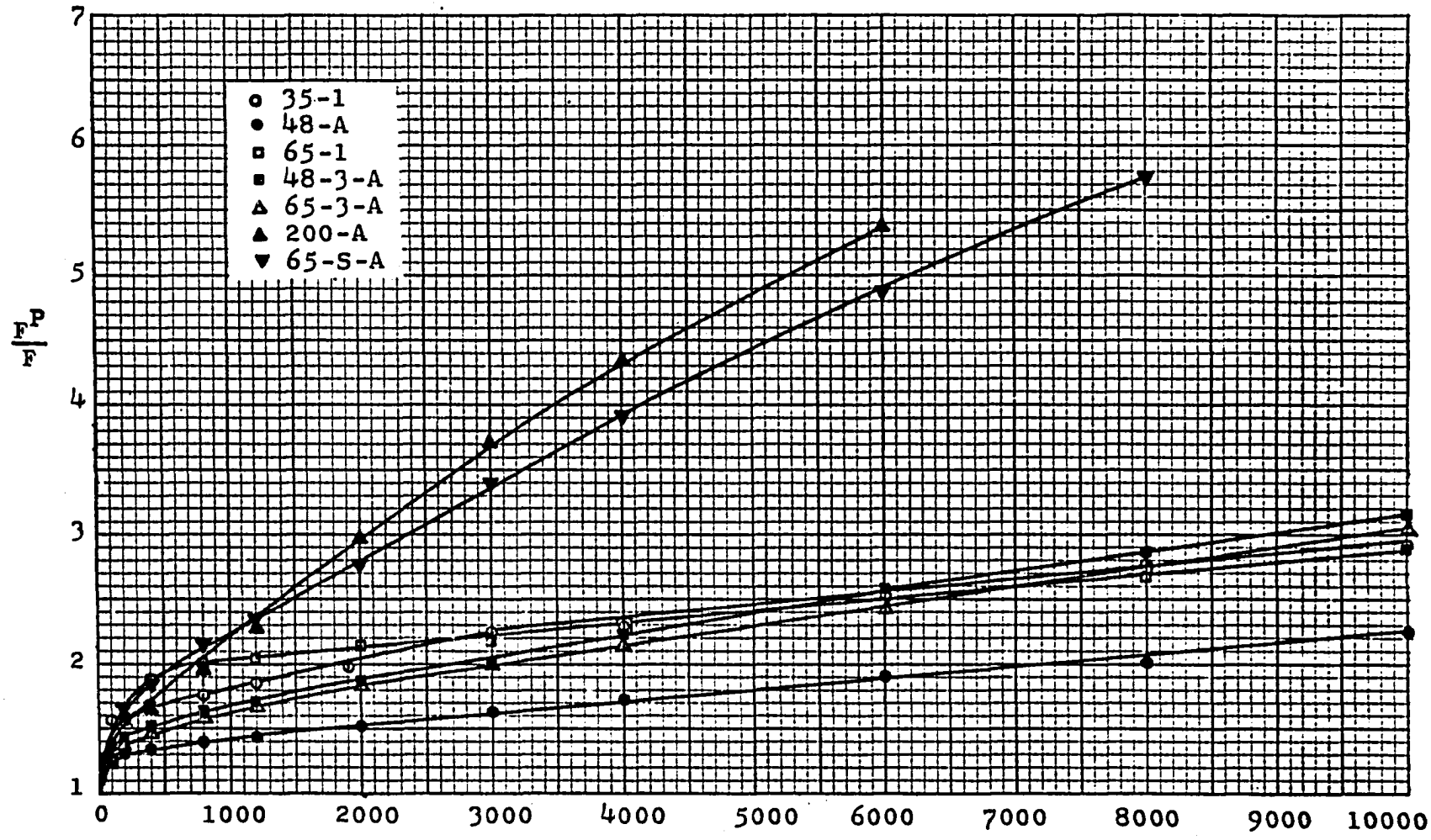

FIG. 12.--RELATIVE FORMATION RESISTIVITY FACTOR VS. PRESSURE

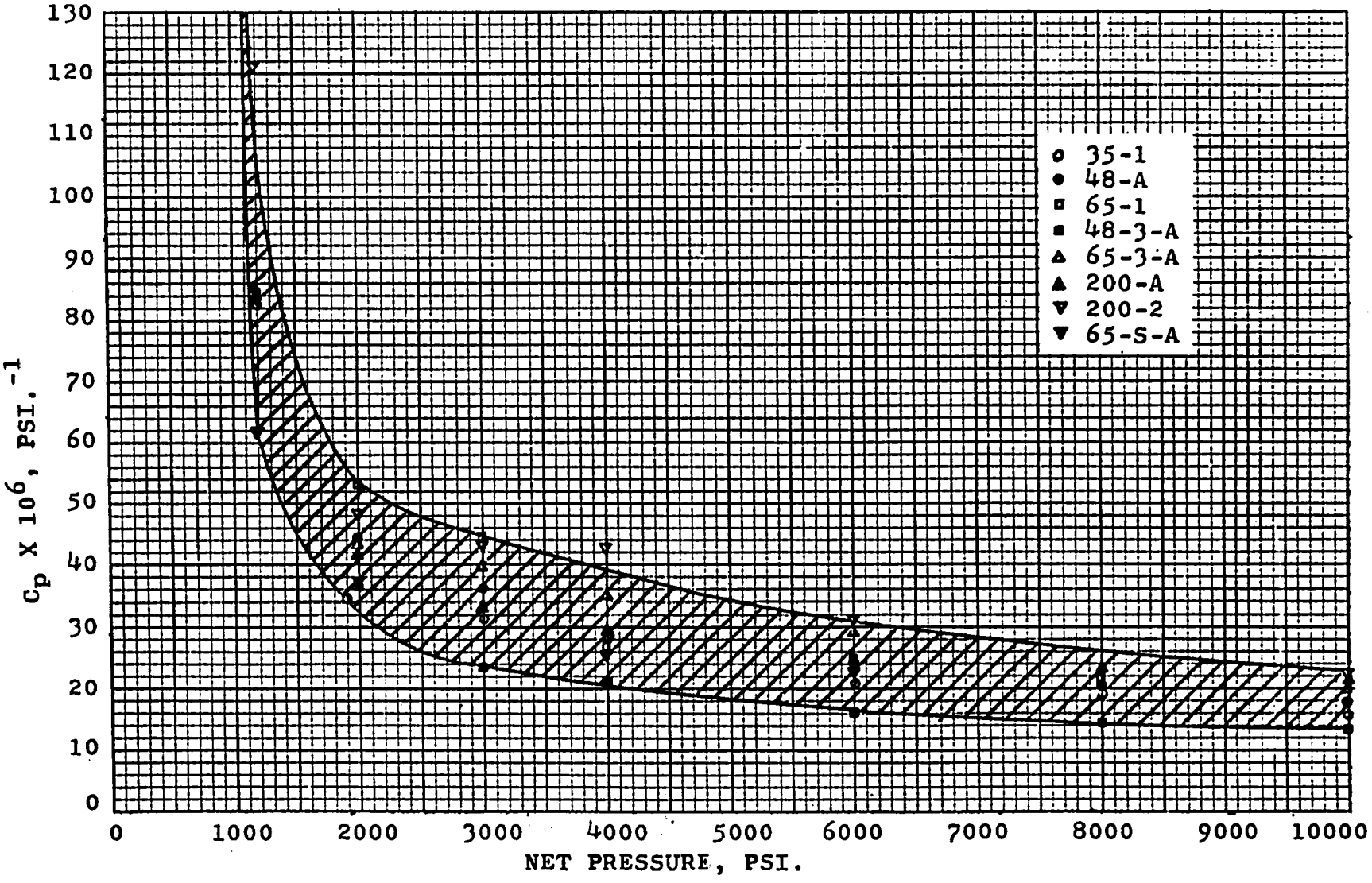

FIG. 13.--PORE VOL. COMPRESSIBILITY VS. NET PRESSURE

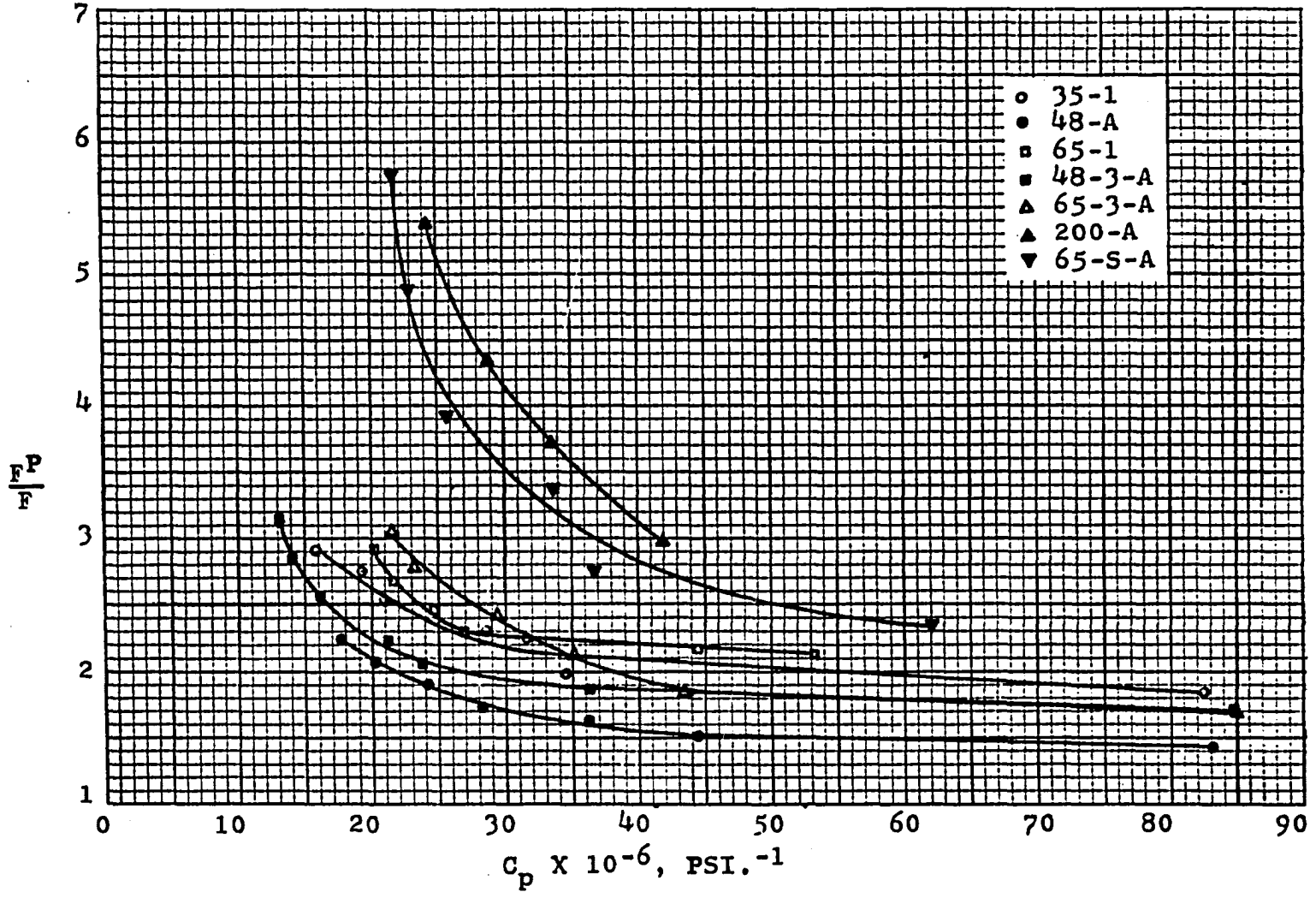

FIG. 14.--RELATIVE FORMATION RESISTIVITY FACTOR VS. PORE COMPRESSIBILITY

in volume but it does not indicate in what manner this reduction is occurring. For example, it would be possible for two porous materials having the same pore geometry and compressibility to compress in a completely different manner on a microscopic basis. In one, the pore volume change might be occurring primarily in the larger pores, whereas, with the other, the bulk of the pore volume change could be in the smaller pores. This is indicated in this study. All of the cores were similar in materials used, porosity, and compressibility and, yet, the change in relative formation resistivity factor cannot be specifically related to compressibility. Or, as taken from Hilchie's paper, "as compressibility is a function of pore volume change and resistivity is more than just that, the intercorrelation (between relative formation resistivity factor and compressibility) is not a logical place to start." The microscopic aspect of pore volume change which is essentially "masked" in the compressibility parameter is, therefore, felt to be a necessary part of any correlation concerning resistivity behavior in a porous media under pressure.

As indicated by Figure 12, there is a rapid initial change in resistivity which is due primarily to the large initial compressibility of these synthetic cores. After the high initial changes in resistivity and pore volume, the rate of change occurring in these two parameters diminishes considerably. It can also be seen that the rate of change

in relative formation resistivity factor above 400 psi. are to some extent different for the different cores. Based on this figure, however, there appears to be no definite relationship.

A careful analysis of this data, on the other hand, seems to indicate that the large initial changes in resistivity and pore volume are tending to mask the overall picture. In order to eliminate this effect, it was decided to refer all of the resistivity data above 400 psi. to the same reference point. Elimination of the effect of pressure below 400 psi. is accomplished simply by subtracting the relative formation resistivity factor at 400 psi. from the value observed at net pressure P. The change in the relative formation resistivity factor occurring above 400 psi. for each core can then be observed in relation to the change in this property above 400 psi. for the other cores. The results obtained from this analysis, shown in Figure 15, are rather dramatic.

Surface Area Relationship

A distinct relationship is apparent between the total change and also the rate of change in the relative formation resistivity factor above 400 psi. and the surface area theoretically calculated for the core. Some relationship such as this was, of course, anticipated from Hilchie's study since he noticed a relationship existing between the relative

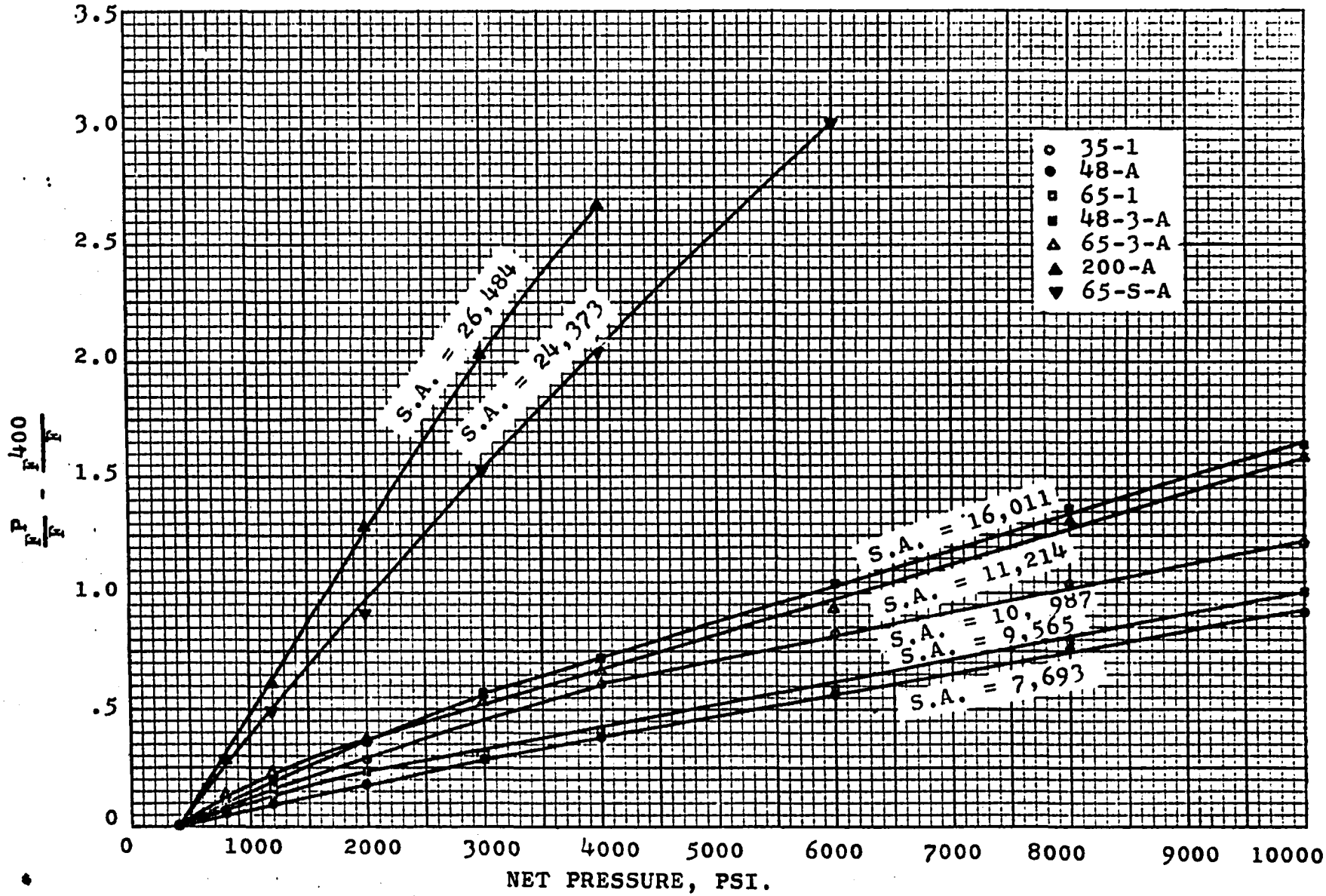

FIG. 15.--CHANGE OCCURRING IN RELATIVE RESISTIVITY RATIO ABOVE 400 PSI.

formation resistivity factor and the number of small pores below 0.5 microns. In this study, however, a relationship between the total number of small pores below .5 microns did not appear to be the answer in itself. This led to the use of a more comprehensive correlating parameter, namely surface area. In this way, rather than consider only the very small pores, a more general parameter is used which will consider, in essence, the relative effect of all the pores. The influence of the small pores on this parameter is, however, the most important single factor, although the contribution of the whole pore range is included.

A uniform difference in the relative formation resistivity factor with surface area is not apparent but this is due to the inherent inaccuracy in determining the surface area. For example, if a higher degree of accuracy were available, the surface area of core 48-3-A might be found to be 12,000 cm^2/cm^3, rather than the calculated value of 16,011 cm^2/cm^3. This analysis, therefore, precludes any quantitative analysis, but rather only permits a qualitative study. The important factor which should be pointed out here is that the theoretical surface area calculated for all of the synthetic cores was calculated in exactly the same manner. Therefore, the surface area values used, no matter as to how non-representative they might be, are at least relative. In this way, it is felt that the relative relation of each core with

respect to their actual surface area has been accomplished.

One interesting observation which can be made with regard to the data presented in Figure 15 is the large increase in relative formation resistivity factor which occurs in the cores having a calculated surface area greater than 16,000 cm^2/cm^3. This indicates that there is possibly a critical surface area above which the increase in relative formation resistivity factor is magnified.

The significance of sample 65-S-A should be pointed out. This particular sample was fabricated from sand rather than the beads in order to provide an insight into the effect of a different material. It has a much higher porosity along with a low permeability. Also, the pore size distribution does not indicate a preferential pore size and yet, with all these differences, the change occurring in the relative formation resistivity factor with pressure fits extremely well the general relationship observed with respect to surface area. On the other hand, a distinct influence of material on the change in relative formation resistivity factor due to temperature was noted, as expected, and will be discussed later.

Theoretical surface area calculations were made on the five natural cores run by Hilchie. These calculations

are based on the pore size distribution curves presented for these cores. The pore size distribution calculations which were subsequently made from this data, are presented in Appendix C. One difference in calculating these surface areas with respect to those calculated for the synthetic cores is to be noted. When calculating the surface area of the synthetic cores, the same incremental radii were used in all cases for the purpose of consistency. This was not possible, however, when using the pore size distribution curves for the natural cores. For example, the pore size distribution for these cores was represented incrementally below 1.0 micron to varying degrees. Therefore, surface area calculations were made over different intervals below 1.0 micron, depending on the increments chosen by the author. The definition of very small increments as shown for the Dean sand and the Paradox limestone are, however, of critical importance since the bulk of their pores is in the pore size range below 1.0 micron. Two minor discrepancies in this data were noted when comparing these graphical results with respect to the pore size information tabulated in Table III, page 52, of Hilchie's work. The table indicates that the Briar Hill sample has 18 percent of its pore volume less than 0.5 microns with a total volume of 23 percent below 1.0 micron. The pore size distribution curve, however, indicates 18 percent of the pore volume is below 1.0 micron. The tabulated values were used in this case. It was also noted in the table that the

Bandera sand should have 31 percent of its pore volume below .5 microns, whereas the graph indicates 32 percent. The capillary pressure curve would have been useful in relieving this difference. The graphical analysis of 32 percent was used with all the pores below 0.3 microns being weighted the same. As can be seen in Figure 16, the relative formation resistivity factor also increases with the calculated values of surface area. It must be pointed out again that these are not absolute values of surface areas but only "pseudo" values as calculated from pore size distribution data. These calculations on the natural cores, although not as applicable as to the simpler geometry of the synthetic cores, can still be used as a guide. In any case, the utility of the surface area concept as a characterizing parameter is apparent even though it is not an absolute value.

Influence of Sample Character

A close examination of Figure 12 also reveals another interesting aspect worthy of additional evaluation. As can be seen, the rates of change in the relative formation resistivity factors of these cores are similar on a group basis. In other words, at sufficiently high pressures (approximately 3000 psi. for core 35-1) the slopes of the curves for 48-A, 65-1 and 35-1 are essentially the same while the slopes of 48-3-A and 65-3-A are similar. This immediately recalls the bead combination utilized in preparing the unconsolidated

FIG. 16.--THE EFFECT OF OVERBURDEN PRESSURE ON ROCK RESISTIVITY (FROM HILCHIE[20])

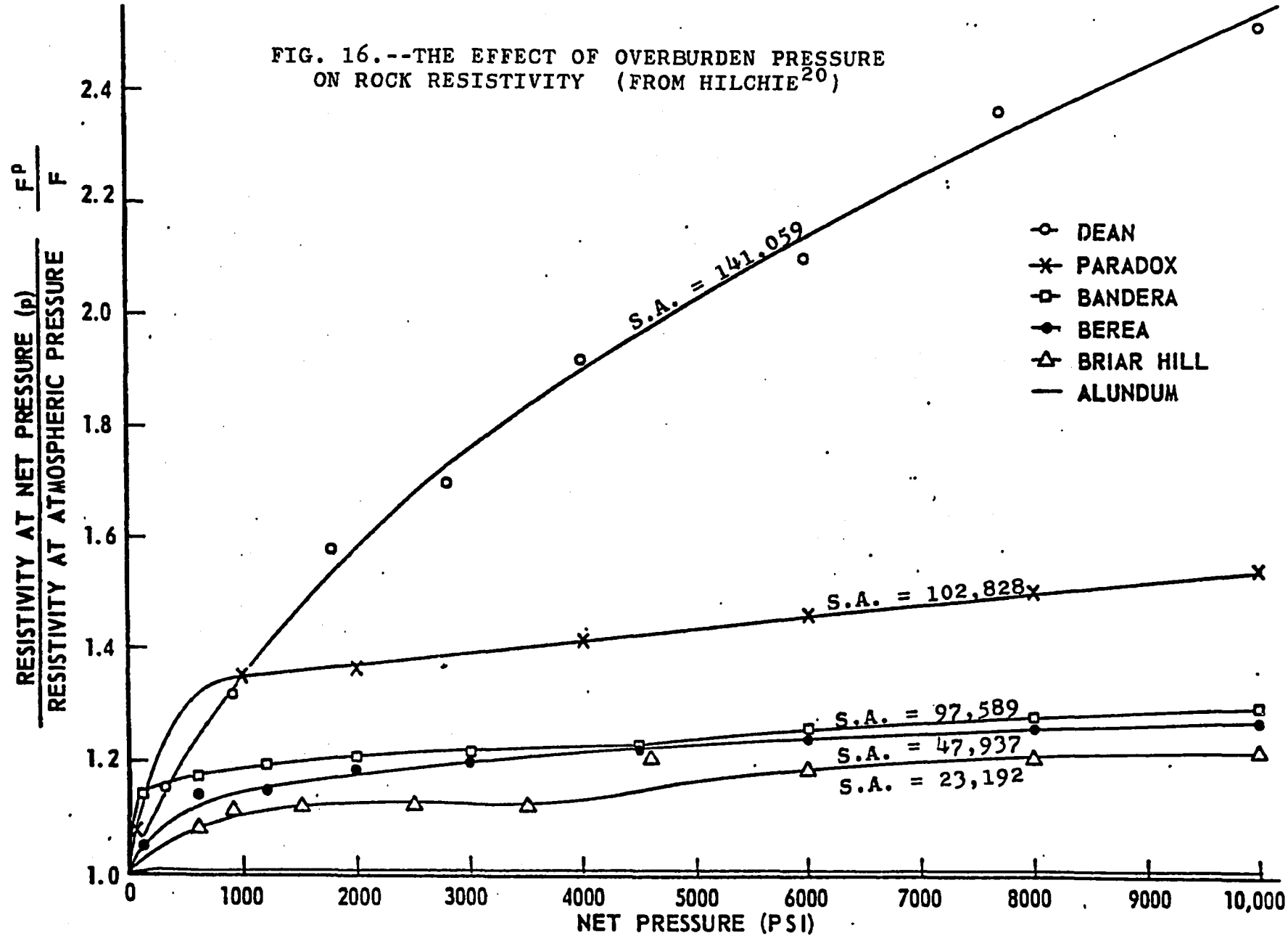

packs and suggests the influence of the matrix arrangement. As previously discussed, the synthetic cores were made with varying bead combinations and size ratios. The first three cores mentioned here (48-A, 65-1 and 35-1) all consisted of two bead sizes in which the ratio of the sizes was about 0.2. Pack design of these three was almost exactly the same and, therefore, can be considered for purposes of this discussion, as Group I. The two cores (48-3-A and 65-3-A) are different in pack design from those in Group I. These two contain three different bead sizes and can be considered as Group II with Group III being the sample containing the two small beads where the ratio between the two is high (number 200 cores). The similarity of slopes in each group indicates that the character of the matrix is also an important parameter. This character appears to be the determining factor as to how the structure reacts under pressure. Specifically, how the grains are deformed and shift, how the pores are decreased in size and close, and where and how the grains are in contact with other grains, to name a few. This has been pointed out by Hilchie, who noted that the slopes of the sands (Briar Hill, Berea and Bandera) were similar with the limestone (Paradox) and shaly sand (Dean) being different. These natural cores could then be labelled Groups I, II, and III, respectively. A separation of natural rocks into one of these three groups with respect to matrix character is, therefore, deemed an essential step in evaluating the effects

of pressure on the relative formation resistivity factor.

The similar relationship of the curves of the groups formed with the synthetic cores and those groups comprising the natural cores is striking. The greater magnitude of the relative formation resistivity ratio in the synthetic cores is probably associated with the larger total pore volume change which in turn would emphasize the mechanisms influencing this change. Both of these sets of data tend to support the generality that rocks with a similar matrix character (lithology) would tend to have similar rates of change of relative formation resistivity factor with pressure, with the magnitude of this change in each group being a function of the surface area.

Comparison of Similar Cores

Two of the number 200 cores were run under both pressure and temperature influences. It was originally decided to run core number 200-2 for these data since its low permeability was felt indicative of what might be considered a lower limit in the construction of a core having very small pores. Due to the very large change in the relative formation resistivity factor data it was deemed necessary to validate the results obtained with this core. Core number 200-A was used for this verification and the same general change was observed with the variation being slightly less for sample 200-A. Good agreement was obtained with the results being presented in Figure 17. A problem arose as to the surface area of these cores.

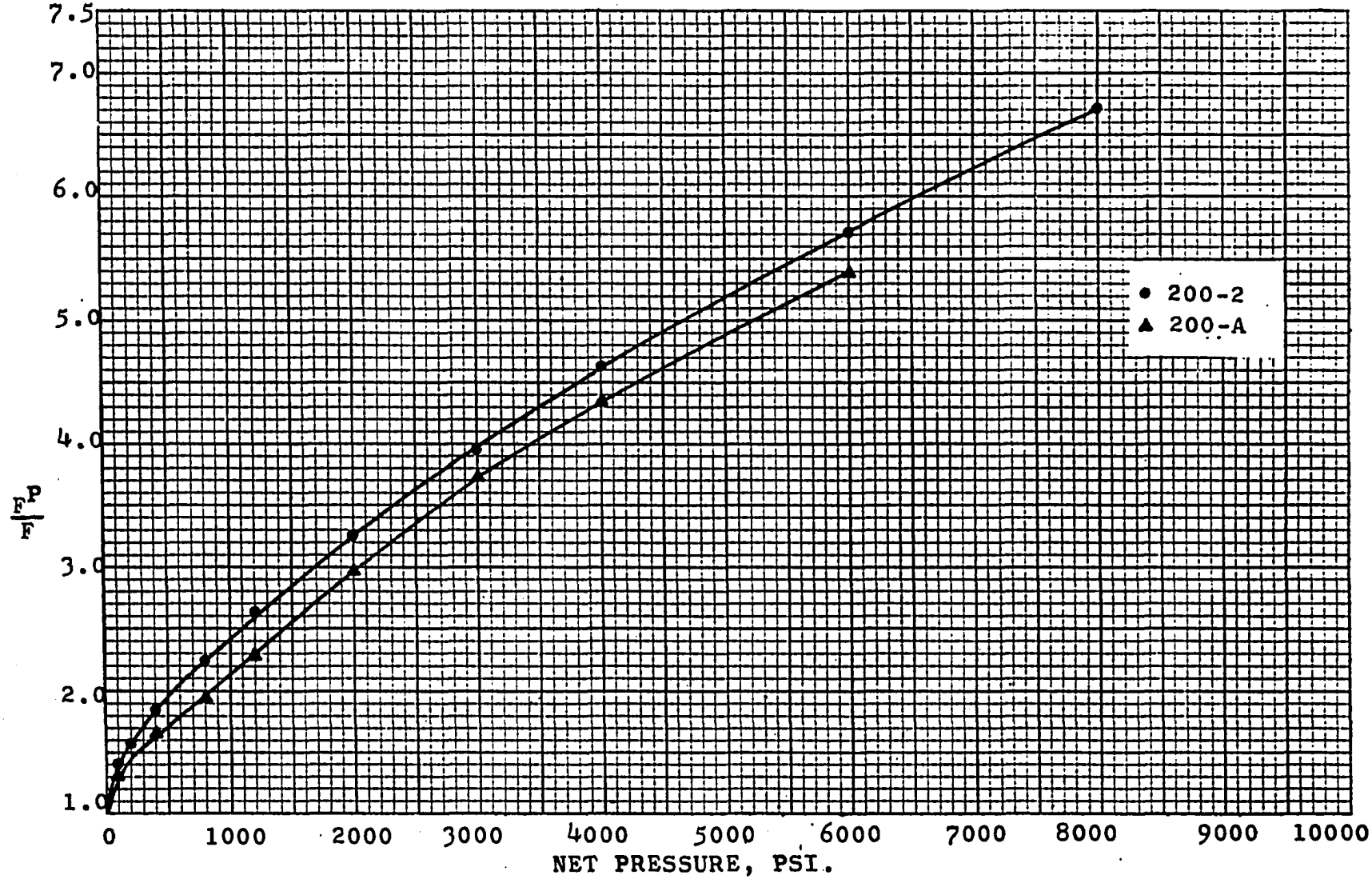

FIG. 17.--RELATIVE FORMATION RESISTIVITY FACTOR VS. NET PRESSURE (COMPARISON RUNS)

Since only one pore size distribution curve was available for these number 200 cores, only one theoretical surface area per unit pore volume value was calculated. Using this value on each core would naturally result in a higher "pseudo" surface area being assigned to the higher porosity core. This was resolved by assuming that the original pore size distribution data would be more nearly representative of core 200-A than of 200-2. Actually, this choice was not necessarily an assumption but a rather necessary decision. As previously stated, the mercury injection plug was obtained from between cores numbered 1 and A and, therefore, the mercury injection test was performed on a sample having a greater proximity to 200-A than to 200-2. Also, as pointed out in Table 5, the $\Delta\phi$ value between the mercury injection plug and core 200-2 is large with respect to that obtained with 200-A. In fact, all the mercury injection samples represented the cores studied very well, porosity wise. Therefore, the results obtained with core 200-A are considered the basic data with the results of core 200-2 being merely included as a verification-type run with no "pseudo" surface area value being assigned to it.

Evaluation of Cementation Factor

A knowledge of the pore volume change and resistivity variation occurring at each incremental step in pressure also allows an evaluation to be made of the variation in cementation factor, m, defined in Archie's equation, $F = \phi^{-m}$. This

TABLE 5

COMPARISON OF SAMPLE AND PORE SIZE DISTRIBUTION PLUG POROSITIES

Core Number	Core Porosity	Porosity of Plug Used in Mercury Injection Test	$\Delta\phi$ (Core ϕ - Plug ϕ)
35-1	12.82	13.0	-0.18
48-A	14.70	13.9	+0.80
65-1	14.90	13.5	+1.40
48-3-A	16.70	15.9	+0.80
65-3-A	13.69	13.25	+0.44
200-A	16.12	16.67	-0.55
65-S-A	21.35	22.20	-0.85
200-2	13.52	16.67	-3.12

change in cementation factor is illustrated in Figure 18. All of the cores exhibit essentially the same behavior - an initial, large decrease in Δm after which Δm is found to increase. This increase in Δm is found to be systematic if the initial pressure effects are eliminated by referring the change of Δm occurring in all the cores to a common reference point at a higher net pressure. This was accomplished by relating all the changes in cementation factor at a net pressure of 1200 psi. This change in cementation factor above 1200 psi. ($\Delta m = m^{P} - m^{1200}$) is shown in Figure 19. The overall trend of this data indicates a generally increasing change in Δm with increasing surface area of the core. Core number 65-1 appears to be an exception with an increase in Δm not being observed until the net pressure reached 3000 psi.

One interesting point about these data is that the changes in cementation factor for the cores having low surface areas was small, but as the surface area increased, these changes became quite large. In fact, it appears that for a synthetic core exhibiting a surface area of 16,000 cm^2/cm^3 or more, a significant change in cementation factor above 1200 psi. could be expected. Once again it appears that a critical surface area is reached beyond which the change exhibited in this parameter, m, becomes quite large.

Relationship of Surface Area with Pore Structure Change

It has been noted in previous work[12, 20] that the

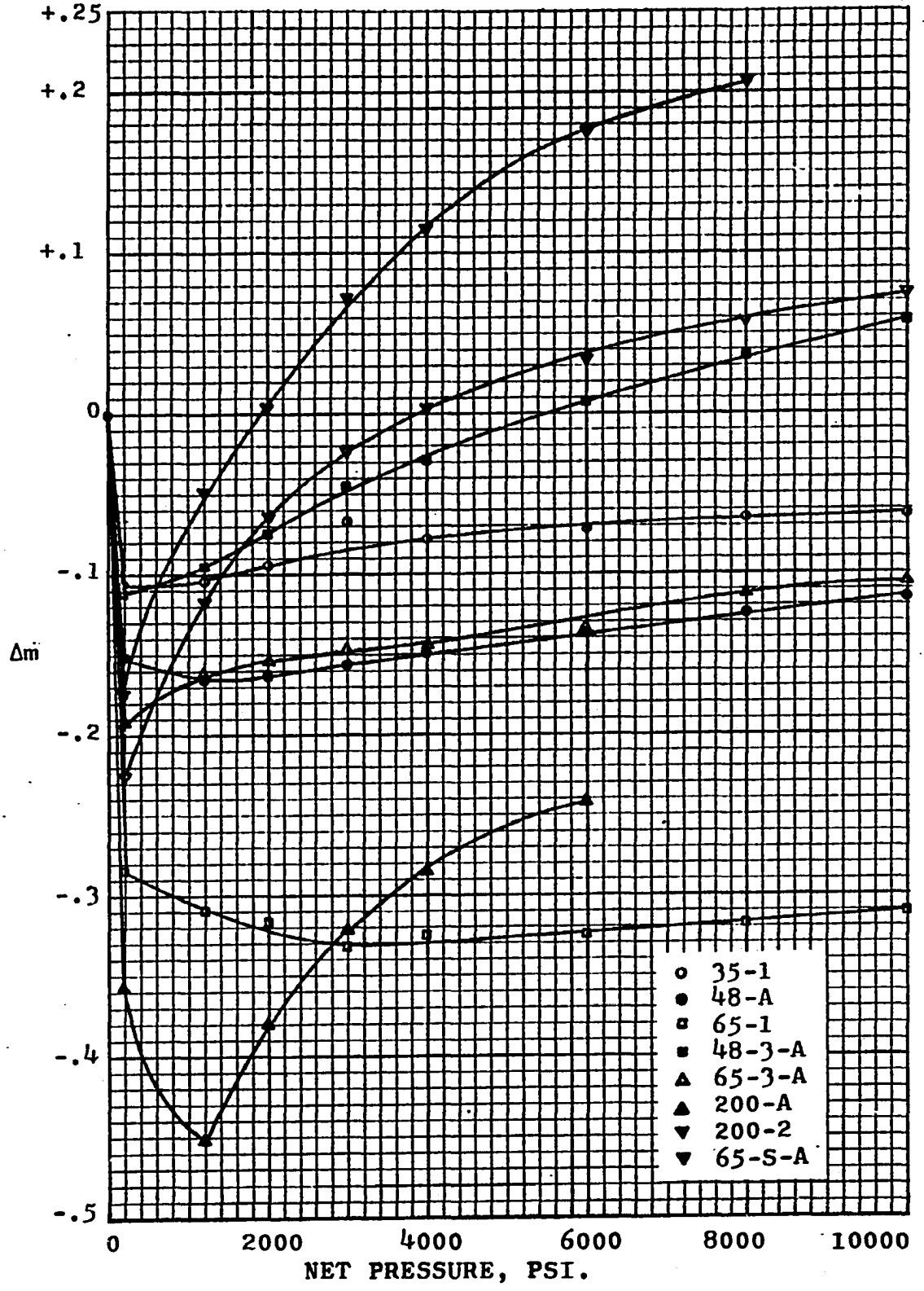

FIG. 18.--CHANGE IN m ($F = \phi^{-m}$) WITH NET PRESSURE ON SYNTHETIC CORES

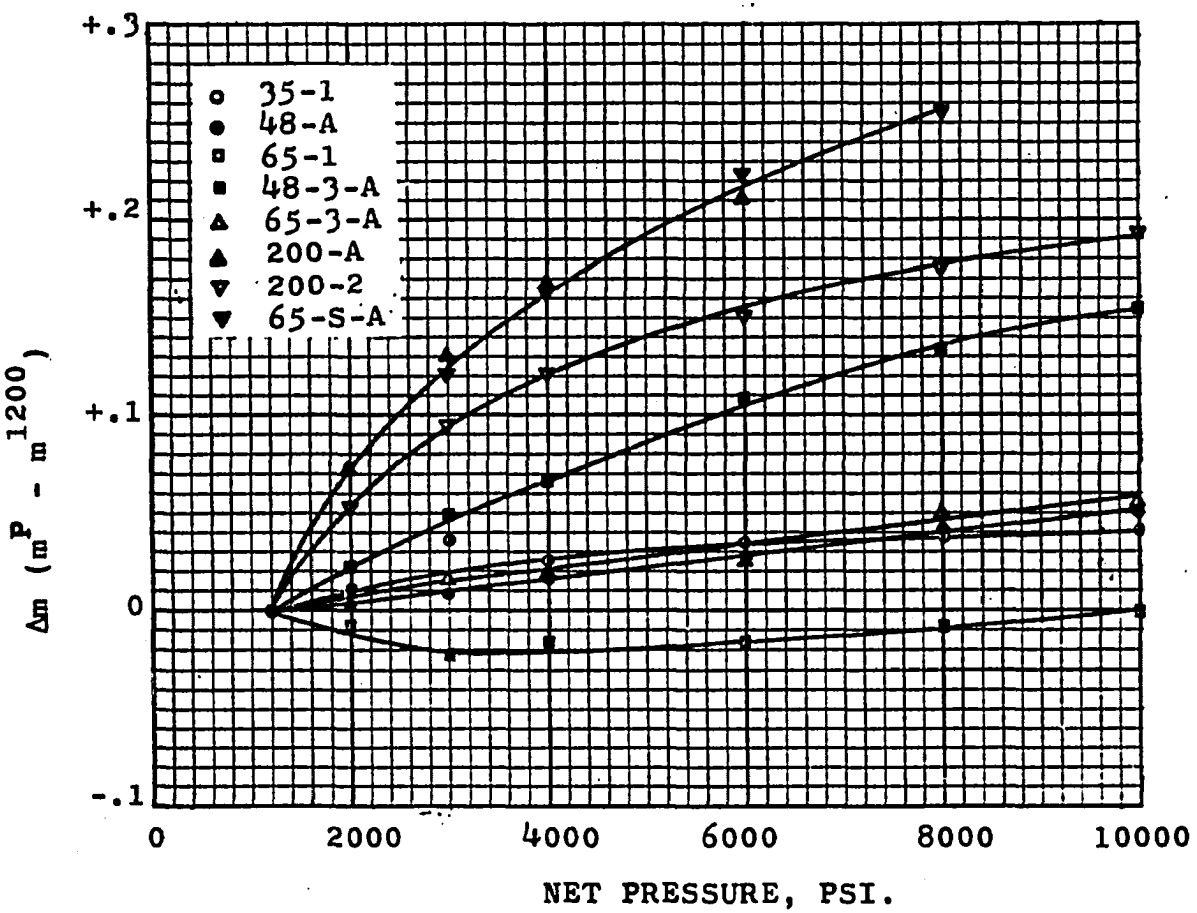

FIG. 19.--CHANGE IN m ($\Delta m = m^P - m^{1200}$) WITH NET PRESSURE

increase in formation resistivity factor due to pressure cannot be totally accounted for by a consideration of the pore volume change alone. This observation, as stated by Fatt,[12] is:

> "Here it is observed that the increase in formation factor for a given core with decrease in porosity during compression is more rapid than would be expected from the average line of formation factors versus porosity. This means that compression of the rock causes a more radical change in pore structure than does the change in porosity from sample to sample caused by the geological processes that reduce porosity."

One approach for explaining this rapid change in resistivity due to compression pointed out by Fatt would be with respect to the radical changes occurring in the pore structure itself.

The concept of constriction should be considered an important influence on formation resistivity. The constriction factor is an assessment of the variation in the cross-sectional area of the pore network. Owen's model indicates that for the same rock porosity and tortuosity an increasing constriction factor leads to increasing formation factors. This concept can be related to the influence of pressure on porous media. As pressure is applied to the media, an increase in formation factor will be observed due to the reduction in total pore volume alone. At the same time, however, if the constrictions are being closed at a greater rate than the larger pores, the constriction factor, as compared with the original constriction factor, will be increased, producing an even larger increase in formation factor than

expected.

From Figure 15, it can be seen that the relative formation resistivity factor increases with respect to surface area. However, surface area can easily be shown to be closely asscciated with the constriction factor. It is known that for two equal volumes of different sized particles the one with the smaller particles will have the greater surface area. There will also be more of the smaller grains, more grain to grain contacts and more relative changes in the sizes of the pores formed by the smaller grains. This can be descriptively illustrated as shown in Figure 20.

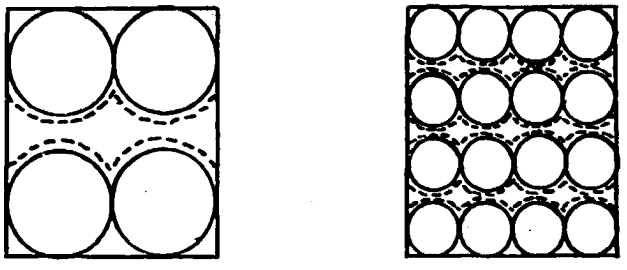

FIG. 20.--DESCRIPTIVE ILLUSTRATION OF GREATER NUMBER OF CONSTRICTIONS ASSOCIATED WITH SMALLER GRAINS

From this, it can be deduced that a greater surface area normally will be accompanied by an increase in the number of constrictions present in the pore channels formed. Therefore, it can be seen that an explanation of the change in formation resistivity factor on the basis of pore structure change alone can be readily tied to surface area variation by using the concept of the constriction factor.

The models also indicate that an increase in "m" with pressure, which is indicative of an increase in constriction factor, implies that the small pores are closing at a faster rate than the large pores. Conversely, a decrease in "m," as noted initially with the synthetic cores, indicates a decrease in the larger pores at a greater rate than the smaller pores. This concept, therefore, provides a reasonable explanation of the initial behavior displayed by these synthetic cores, since the large initial compressibility is probably due to a rapid decrease in the large pores. Once a more stable, or less compressible system is attained, however, the closing of the small constrictive pores becomes greater with respect to the closing of the larger pores.

Changes could also occur in tortuosity as well as constriction. In fact, this might be attributed to the change in "m" observed for core 65-S-A. The similar change in "m" of 65-S-A with respect to that of 200-A might be indicative of a faster rate of tortuosity increase in 65-S-A. The increases in tortuosity are due to the closing of passages causing current flow channels to be diverted with a subsequent increase in the average path length (tortuosity).

Double Layer Concept

The electrical double layer is another potential factor influencing the high rate of resistivity change. The double layer describes the nature of the distribution of the ions

in the electrolyte in the presence of a solid. A double layer will be present to some extent anytime a solid and liquid interface exists. As expressed by Adam,[1] "At any phase boundary there exists an electrical double layer, the positive and negative charges (ions, electrons, sometimes the opposite ends of dipoles in molecules near the surface) being distributed so that, on the average, the positive charges are nearer to one phase than the other."

Since all solids found in nature are assumed to have an imbalance of electrostatic forces at their outer surface, there will be an equalizing buildup of charges in the electrolyte at the solid surface. These charges, which form the double layer, could either be positive or negative, depending on the particular solid surface exposed. It is known, for example, that natural colloidal shales and clays will absorb more negative ions than positive ions from an ionic solution.[38]

The electrical double layer concept is described in a number of sources including the works of Adam,[1] Adamson,[2] and Glasstone.[17] The double layer model as it is now generally conceived was proposed by Stern. According to the Stern theory, the double layer consists of a first rigidly bound or fixed layer and a second, diffuse layer of less rigidly bound ions. A diagrammatic sketch illustrating this concept is shown in Figure 21.

The schematic system presented in Figure 21 shows a negatively charged surface with a corresponding buildup of a

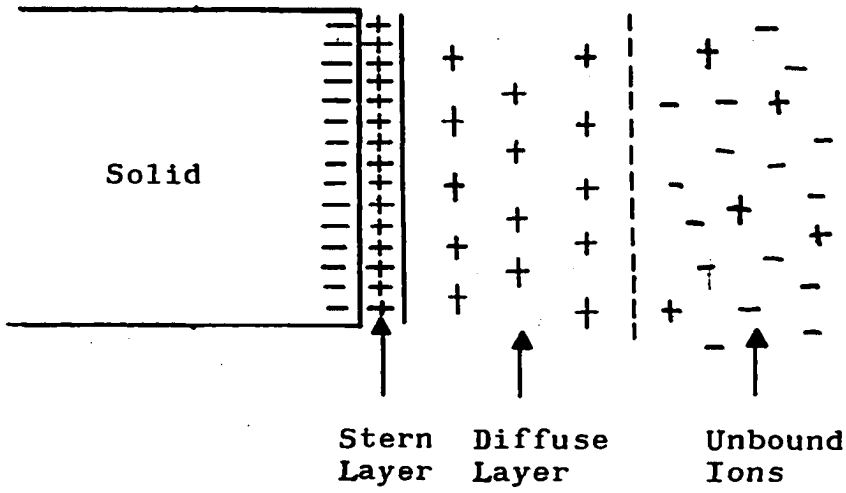

FIG. 21.--ELECTRICAL DOUBLE LAYER CONCEPT

double layer containing positive charges. "The distance through which the surface charge is operative, the thickness of the double layer, is determined essentially by the concentration and kind of ions in the solution in equilibrium with the surface."[38] The Stern layer, however, has been found to have an approximate thickness of a molecular diameter.[17] The mean thickness of the diffuse ionic double layer will be on the order of 10^{-5} to 10^{-6} cm. for aqueous systems.[9] These thicknesses are of course only approximations, since the effectiveness of the double layer is dependent on the particular surface and electrolyte in question.

Double Layer Influence at Static Conditions

First, consider a cross-section view of a single rock pore as shown in Figure 22.

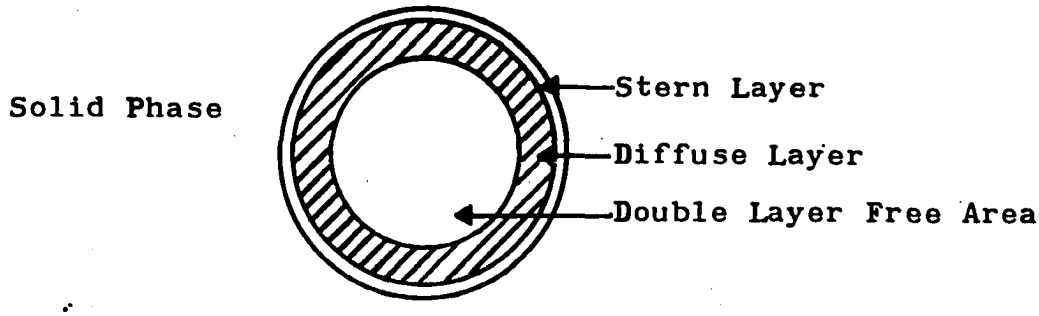

FIG. 22.--CROSS SECTION OF PORE INCLUDING DOUBLE LAYER

The presence of the double layer on the surface of the pore represents an area in which the ions are either rigidly or semi-rigidly bound to the charged solid surface. This, then, indicates that essentially two different paths are available for current flow although the pore is completely filled with only one electrolyte phase. These two current paths are depicted schematically in Figure 23. A sharp boundary between the diffuse layer and inner area is indicated in both Figures 21 and 22, although in reality the diffuse layer is a gradual transition from rigidly bound to non-bound charges.

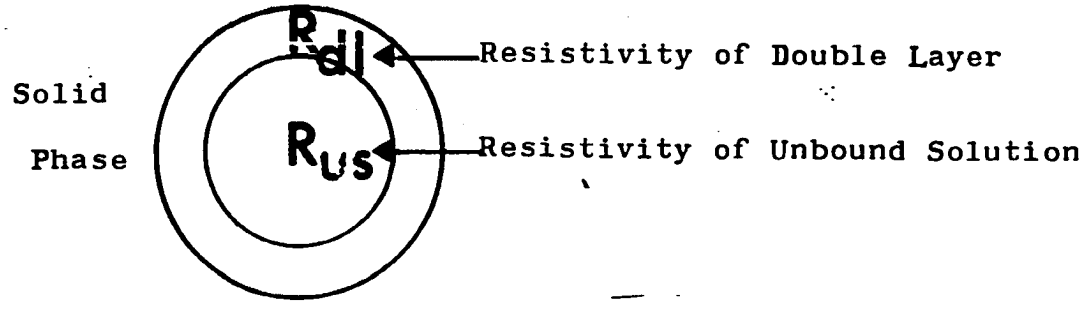

FIG. 23.--CROSS SECTION OF PORE INDICATING TWO DIFFERENT RESISTIVITY PATHS

The presence of the electrical double layer essentially produces a parallel circuit for current flow consisting

of two concentric paths of different resistivity.

The thickness of the double layer in a pore is a function of the properties of the particular solid and liquid in equilibrium. However, in order to obtain some concept as to the relative size of the double layer with respect to the pore itself, the assumption of a double layer thickness on the order of 10^{-6} cm. appears feasible. Using this assumption the ratio of pore radius to double layer thickness in a pore having a radius of one micron would be 100:1 and for a pore having a radius of 0.5 microns, the ratio would be 50:1. From these figures, the thickness of the double layer is becoming increasingly large with respect to pore size. By the same reasoning, then, it can be said that as the pore size decreases, the relative importance of the double layer path for current flow becomes increasingly important. A diagramatic sketch showing the relationship just described is given in Figure 24.

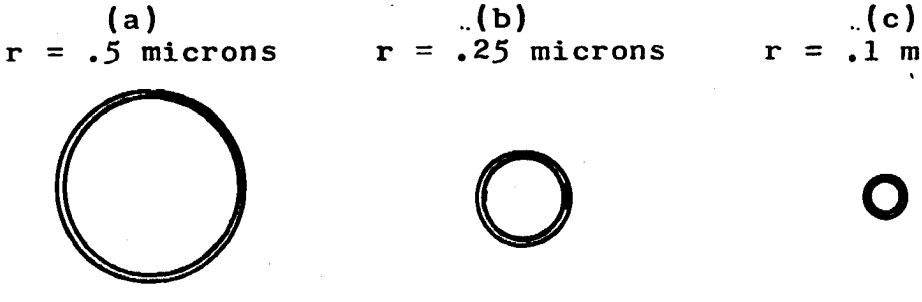

FIG. 24.--SKETCH SHOWING RELATIVE IMPORTANCE OF DOUBLE LAYER PATH WITH RESPECT TO TOTAL PORE SIZE

From this, it can be deduced that as the pore sizes in a porous media become smaller and smaller, the overall influence

of the double layer, with respect to the current flow within the pore structure becomes increasingly important.

The magnitude of the resistivities in each of these paths with respect to one another has not been discussed up to this point. However, in order to examine the relative magnitude of these resistivities, it is necessary to understand the factors influencing their current carrying capacity. Considering the basic description of the double layer itself, it can be seen that the ions in this double layer are either totally or partially bound by the surface charge of the solid. This means that the mobility of these ions will be reduced due to this binding effect. If this were the only factor to be considered, it would be obvious that the ability of the ions in the double layer to carry current would be reduced with respect to the free ions in the inner portion of the pore. It has been shown in work by Winsauer and McCardell[38] that the initial concentration of the saturating solution in the porous media must be considered. Their work was conducted on shaly sands (shales have a very effective double layer, probably much greater than that existing on other surfaces occurring in natural rock). They found that shaly sands in the presence of dilute solutions of electrolyte exhibited a greater double layer conductivity than the conductivity of the double layer free solution. This was explained as being due to the excess ions present in the double layer required to satisfy the surface charge. This action, in turn, reduced the

concentration of the electrolyte in the inner portion of the pore (double layer free area). The excess ions in the double layer, even though they are bound by the surface charge, can produce a greater total current carrying capacity than the inner portion which has been, correspondingly, reduced in concentration. It was found, however, that as the concentration of the solution used in saturating the porous media was increased, the conductivity of the inner portion increased with respect to that of the double layer. In most cases, if the concentration of the electrolyte is high enough, the conductivity of the electrolyte solution in the double free layer will become the larger of the two.

The previous analysis points out the reason for using highly saline solutions when measuring formation resistivity factors of natural rocks in the laboratory. It is the only way a constant formation resistivity factor for many natural rocks can be determined. Once an electrolyte having a sufficiently high ionic concentration is used, the conductivity of the double layer is essentially obviated with respect to the conductivity of the double layer free area. It can be concluded from this that it is possible to have a double layer with a resistivity less than, equal to, or greater than the resistivity of the inner portion (double layer-free area) of the pore, depending upon the particular surface and surface charge and the solution within the pore space. It would be unlikely that any particular system would have paths providing

equal conductivity. The most probable case, when using a fairly saline solution, is the one where the double layer free area is more conductive than the double layer itself.

Considering, now, the effect of this double layer in a porous media, the following hypothesis can be made. First, assume that the double layer resistivity is greater than the resistivity in the double layer free area, which is the most likely case. Next, consider a hypothetical situation where two cores are available, each having exactly the same porosity with one core having a smaller pore size than the other. For example, with reference to Figure 24, one core would have pores as indicated in (a) and one have pores as indicated in (c). A higher total resistivity would be measured for the smaller pored core than for the large pored core due to the influence of the double layer itself (assuming that the tortuosity and constriction factors of the two systems were equal). In other words, what is being suggested is essentially an "ELECTRICAL CONSTRICTION FACTOR" arising from the influence of the double layer. This electrical constriction concept would, of course, operate (for more resistive double layers) in the same manner as the geometric constriction factors. There is one important difference, however. Whereas the geometric constriction factor is due to the solid matrix, this constriction is occurring in the pore space itself. Therefore under certain conditions an erroneous formation factor could be measured in a completely saline water

saturated system. If the condition were to arise where the double layer influenced a relatively important portion of the pore space and it was the more resistive path, the results could be similar to those obtained when a non-conducting liquid such as residual oil is present.

Double Layer Influence Associated with Compression

When considering the effect of pressure on the formation resistivity factor the electrical constriction concept could have a very definite influence. As external pressure is applied to the core, the pore sizes will be reduced. If a pore has a radius of 0.5 microns at atmospheric conditions and an external pressure is applied with a corresponding reduction of this pore to a radius of 0.1 microns, then the influence of the double layer path has been increased. This is illustrated in Figure 24. This, of course, assumes that the double layer thickness will not be essentially altered during the compression process. During this compression process, water if forced out of the core and the system must return to electrical equilibrium. If the double layer reforms or equalizes with approximately the same thickness, then the only change taking place is the decrease in size or area of the more conductive path in the center of the pore.

This double layer mechanism can now be seen to be a potential factor on the change in formation resistivity factor with pressure. No matter what its relative resistivity

relationship with the double layer free area of the pore (unless the two are equal) a change in the proportional influence of these two paths occurs during compression. This will be true even if the effects of the double layer are obviated at atmospheric conditions by using a saline water as the electrolyte. However, in view of the previous discussion, its effect would probably be relatively small except in the small pores. In other words, with a small decrease in a large pore, the relative increase in the size of the double layer with respect to the double layer free inner area would be small. On the other hand, its effect in small pores could be quite large. Therefore, it is felt that the effect of the double layer will be governed by the number of small pores. By the same token, it can be stated that the greater the number of small pores, the greater the surface area. This, then, leads to the implication that surface area is also an indicator of the magnitude of the double layer effect.

Applying this concept to the changes occurring in the cementation factor, m, a coordinated picture can be obtained. The initial decrease in Δm was felt to be due to the closing of the larger pores. If this is true, the influence of the double layer will be low. However, when the small pores begin to close at a faster rate, the influence of the double layer will increase, which, in turn, will be associated with an increase in the formation resistivity factor. These concepts fit in very well with the observed changes of the cementation

factors of both the natural cores of Hilchie and the synthetic cores studied here. One important aspect with respect to the Δm data of Hilchie as shown in Figure 25 can be explained here. It was noted that the shale core (Dean) exhibited a decrease in separation with respect to the sandstone samples. This could easily be explained by the double layer concept. It is possible that for this particular sample the salinity of the water used, although relatively high, was not high enough to allow the double layer free area to have a higher conductivity. In all respects, at atmospheric conditions, this relatively saline solution probably did lessen the effect of the double layer to a negligible extent. However, if the double layer were still the more conductive, then an increase in pressure would expand the effects of a more conductive path. This, in turn, would tend to have a decreasing effect on the formation resistivity factor. Thus, it would be tending to oppose the effect of increasing the formation resistivity factor being induced by the changing pore geometry (geometric constriction factor increasing).

The association of this double layer concept with clay might also be used as a supporting point for the empirical relationship of formation resistivity factor with clay content as proposed by Hilchie. It would be expected that the influence of the double layer would have an increasing influence on the formation resistivity factor under pressure since clay has a very effective double layer. If, as in most

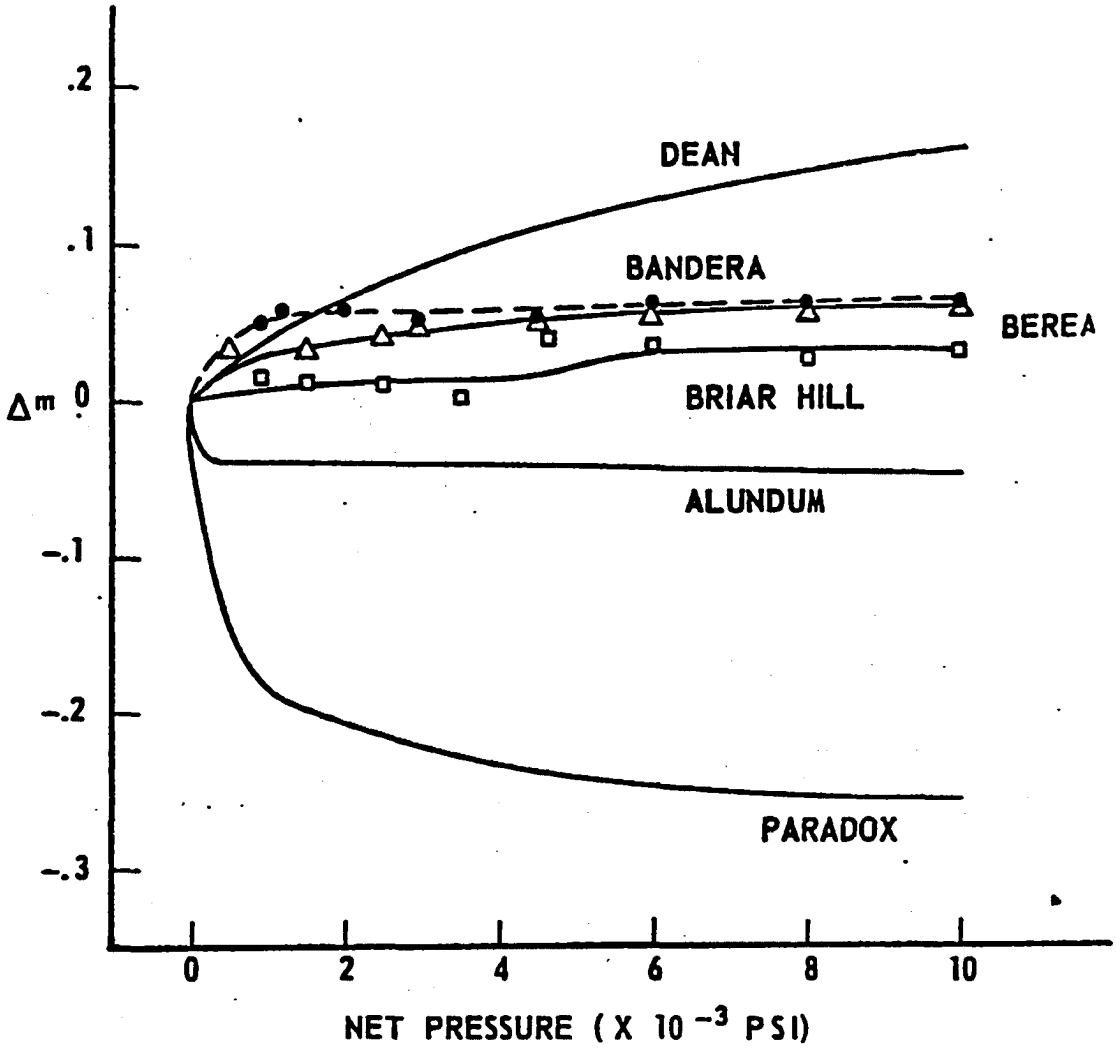

FIG. 25.--THE CHANGE IN m ($F = \phi^{-m}$) WITH NET PRESSURE ON NATURAL CORES (FROM HILCHIE[20])

cases, the double layer is more resistive than the double layer free area of the pore an increase in the percentage clay should engender a corresponding increase in formation resistivity factor.

Summary of Pressure Effects

The "cementation" factor proposed by Archie represents the effect of all the numerous, interrelated parameters which are characteristic of natural rocks. The variation in "cementation" factor required to correlate the formation resistivity factor with porosity for consolidated media can, in turn, be effectively ascribed to three parameters tortuosity (t), pore constriction factor (PC) and electrical constriction factor (EC)

$$m = f\ (t,\ PC,\ EC) \qquad (13)$$

or

$$F = f\ (\phi,\ t,\ PC,\ EC) \qquad (14)$$

It has also been pointed out that, in order to obtain a true formation resistivity factor which is representative of the pore volume, a highly saline saturating solution is generally necessary in order to negate the effects of the "conductive solids" (double layer). If this is done, then the influence of the electrical constriction is essentially nullified with the relationship reducing to:

$$F = f\ (\phi,\ t,\ PC) \qquad (15)$$

Subjecting a rock to pressure will, of course, reduce the porosity, but the formation resistivity factor changes at a more rapid rate than can be accounted for solely by the change in porosity. This indicates that the other functional

parameters (t, PC, EC) are also changing. A prediction of porosity at another pressure condition, therefore, requires a method of predicting the influence of these three parameters.

As indicated by this study, a definite relationship exists between the theoretically calculated surface area and the change in relative formation resistivity factor. The surface area has also been qualitatively shown to be closely associated with each of the three influencing parameters such that

$$(t, PC, EC) = f\ (SA) \qquad (16)$$

It should be emphasized that the separate effects of these three parameters, as associated with the microscopic mechanisms occurring during compression, cannot be disassociated from each other. Nevertheless, it appears that their combined effect can be satisfactorily ascertained by the surface area concept. This indicates that an equation of the form

$$\frac{F^P}{F} = f\ (SA) \qquad (17)$$

will provide a suitable approach for predicting the effect of pressure on the formation resistivity factor. The use of a closely associated parameter such as $PV<0.5$ (used by Hilchie) may, for all practical purposes, be adequate for natural rocks, although surface area is a more encompassing parameter. Development of relationships such as Equation 17 should, however, be done on a group basis with respect to rock character (lithology).

Temperature Data

The effect of temperature on the synthetic samples at a constant net stress is graphically illustrated in Figure 26. The results, in general, indicate initial increases in the relative formation resistivity factor up to approximately 240° F. This rate of increase appears to accelerate with the surface area of the core. For the cores with a low surface area (48-A and 65-1), the initial change in the relative formation resistivity factor appears to be almost nil, although, as the surface area of the core increases, the increase occurs sooner. The consistency of this variation in initial formation resistivity factor change with surface area of the core is very pronounced. The very consistency of the data up to 240° F. indicates a definite influence of the small pores on the initial change occurring in the relative formation resistivity factor.

For all of the bead cores, another notable observation can be made. In the vicinity of 200-240° F., the relative formation resistivity factors seem to converge. Above 240° F. a single curve suffices. One exception to this is noted in the strange behavior of core number 200-A. For this particular core, an abrupt decrease in the relative formation resistivity factor occurs above 240° F., with the minimum probably being in the vicinity of 280° F. After this sudden decrease, an increase is again observed. The other bead cores display a relatively stable situation existing between 240

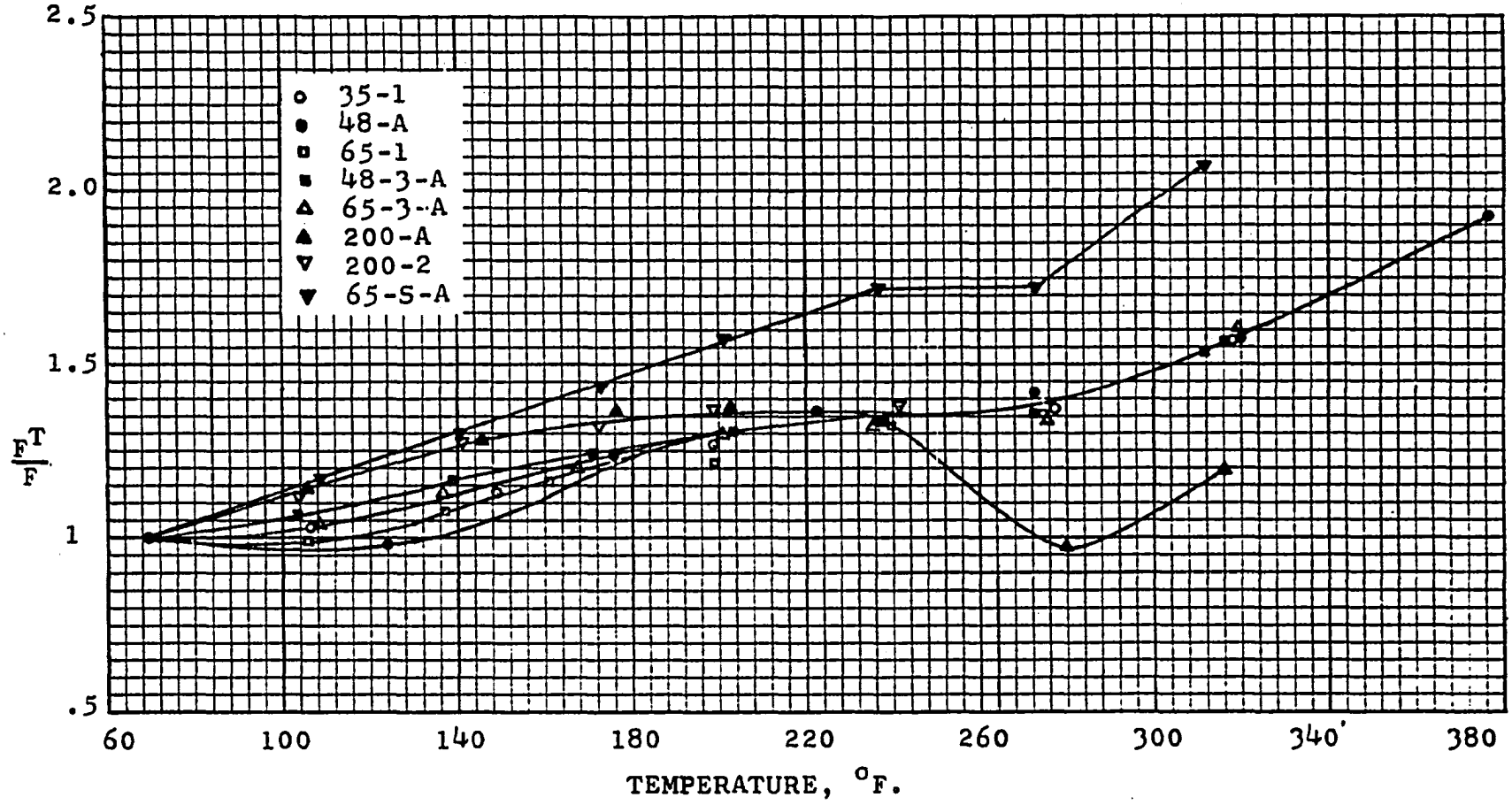

FIG. 26.--RESISTIVITY CHANGES DUE TO TEMPERATURE

and 280° F., with a subsequent increase being noted above 280° F.

One interesting aspect of this study is the difference in trend noted with the sand sample. At the low temperatures, up to approximately 140° F., the sand core seemed to vary similarly to the bead cores, although it changed at a slightly greater rate than would be expected from its surface area. This rate of change continued, in almost a straight line relationship, to approximately 240° F. At this point, as with all the bead cores except 200-A, a static condition seemed prevalent until the formation resistivity factor began to increase again above 280° F.

The above behavior of these synthetic cores with respect to the effect of temperature, can be divided into three separate, distinct phases. The first phase might be considered the behavior exhibited by the cores up to a temperature of 240° F. The second phase would be from approximately 240-280° F. with the third phase occurring at temperatures above 280° F.

In the first phase, an essentially increasing relative formation resistivity factor is noted which is indicative of a generally increasing constriction factor (closing of the smaller pores). It also appears that the rate of increase is more rapid as the surface area of the core increases. The bead cores exhibit a total increase in relative formation resistivity factor from 1.00 at 70° F. to a value of

approximately 1.35 at 240° F. The sand core, on the other hand, increases to about 1.72 at 240° F. With respect to this phase, it might be stated that the total change is a function of composition although the rate at which this change occurs is a function of surface area.

Comparing the results occurring in this initial phase with respect to the observations made by Hilchie on the natural cores, it can be seen that, in both cases, the initial behavior seemed to be governed by the smaller pores. However, the results appear to be directly contradictory. In the natural cores studied by Hilchie, an initial decrease was observed to some minimum value after which an increase was apparent. The magnitude of this minimum relative formation resistivity factor was apparently a function of the percent of the pore volume having a pore radii less than 0.5 microns. The lowest minimum is associated with the core having the greatest pore volume less than 0.5 microns. This was hypothetically explained by Hilchie as possibly being the result of the thermal expansion of the rock grains causing the small pores to open, thereby reducing the resistivity in somewhat the reverse of what happens when the rock is subjected to pressure. This explanation assumes, therefore, that the expanding rock grains, working against each other, force the rock to expand with a resulting increase in size of the pores. Therefore, the more small pores present, the greater will be the resultant effect of their opening. The same type of

hypotheses might be applied to the synthetic cores. The initial increase in temperature would, of course, cause the matrix material to expand. However, as opposed to natural rock, the expanding beads and sand do not work against each other and open pores. This is probably the case, since the packing of a natural matrix is essentially at a minimum, whereas, the packing of the synthetic systems is, in all probability, not the minimum arrangement possible. If this be the case, the increase in temperature and resultant increase in bead and sand size would tend to produce a minimum packing in which the grains, instead of working against each other, would have a tendency to expand into less stable, unsupported areas.

The second phase might be indicative of that point where the beads begin to work against each other. If this is the case, then the tendency would be for the relative formation resistivity ratio to reduce or at least to offset any further increase. In fact, the behavior of core 200-A indicates that the pore passages are being opened. This is very possible since in the ratio between the bead sizes used was the greatest. In other words, the small beads were not too much smaller than the large beads. In this case, then, the "fitting" of the smaller beads in between larger beads is less likely. Therefore, on expansion, the beads in this particular pack would probably begin to work against each other sooner. Therefore, it appears that the packing arrangement

existing in the matrix itself governs the temperature effect to some extent.

The third phase probably indicates the point at which the epoxy cementing material exhibits plastic deformation. It is indicated that, at a temperature of about 280° F. and a net pressure of 1000 psi., the plastic deformation of the epoxy allows the rigid framework of the core to "breakdown" with a resulting decrease in overall pore sizes, closing of the pores, and, in general, alteration of the grain-to-grain matrix system. As can be seen, a more or less radical increase in the relative formation resistivity factor above 280° F. occurs.

Resistivity measurements were made on all cores up to 320° F., except for core 200-2, where sleeve failure occurred in the vicinity of 240° F. The first core measured (48-A) was measured up to 380° F., but the large increase in relative formation resistivity factor indicated that the core might be failing. Therefore, subsequent cores were only measured to 320° F.

The difficulty encountered with the high pressure pore volume change system drastically reduced the amount of data collected. In fact, reliable $\Delta\phi$ data were obtained on only three cores. However, it is believed that the uncertainty with respect to how the total volume of the system is being affected by the increased temperature of the cell makes these data essentially unreliable. In order to account for the

effect of thermal expansion of the water, it was necessary to assume that only the core itself was affected by the temperature change and consequently the water existing in the line near the cell was assumed to be at ambient temperature. Furthermore, the exact porosity of the stressed core is not exactly known and it is believed that the presence of an internal pressure operating with an external pressure to form the net stress of 1000 psi. greatly affected these synthetic cores. As has been shown, these cores are somewhat sensitive to initial compression effects. It appears, based on the formation resistivity factor values obtained at the initial stress, that the cores reacted in a manner that resulted in a lower formation factor measurement than expected. These observed formation resistivity factors, at ambient temperature and under a net stress resulting from both internal and external pressure, were all lower than the value measured at ambient temperature and atmospheric internal--1000 psi. external net stress. This is also true of natural cores but the effect observed is higher in the synthetic cores. Therefore, the porosity that actually exists in the core when it is stressed internally and externally is uncertain. Thermal expansion data for sodium chloride solutions are shown in Figure 43 (Appendix B). These data are not available above 200° F. and it appears that at this point the brine and pure water expansion data are beginning to deviate. Therefore the expansion of the saline solution can only be corrected

reliably up to about 240° F. In spite of these problems an attempt has been made to "approximate" the pore volume change occurring in the cores during temperature increases to 240° F. These data are shown in Figure 27. The pore volume change is plotted as percentages of the total change that seemingly occurred to 240° F. This graphical analysis indicates that for core 48-3-A, a larger percent of the change occurred in the 104°-140° F. range than anywhere else. A fairly uniform change is observed for core 65-S-A. These data are therefore felt to be in agreement with the observed results and tend to indicate that the change observed in the relative formation resistivity factor up to a temperature of 240° F. is a function of the decrease in pore volume due to thermal expansion of the matrix material.

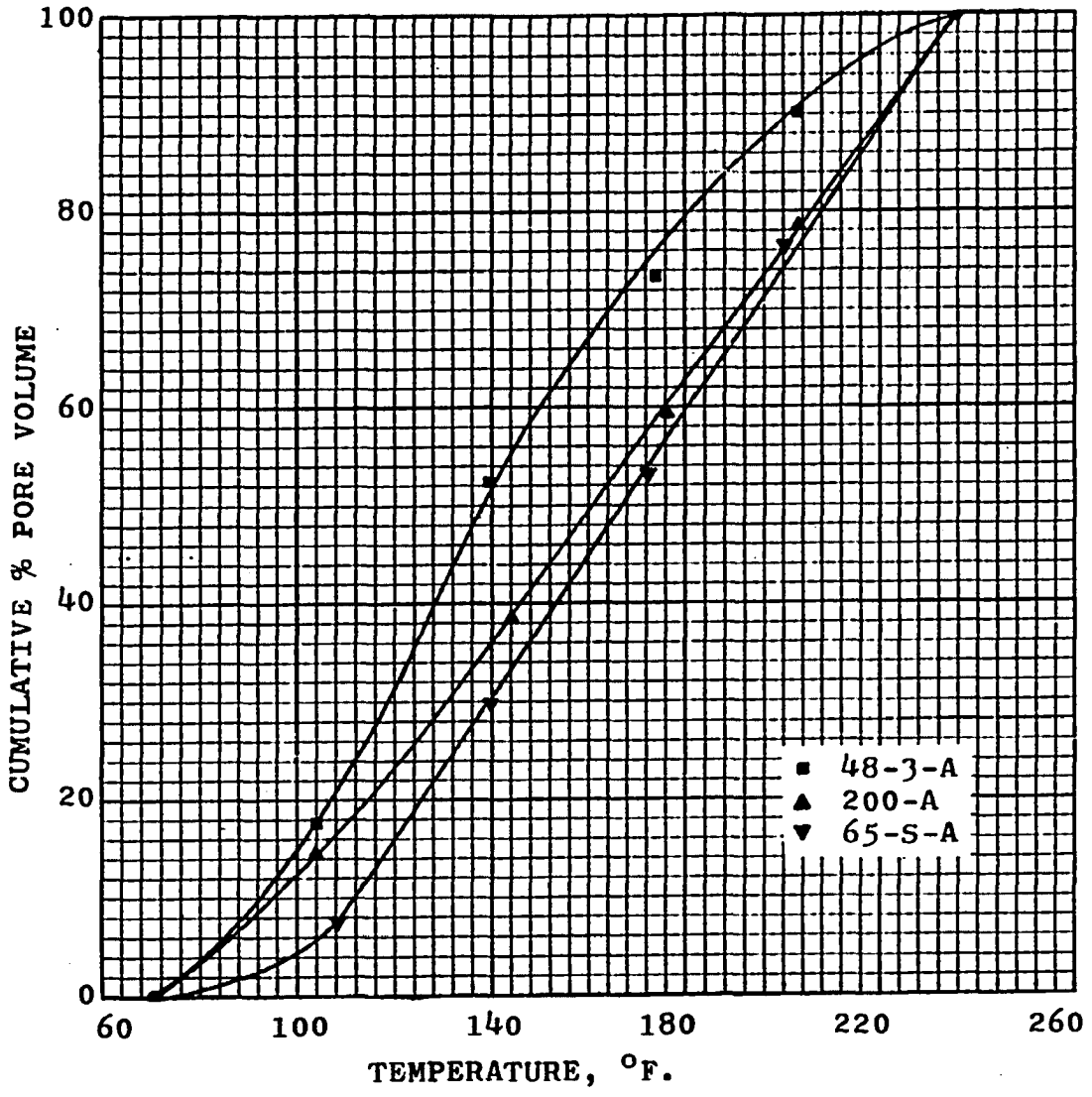

FIG. 27.--CUMULATIVE % PORE VOLUME CHANGE OCCURRING TO 240° F. VS. TEMPERATURE

CHAPTER VI

CONCLUSIONS

This study was originally promulgated on the basis that characterization of the behavior of natural porous media could best be achieved through the systematic investigation of synthetic "rocks." Such artificial media enable one to control the variables in a manner that is impossible with natural rocks. One of the significant contributions of this study has been the development of artificial cores that can be fabricated to possess specific properites and still behave in the same relative manner as natural rocks.

In this study the emphasis has been on the effect of pore size distribution (surface area) on the formation resistivity factor, at varying pressures and temperatures. The use of synthetic cores made it possible to exclude the other parameters. For the cores in question it has been shown conclusively that relative formation resistivity factor may be correlated versus pressure (at constant temperature) with relative surface area as the third parameter. An equivalent result was obtained with temperature rather than pressure as the independent variable.

A relative or pseudo surface area was used rather than

pore size distribution inasmuch as it is more readily identifiable with those factors which are hypothesized to play a role in the reported behavioral patterns. These are:

1. The increase in the length of the mean free path for current flow (increased tortuosity) as pores or constrictions close completely.
2. The increase in the constriction factor due to a more rapid relative decrease in the smaller pores.
3. The effect of pore reduction on the double layer existing at the surface of the rock.

Although it is impossible at this point to quantitatively determine the relative role of each factor, a better qualitative understanding has been provided.

The effect of surface area on temperature behavior is not as well defined because of greater experimental difficulty. However, it is clear that the same basic parameters are involved. It is likely that packing density and other factors that are affected by thermal stresses must also necessarily play a role.

REFERENCES

1. Adam, N. K. Physical Chemistry. Oxford, England: Clarendon Press, 1956.

2. Adamson, A. W. Physical Chemistry of Surfaces. New York: Interscience Publishers, Inc., 1960.

3. Amyx, J. W., et al. Petroleum Reservoir Engineering. New York: McGraw-Hill Book Co., Inc., 1960.

4. Archie, G. E. "The Electrical Resistivity Log As an Aid in Determining Some Reservoir Characteristics," Trans. A.I.M.E., Vol. 146 (1942), p. 54.

5. _____. "Classification of Carbonate Rocks and Petrophysical Considerations," A.A.P.G. Bull., Vol. 36 (1952), p. 278.

6. Atkins, E. R. Jr., and Smith, G. H. "The Significance of Particle Shape in Formation Resistivity Factor-Porosity Relationships," A.I.M.E. Trans., Vol. 222 (1961), p. 285.

7. Chombart, Louis G. "Well Log Interpretation in Carbonate Reservoirs," Geophysics, Vol. 25 (1960), p.779.

8. Dakhnov, V. M. "Geophysical Well Logging," Colorado School of Mines Quarterly, Vol. 57, No. 2. Translated by G. V. Keller from 1959, Russia Edition.

9. Davies, J. T., and Rideal, E. K. Interfacial Phenomenon. New York: Academic Press, 1963.

10. de Witte, L. "Relations between Resistivities and Fluid Contents of Porous Rock," Oil and Gas Jour., Vol. 49 (Aug. 24, 1950), p. 120.

11. Dobrynin, V. M. "Effect of Overburden Pressure on Some Properties of Sandstones," Soc. Pet. Eng. Jour., Vol. 2, No. 4 (1962), p. 360.

12. Fatt, I. "Effect of Overburden and Reservoir Pressure on Electrical Logging Formation Factor," A.A.P.G. Bull., Vol. 41, No. 11 (1957), p. 3456.

13. _____. "Pore Volume Compressibilities of Sandstone Reservoir Rocks," A.I.M.E. Trans., Vol. 213 (1958), p. 362.

14. Fricke, H. "A Mathematical Treatment of the Electric Conductivity and Capacity of Dispersed Systems," Phy. Rev., Vol. 24 (1924), p. 575.

15. Furnas, C. C. "Grading Aggregates: PT. I. - Mathematical Relations for Beds of Broken Solids of Maximum Density," Ind. and Eng. Chem., Vol. 23, No. 9 (1931), p. 1052.

16. Glanville, C. R. "Laboratory Study Indicates Significant Effects of Pressure on Resistivity of Reservoir Rocks," Jour. Pet. Tech., Vol. 11, No. 4 (1959), p. 20.

17. Glasstone, S. An Introduction to Electrochemistry. New York: D. Van Nostrand Co., Inc., 1942.

18. Glumov, I. F., and Dobrynin, V. M. "Changes of Specific Resistivity of Water Saturated Rocks under the Action of Rock and Reservoir Pressures," Priklad. Geofiz., No. 33 (1962), p. 190.

19. Guyod, Hubert. "Electrical Well Logging," The Oil Weekly, Aug.-Dec., 1944.

20. Hilchie, D. W. "The Effect of Pressure and Temperature on the Resistivity of Rocks." Unpublished Ph.D. dissertation, The University of Oklahoma, 1964.

21. Hubbert, M. King, and Willis, D. G. "Mechanics of Hydraulic Fracturing," A.I.M.E. Trans., Vol. 210, (1957), p. 153.

22. Lynn, R. D. "Effect of Temperature on Drilling Mud Resistivities," T.P. No. 1302 G. Annual Fall Meeting, Soc. of Pet. Eng. of A.I.M.E., Dallas, Texas, Oct. 4-7, 1959.

23. Long, G., and Chielci, G. "Salt Content Changes Compressibility of Reservoir Brines," The Pet. Engr., 1961, p. B-25.

24. Maxwell, J. C. A Treatise of Electricity and Magnetism. New York: Dover Publications, Inc., 1954 Reproduction of 1891 Edition.

25. Microbeads, Inc., Company Technical Literature, Jackson, Miss.

26. Muskat, M. The Flow of Homogeneous Fluids through Porous Media. New York: McGraw-Hill Book Co., Inc., 1937.

27. Orlov, L. I., and Gimaev, R. S. "The Influence of Rock Pressure on the Electrical Resistivity of Carbonate Rocks," Priklad. Geofiz., No. 33 (1962), p. 206.

28. Owen, J. E. "The Resistivity of a Fluid Filled Porous Body," A.I.M.E. Trans., 1952, p. 195.

29. Patnode, H. W., and Wyllie, M. R. J. "The Presence of Conductive Solids in Reservoir Rock As a Factor in Electric Log Interpretation," A.I.M.E. Trans., Vol. 189 (1950), p. 47.

30. Pirson, S. J. Oil Reservoir Engineering. New York: McGraw-Hill Book Co., Inc., 1958.

31. Purcell, W. R. "Capillary Pressures - Their Measurement Using Mercury and the Calculation of Permeability Therefrom," A.I.M.E. Trans., 1949.

32. Rayleigh, Lord. "On the Influence of Obstacles Arranged in Rectangular Order upon the Properties of a Medium," Phil. Mag., Vol. 34 (1892), p. 481.

33. Redmond, J. C. "Effect of Simulated Overburden Pressure on the Resistivity, Porosity, and Permeability of Selected Sandstones. Unpublished Ph.D. dissertation, The Penn. State University, 1962.

34. Salwinski, A. "Conductivity of an Electrolyte Containing Dielectric Bodies," J. Chim. Phys., Vol. 23, (1926), p. 710.

35. Towle, Guy. "An Analysis of the Formation Resistivity Factor-Porosity Relationship of Some Assumed Pore Geometries." Proc. of Third Annual Symp. Soc. of Prof. Well Log Anal., Houston, Texas, 1962.

36. Tyler, W. S. The Profitable Use of a Testing Sieve. Cleveland, Ohio: W. S. Tyler Co., Cat. 53, 1957.

37. Winsauer, W. O., et al. "Resistivity of Brine Saturated Sands in Relation to Pore Geometry," A.A.P.G. Bull., Vol. 36, No. 2 (1952), p. 253.

38. Winsauer, W. O., and McCardell, W. M. "Ionic Double-Layer Conductivity in Reservoir Rock," A.I.M.E. Trans., Vol. 198 (1953), p. 129.

39. Wyble, D. O. "Effect of Pressure on the Conductivity, Porosity, and Permeability of Oil Bearing Sandstones." Unpublished Ph.D. dissertation, The Penn. State University.

40. _____. "Effects of Applied Pressure on the Conductivity, Porosity, and Permeability of Sandstones," Jour. Pet. Tech., Vol. 10 (1959), p. 57.

41. Wygal, R. J. "Construction of Models That Simulate Oil Reservoirs," Soc. Pet. Eng. Jour., Vol. 3, No. 4, (1963), p. 281.

42. Wyllie, M. R. J. The Fundamentals of Electric Log Interpretation. New York: Academic Press Inc., 1957.

43. Wyllie, M. R. J., and Gregory, A. R. "Formation Factors of Unconsolidated Porous Media: Influence of Particle Shape and Effect of Cementation," A.I.M.E. Trans., Vol. 198 (1953), p. 103.

44. Wyllie, M. R. J., and Rose, W. D. "Some Theoretical Considerations Related to the Quantitative Evaluation of the Physical Characteristics of Reservoir Rock from Electrical Log Data," A.I.M.E. Trans., Vol. 189 (1950), p. 105.

45. Wyllie, M. R. J., and Spangler, M. B. "Application of Electrical Resistivity Measurements to Problem of Fluid Flow in Porous Media," A.A.P.G. BULL., Vol. 36, No. 2 (1952), p. 359.

APPENDIX A

BASIC CORE INFORMATION

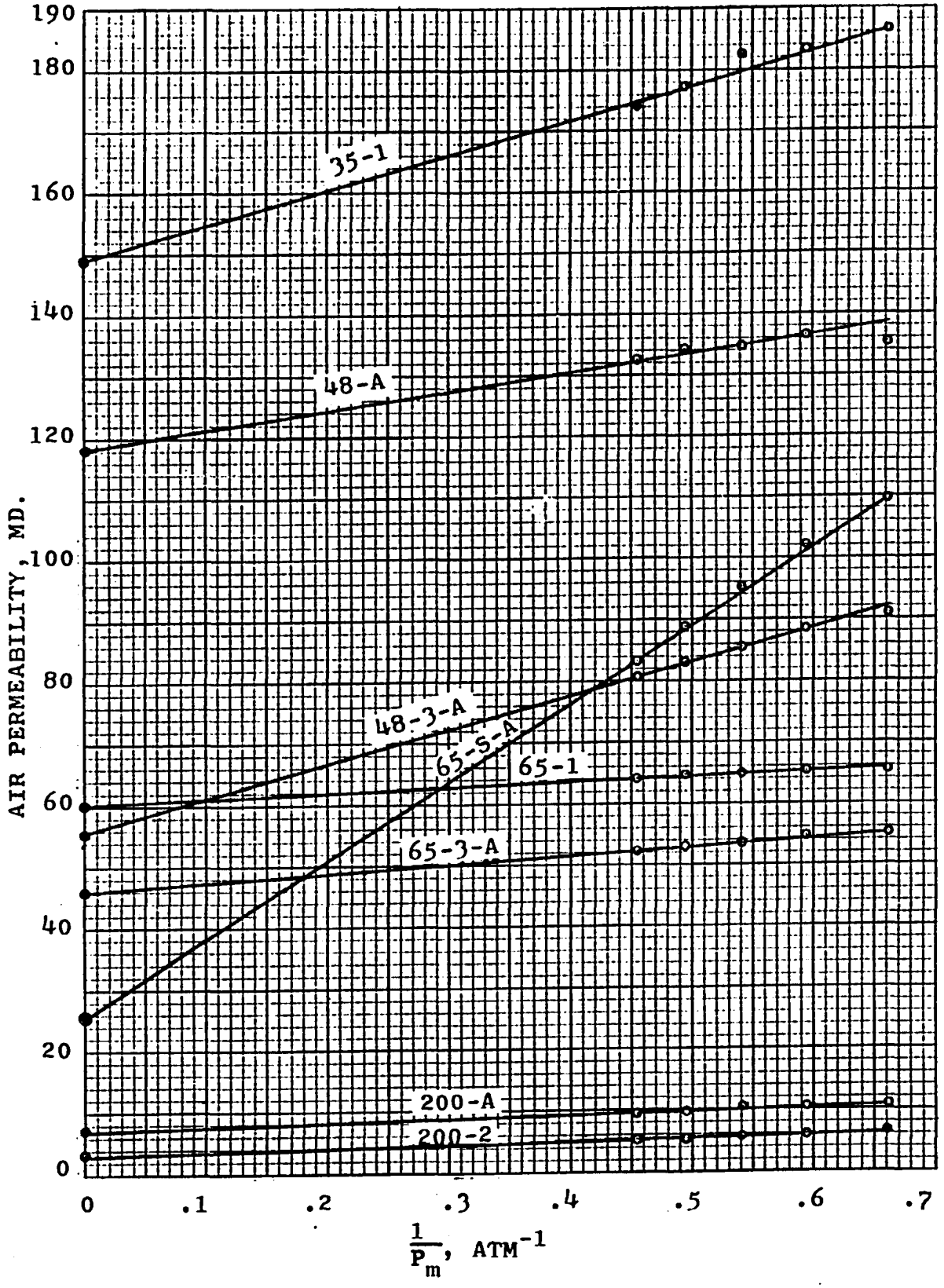

FIG. 28.--KLINKENBERG PERMEABILITY

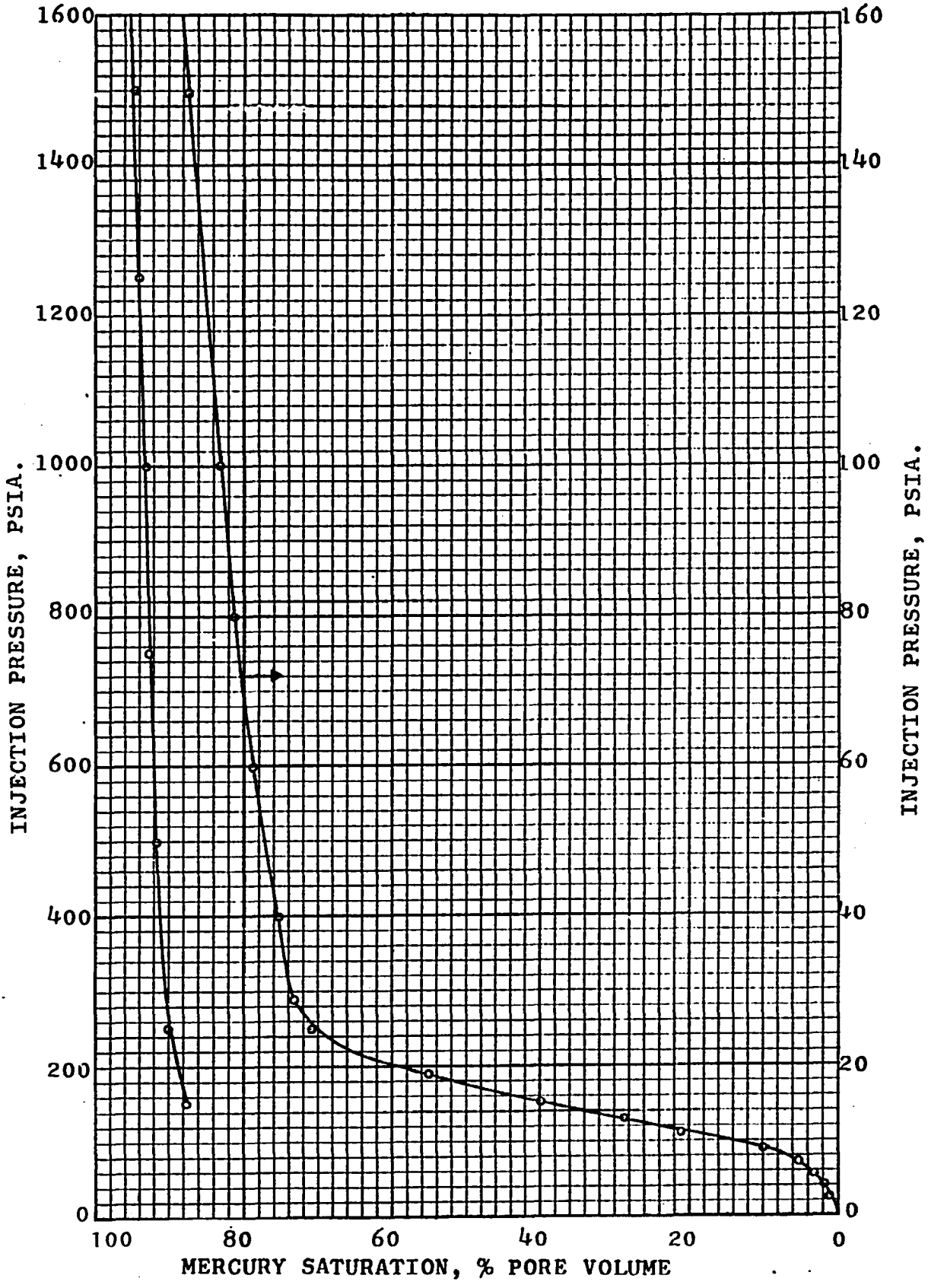

FIG. 29.--MERCURY INJECTION CAPILLARY PRESSURE DATA - CORE 35 (POROSITY = 13%)

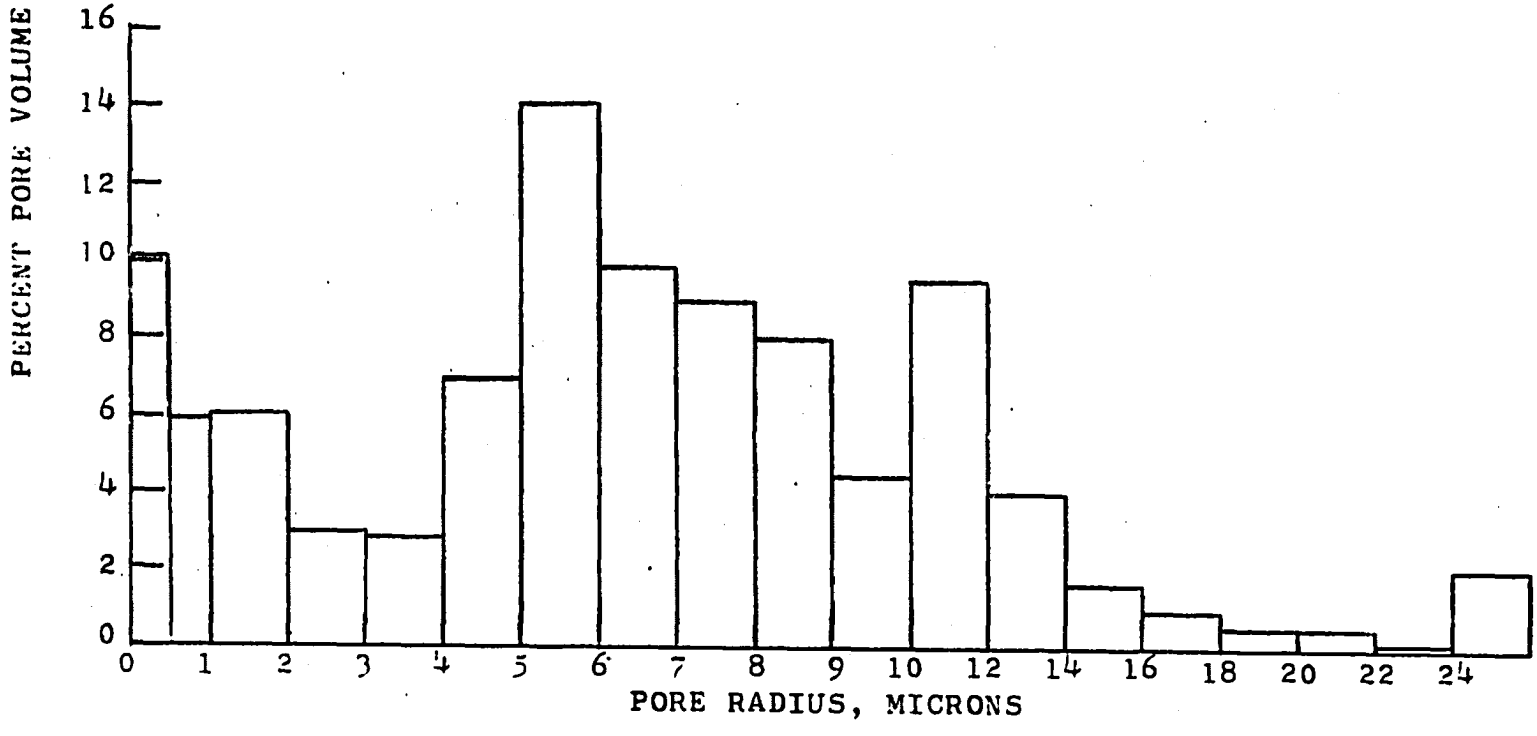

FIG. 30.--MERCURY INJECTION PORE SIZE DISTRIBUTION - CORE 35 (POROSITY 12.8%)

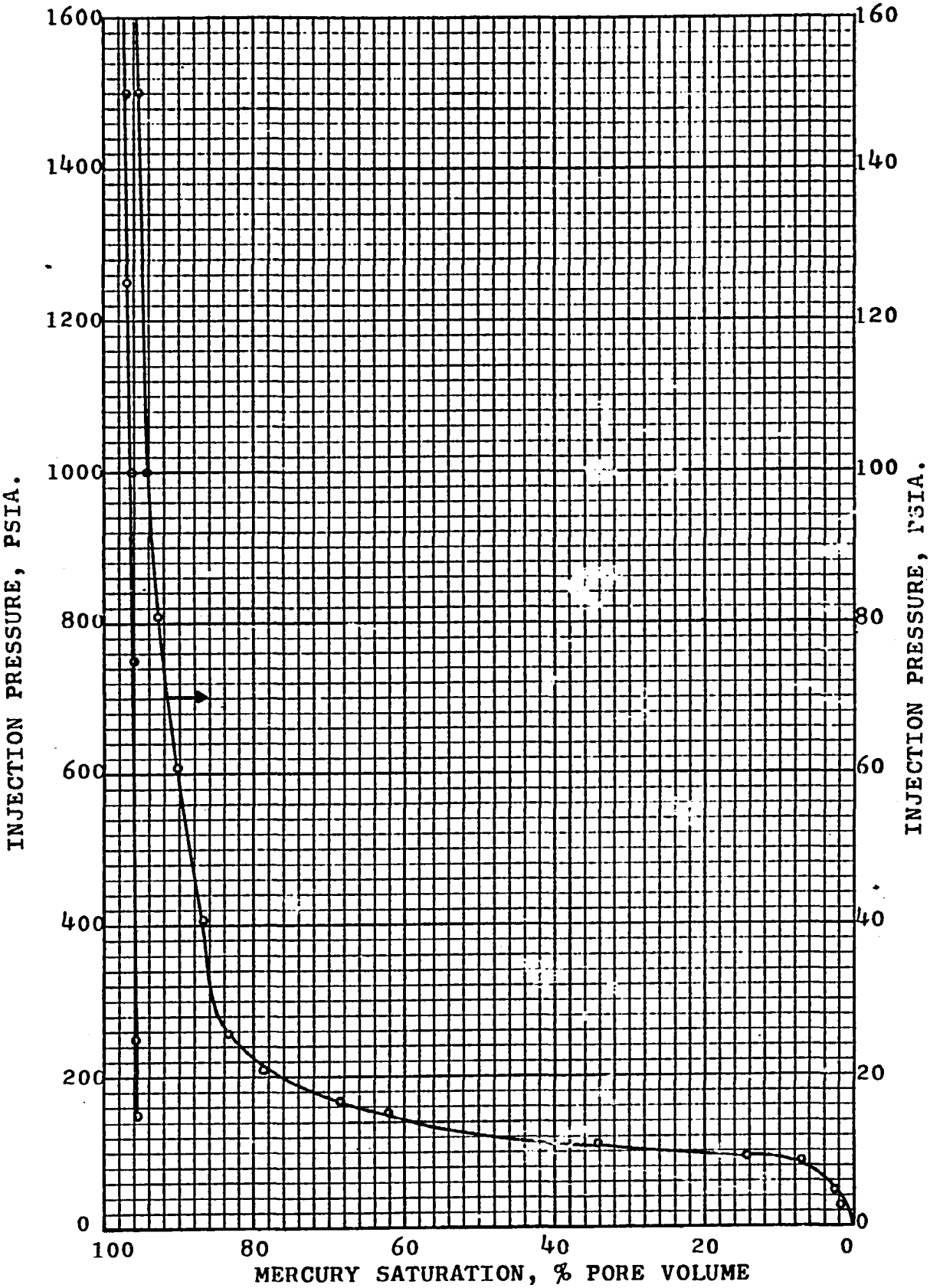

FIG. 31.--MERCURY INJECTION CAPILLARY PRESSURE DATA - CORE 48 (POROSITY = 13.9%)

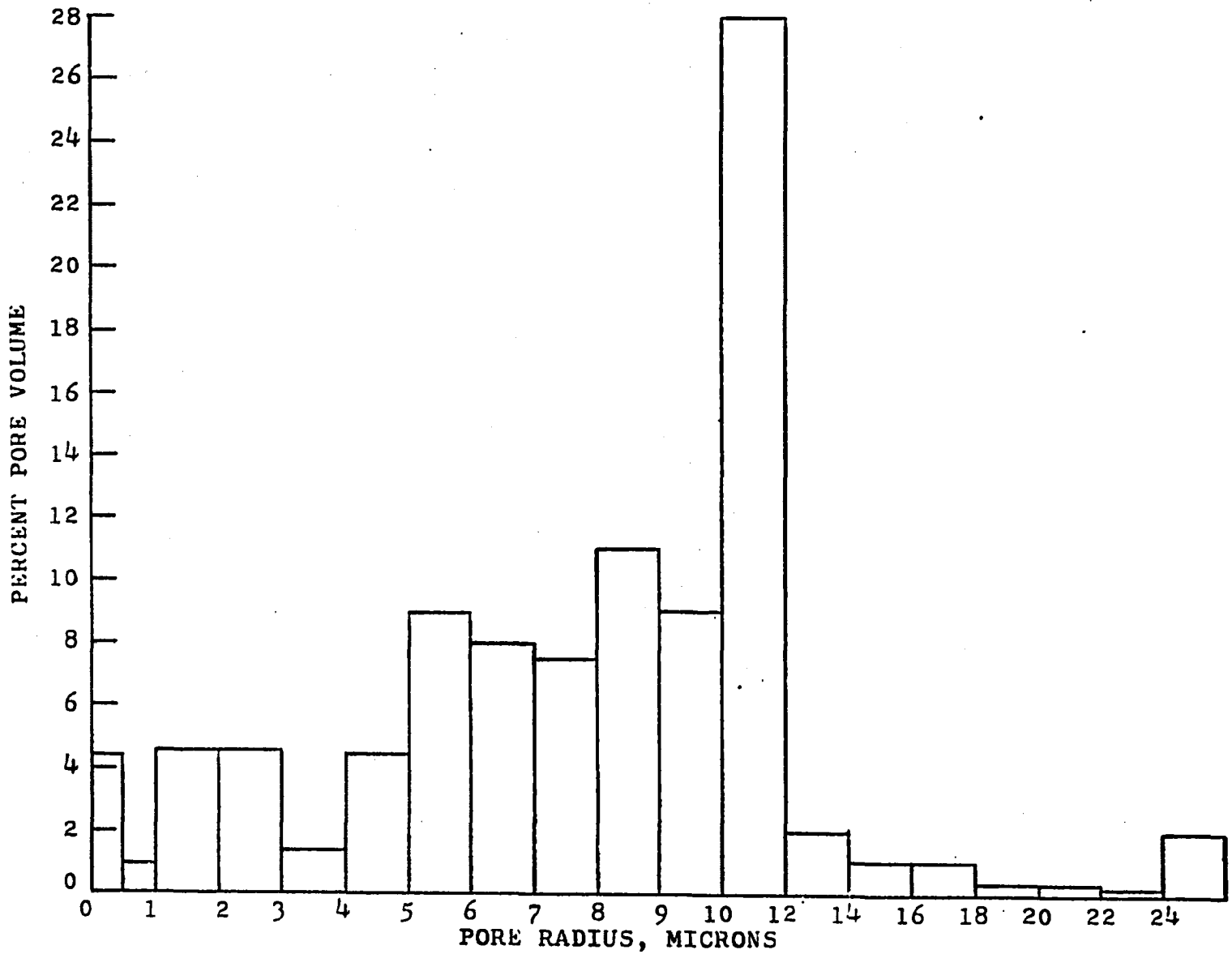

FIG. 32.--MERCURY INJECTION PORE SIZE DISTRIBUTION - CORE 48 (POROSITY 12.9%)

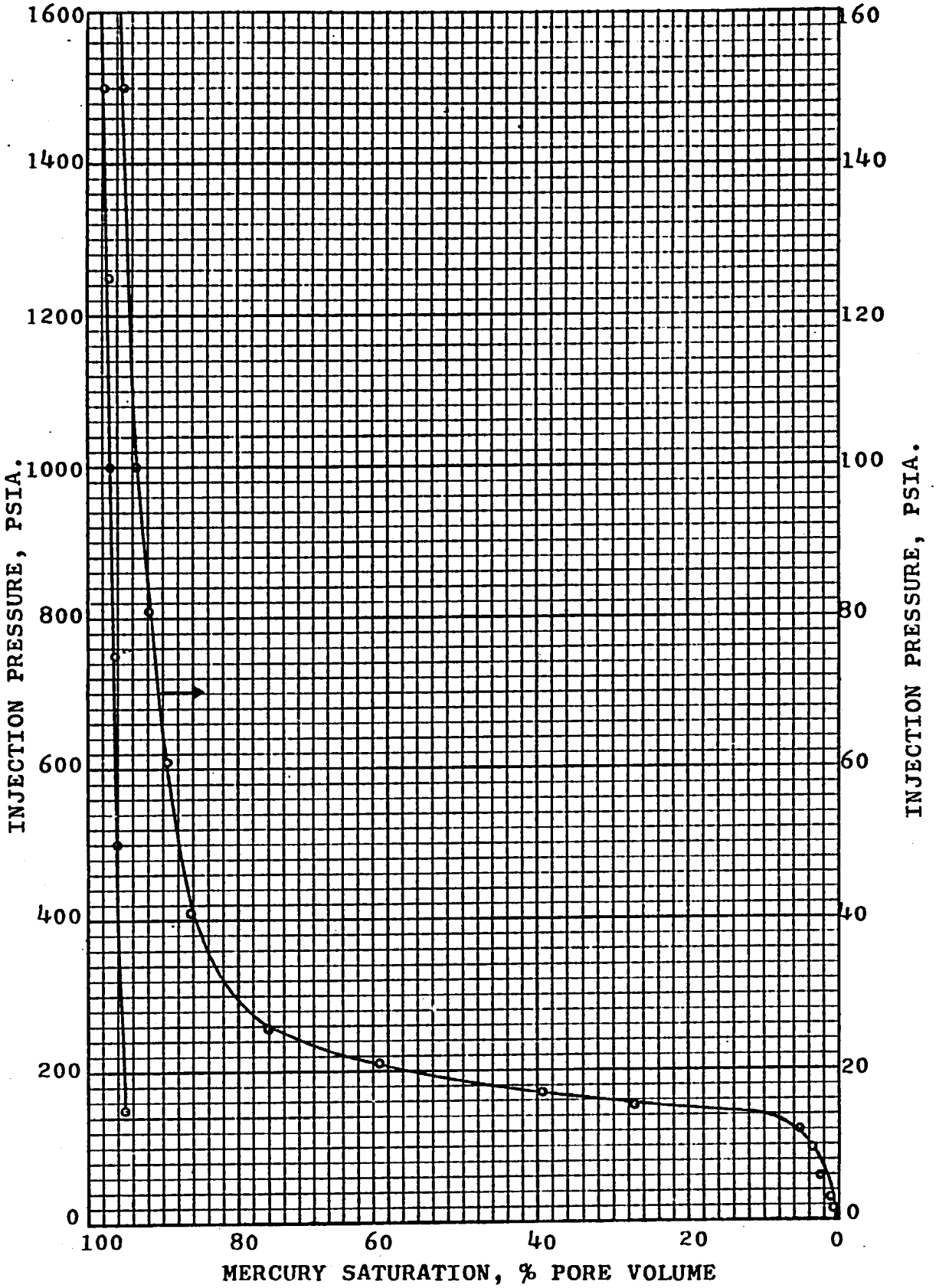

FIG. 33.--MERCURY INJECTION CAPILLARY PRESSURE DATA - CORE 65 (POROSITY = 13.5%)

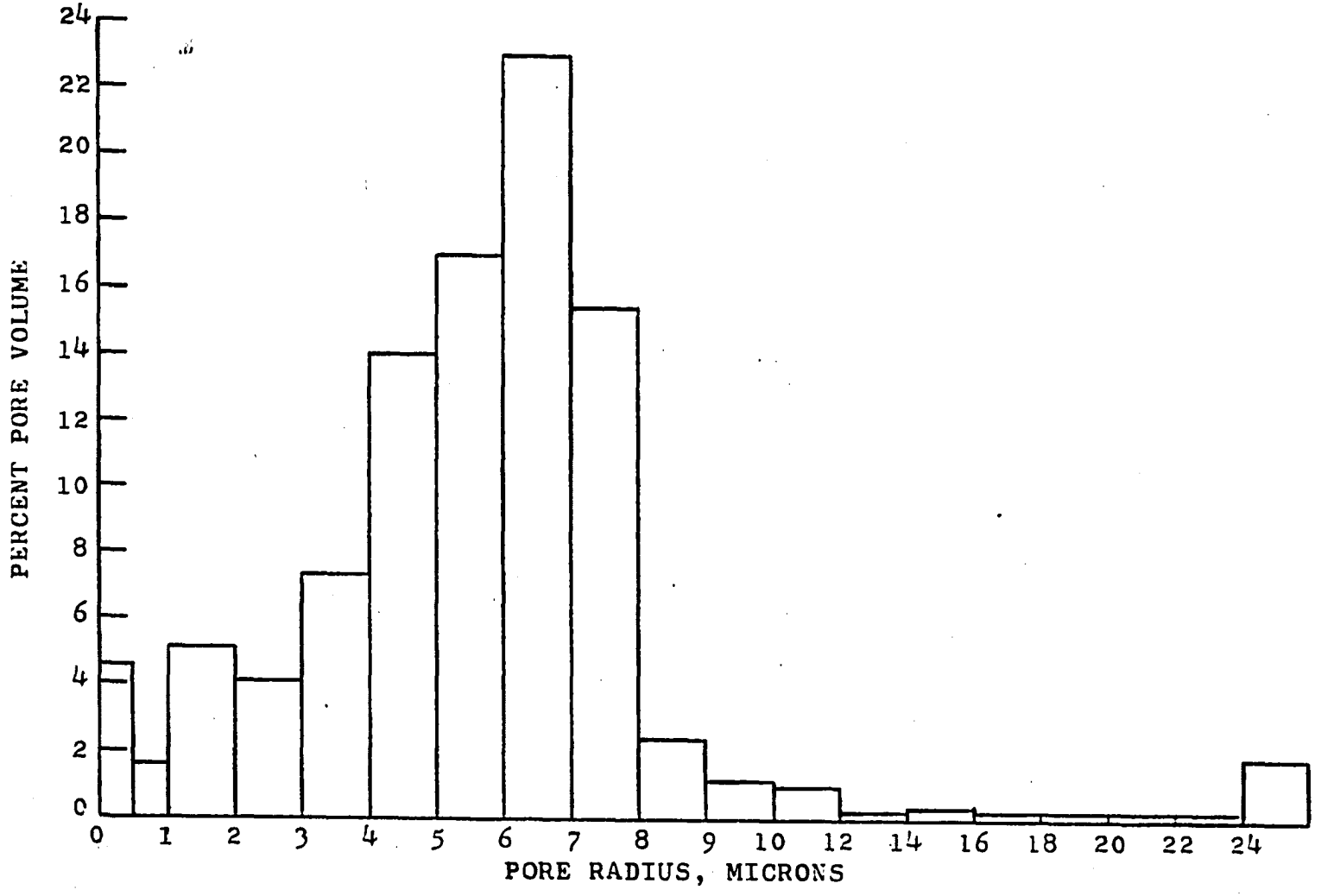

FIG. 34.--MERCURY INJECTION PORE SIZE DISTRIBUTION - CORE 65 (POROSITY = 13.2%)

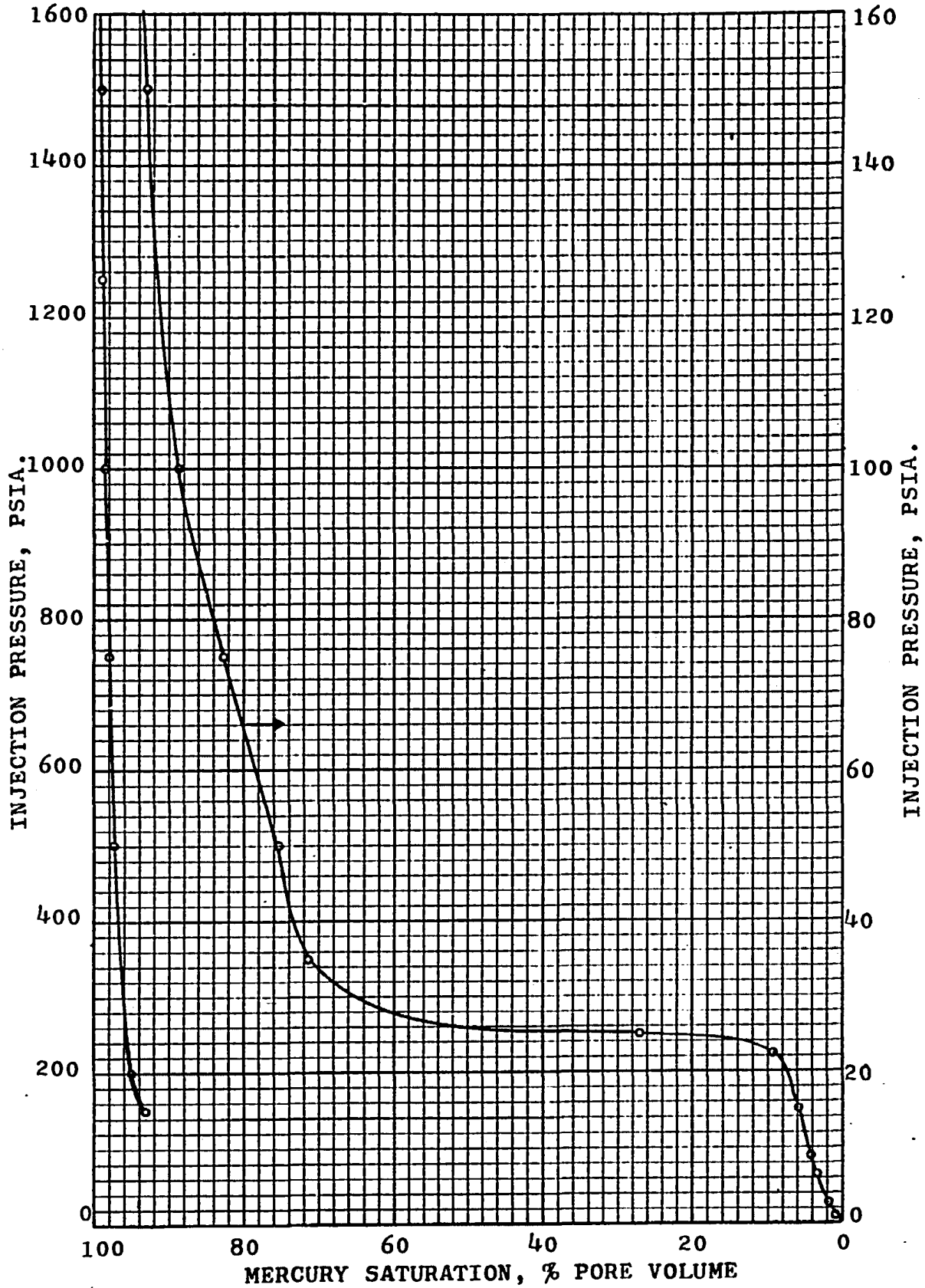

FIG. 35.--MERCURY INJECTION CAPILLARY PRESSURE DATA - CORE 48-3 (POROSITY = 15.9%)

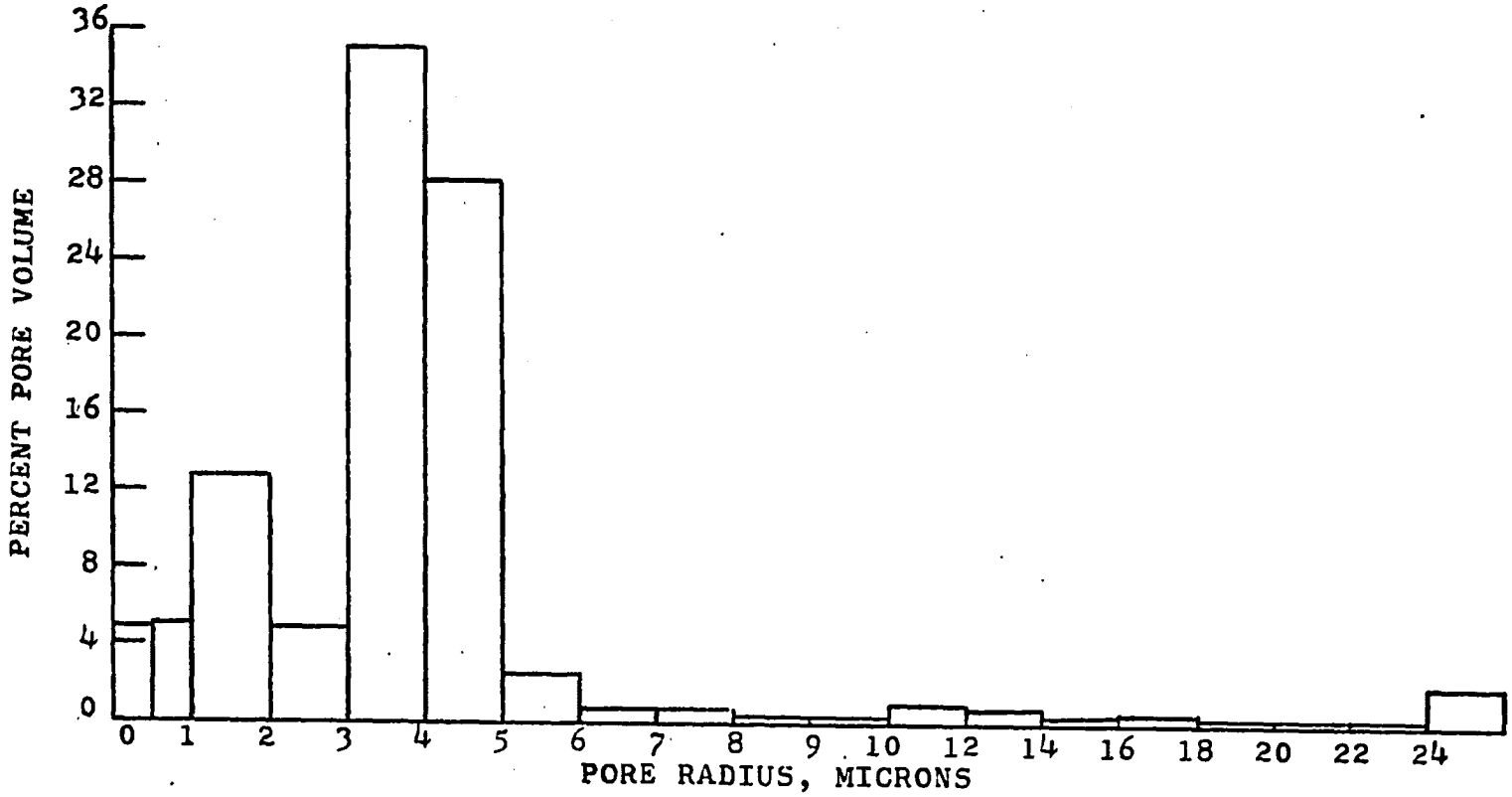

FIG. 36.--MERCURY INJECTION PORE SIZE DISTRIBUTION - CORE 48-3 (POROSITY = 15.9%)

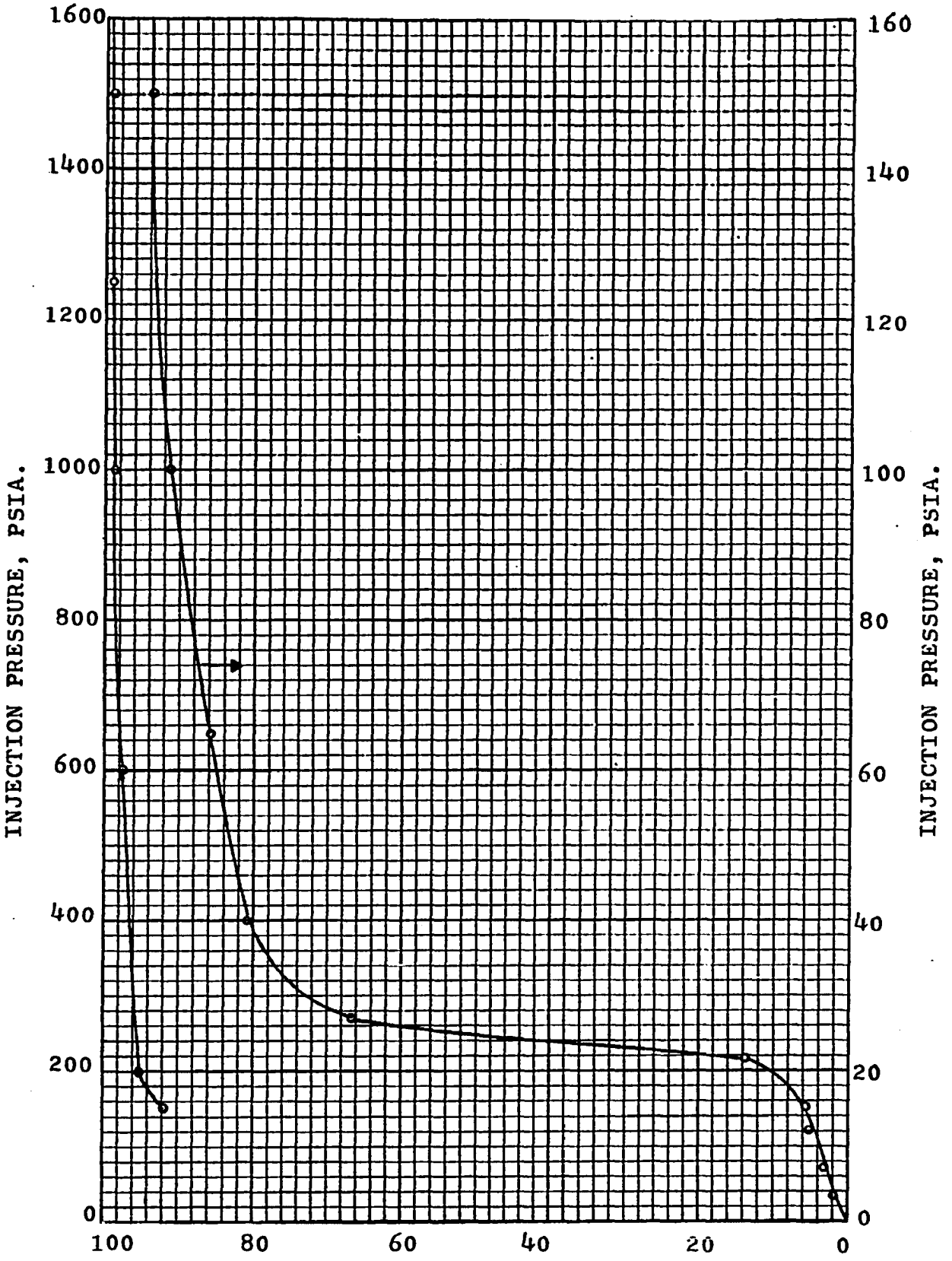

FIG. 37.--MERCURY INJECTION CAPILLARY PRESSURE DATA - CORE 65-3 (POROSITY = 13.25%)

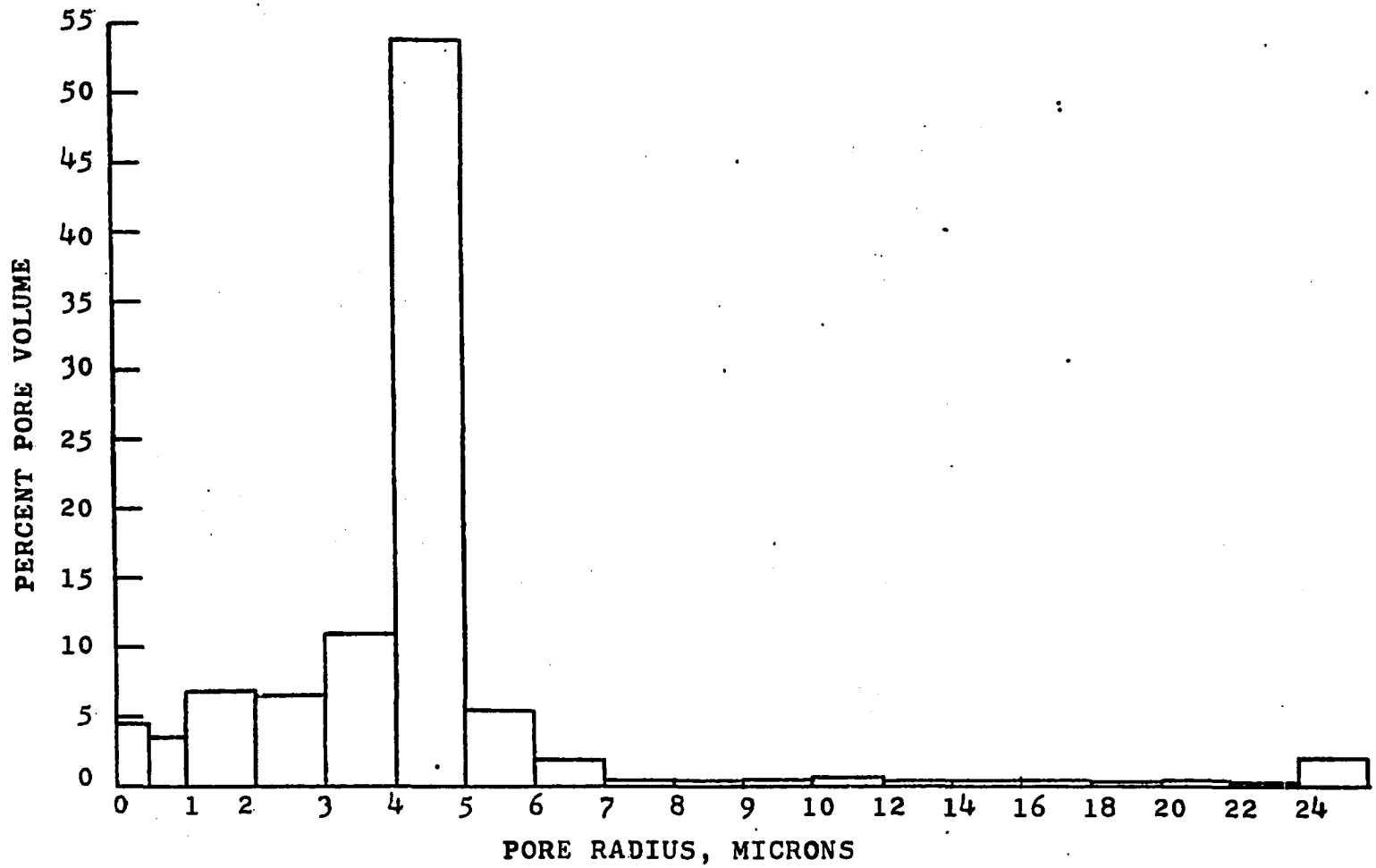

FIG. 38.--MERCURY INJECTION PORE SIZE DISTRIBUTION - CORE 65-3 (POROSITY = 13.25%)

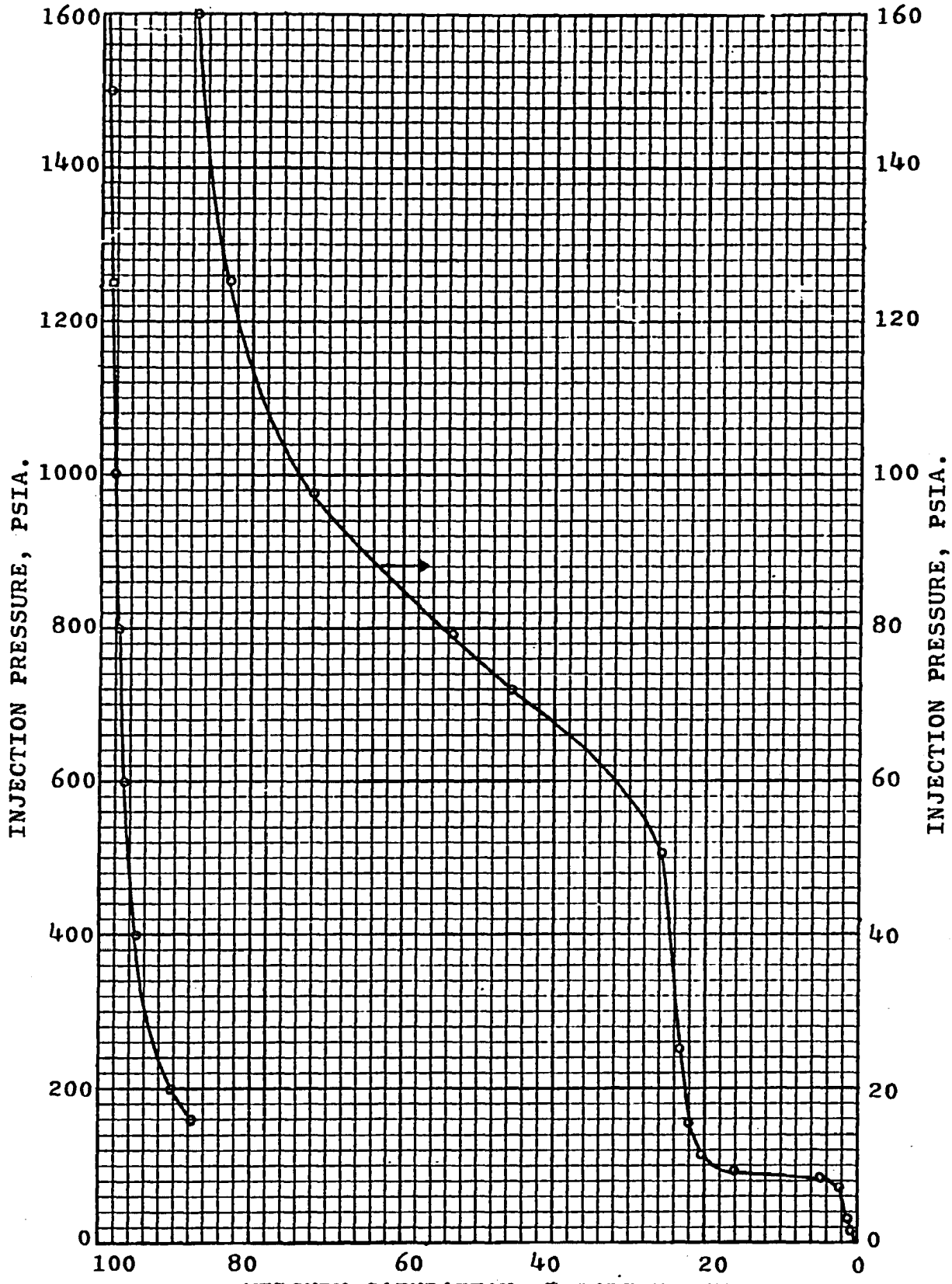

FIG. 39.--MERCURY INJECTION CAPILLARY PRESSURE DATA - CORE 200 (POROSITY = 16.67%)

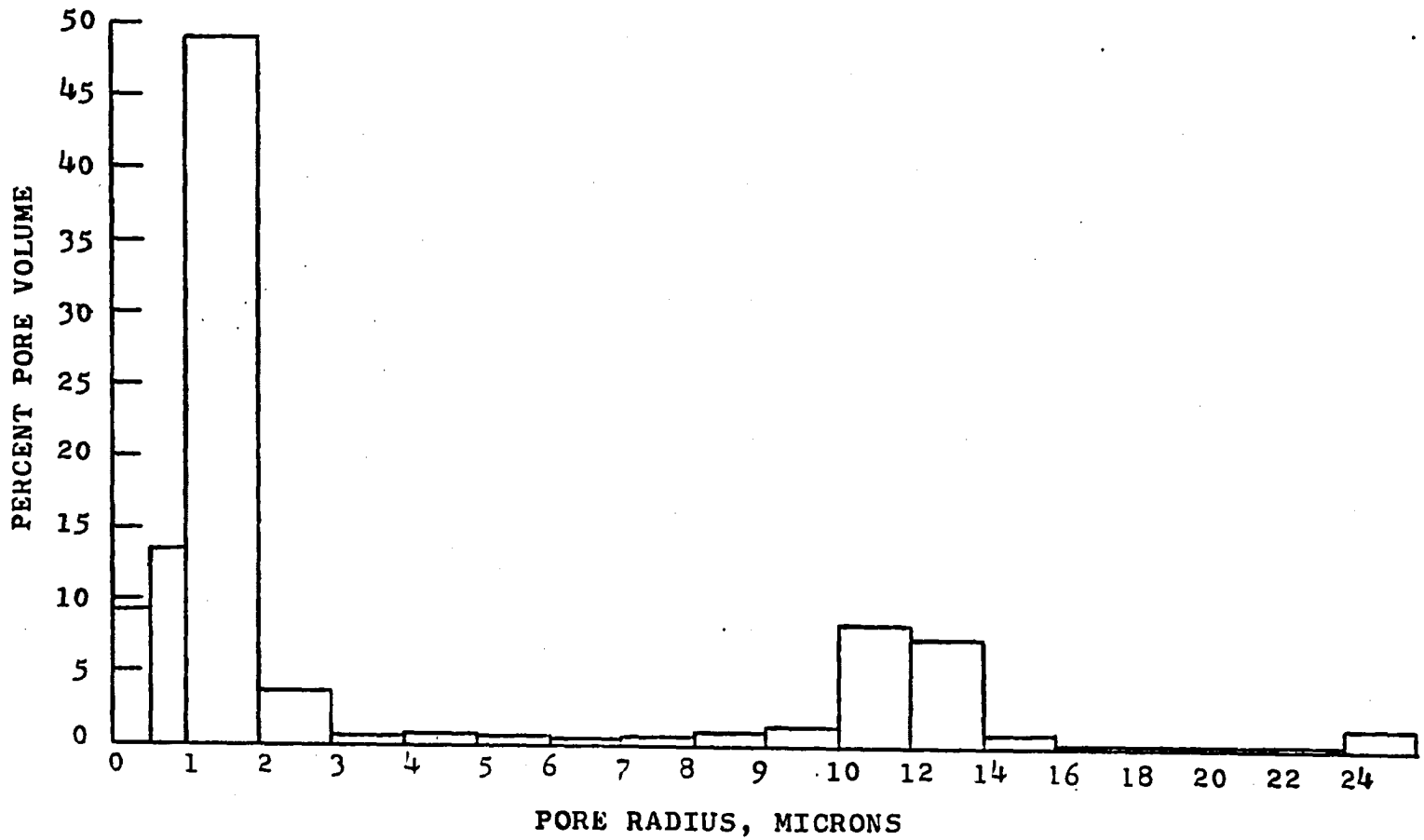

FIG. 40.--MERCURY INJECTION PORE SIZE DISTRIBUTION - CORE 200 (POROSITY = 16.67%)

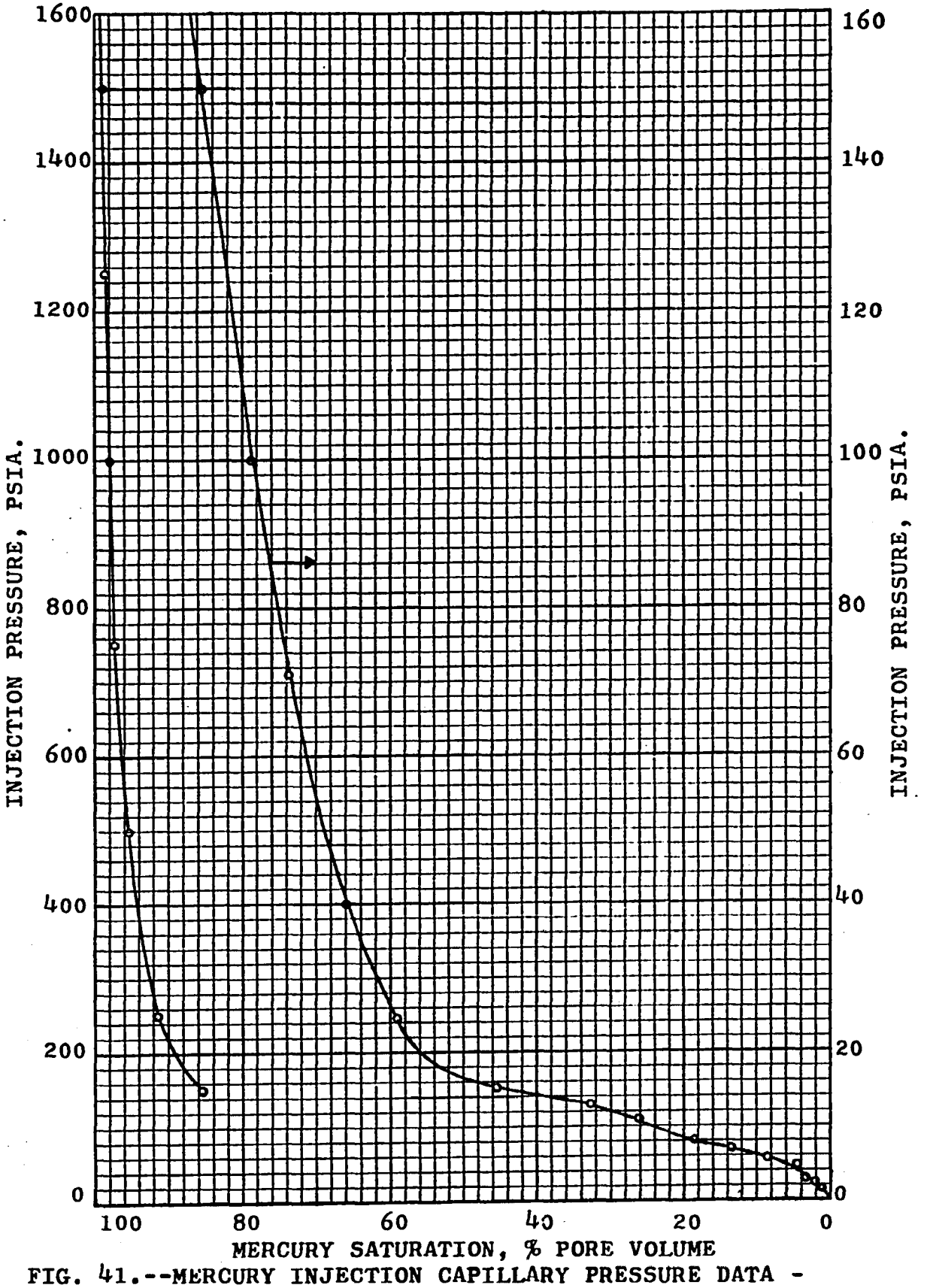

FIG. 41.--MERCURY INJECTION CAPILLARY PRESSURE DATA - CORE 65-S (POROSITY = 22.2%)

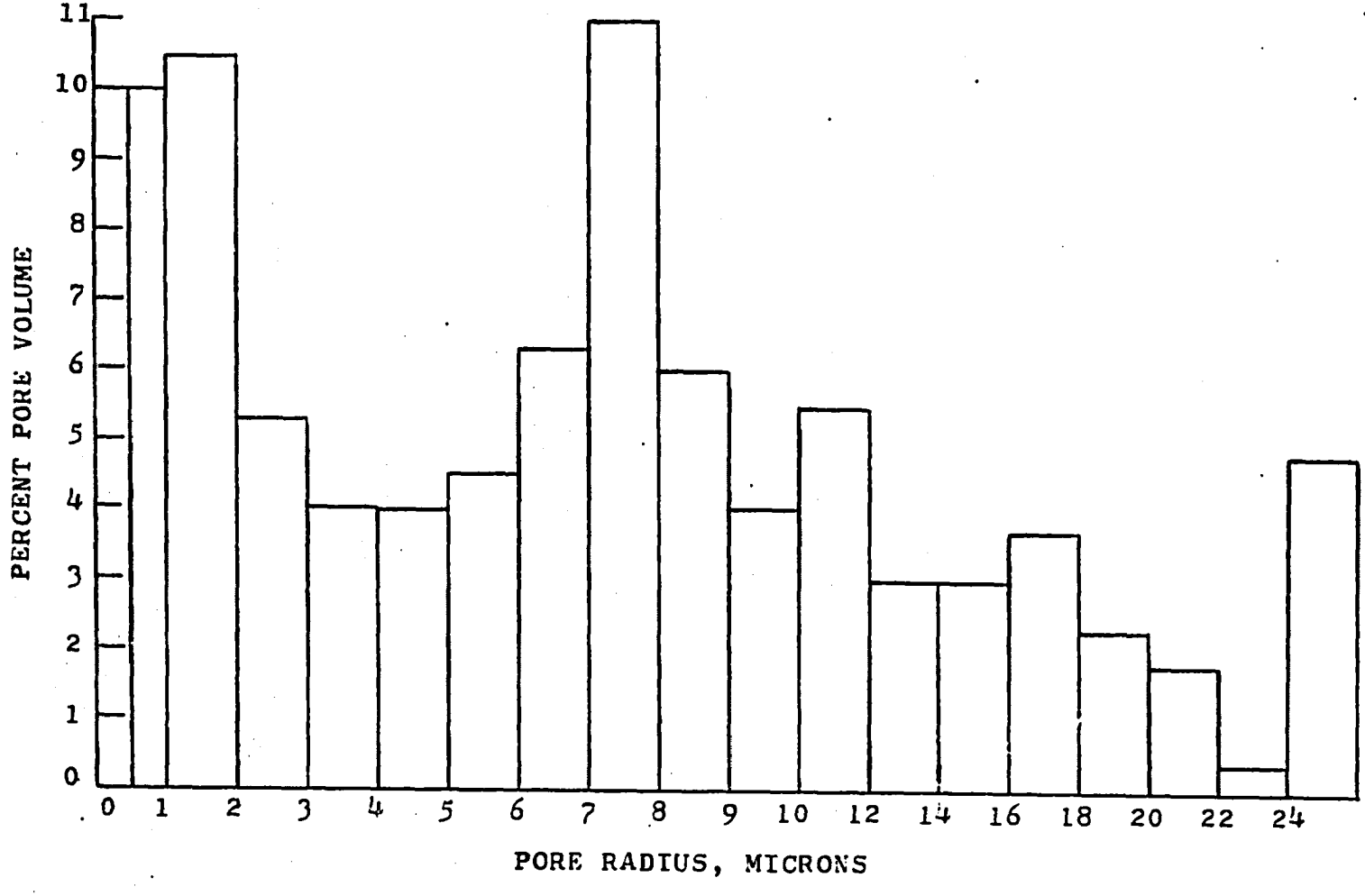

FIG. 42.--MERCURY INJECTION PORE SIZE DISTRIBUTION - CORE 65-S (POROSITY = 22.2%)

TABLE 6

SURFACE AREA CALCULATIONS

Core Number 35-1			
r(microns)	% PV	2(% PV)	$\frac{2(\%\ PV)}{r}$, cm^{-1}
25	2.07	4.14	165.60
23	.21	.42	18.26
21	.62	1.24	59.05
19	.62	1.24	65.26
17	1.03	2.06	121.18
15	1.65	3.30	220.00
13	4.14	8.28	636.92
11	9.82	19.64	1,785.45
9.5	4.65	9.30	978.95
8.5	8.27	16.54	1,945.88
7.5	9.31	18.62	2,482.66
6.5	10.13	20.26	3,116.92
5.5	14.68	29.36	5,338.18
4.5	7.24	14.48	3,217.77
3.5	2.90	5.80	1,657.14
2.5	3.10	6.20	2,480.00
1.5	6.31	12.62	8,413.33
.5	13.25	26.50	53,000.00
			85,702.55

Surface Area = 85,702.55 cm^2/Unit Pore Vol.

Pore Vol. in 35-1 = 7.8574 cm^1

Total Surface Area in 35-1 = 673,399.22 cm^2

Total Surface Area/Unit Bulk Vol. = $\frac{673,399.22}{61.29}$ = $10,987.09 cm^{-1}$

TABLE 6--Continued

Core Number 48-A			
r(microns)	% PV	2(% PV)	$\frac{2(\% PV)}{r}$, cm^{-1}
25	2.0	4.0	160.00
23	.2	.4	17.39
21	.4	.8	38.10
19	.4	.8	42.11
17	1.0	2.0	117.65
15	1.0	2.0	133.33
13	2.0	4.0	307.69
11	28.0	56.0	5,090.91
9.5	9.0	18.0	1,894.73
8.5	11.0	22.0	2,588.23
7.5	7.5	15.0	2,000.00
6.5	8.0	16.0	2,461.53
5.5	9.0	18.0	3,272.27
4.5	4.5	9.0	2,000.00
3.5	1.4	2.8	800.00
2.5	4.6	9.2	3,680.00
1.5	4.6	9.2	6,133.33
.5	5.4	10.8	21,600.00
			52,337.26

Surface Area = 52,337.26/Unit Pore Vol.

Pore Vol. in 48-A = 9.0451 cm^3

Total Surface Area in 48-A = 473,395.75 cm^2

Total Surface Area/Unit Bulk Vol. = $\frac{473,395.75}{61.53}$ = 7,693.73 cm^{-1}

TABLE 6--Continued

Core Number 65-1			
r(microns)	% PV	2(% PV)	$\frac{2(\% PV)}{r}$, cm^{-1}
25	1.8	3.6	144.00
23	.2	.4	17.39
21	.2	.4	19.05
19	.2	.4	21.05
17	.2	.4	23.53
15	.3	.6	40.00
13	.2	.4	30.77
11	.9	1.8	163.64
9.5	1.1	2.2	231.58
8.5	2.4	4.8	564.71
7.5	15.5	31.0	4,133.33
6.5	23.0	46.0	7,076.92
5.5	17.0	34.0	6,181.81
4.5	14.0	28.0	6,222.22
3.5	7.4	14.8	4,228.57
2.5	4.2	8.4	3,360.00
1.5	5.2	10.4	6,933.33
.5	6.2	12.4	24,800.00
			64,191.90

Surface Area = 64,191.90 cm^2/Unit Pore Vol.

Pore Vol. in 65-1 = 7.3983 cm^3

Total Surface Area in 65-1 = 474,910.93 cm^2

Total Surface Area/Unit Bulk Vol. = $\frac{474,910.93}{49.65}$ = $9,565.17\ cm^{-1}$

TABLE 6--Continued

Core Number 48-3			
r(microns)	% PV	2(% PV)	$\frac{2(\% PV)}{r}$, cm^{-1}
25	2.0	4.0	160.00
23	.2	.4	17.39
21	.2	.4	19.05
19	.2	.4	21.05
17	.4	.8	47.06
15	.3	.6	40.00
13	.6	1.2	92.31
11	.8	1.6	14.55
9.5	.3	.6	63.16
8.5	.3	.6	70.59
7.5	.5	1.0	133.33
6.5	.5	1.0	153.85
5.5	2.5	5.0	909.09
4.5	28.2	56.4	12,533.33
3.5	35.0	70.0	20,000.00
2.5	5.0	10.0	4,000.00
1.5	12.9	25.8	17,200.00
.5	10.1	20.2	40,400.00
			95,874.76

Surface Area = 95,874.76 cm^2/Unit Pore Vol.

Pore Vol. in 48-3-A = 10.2265 cm^3

Total Surface Area in 48-3-A = 980,463.23 cm^2

Total Surface Area/Unit Bulk Vol. = $\frac{980,463.23}{61.2363}$ = 16,011.14 cm^{-1}

TABLE 6--Continued

Core Number 65-3			
r(microns)	% PV	2(% PV)	$\frac{2(\% PV)}{r}$, cm^{-1}
25	2.1	4.2	168.00
23	.1	.2	8.10
21	.2	.4	19.04
19	.1	.2	10.53
17	.3	.6	35.29
15	.3	.6	40.00
13	.3	.6	46.15
11	.7	1.4	127.27
9.5	.5	1.0	105.30
8.5	.3	.6	705.88
7.5	.4	.8	1,066.67
6.5	1.9	3.8	584.62
5.5	5.5	11.0	2,000.00
4.5	53.8	107.6	23,911.10
3.5	11.0	22.0	6,285.71
2.5	6.5	13.0	5,200.00
1.5	6.9	13.8	9,200.00
.5	8.1	16.2	32,400.00
			81,914.26

Surface Area = 81,914.26 cm^2/Unit Pore Vol.

Pore Vol. in 65-3-A = 8.0243 cm^3

Total Surface Area in 65-3-A = 657,304.60 cm^2

Total Surface Area/Unit Bulk Vol. = $\frac{657,304.60}{58.6143}$ = 11,214.10 cm^{-1}

TABLE 6--Continued

Core Number 200			
r(microns)	% PV	2(% PV)	$\frac{2(\% PV)}{r}$, cm^{-1}
25	1.5	3.0	120.00
23	.1	.2	8.70
21	.1	.2	9.52
19	.1	.2	10.53
17	.1	.2	11.76
15	.9	1.8	120.00
13	7.5	15.0	1,153.85
11	8.5	17.0	1,545.45
9.5	1.5	3.0	315.79
8.5	1.0	2.0	235.29
7.5	.7	1.4	186.66
6.5	.5	1.0	153.85
5.5	.6	1.2	218.18
4.5	.8	1.6	355.56
3.5	.6	1.2	342.86
2.5	3.7	7.4	2,960.00
1.5	49.0	98.0	65,333.33
.5	22.8	45.6	91,200.00
			164,281.33

Surface Area = 164,281.33 cm^2/Unit Pore Vol.

Pore Vol. in 200-A = 9.4128 cm^3

Total Surface Area in 200-A = 1,546,347.30 cm^2

Total Surface Area/Unit Bulk Vol.= $\frac{1,546,347.30}{58.3861} = 26,484.8\ cm^{-1}$

TABLE 6--Continued

Core Number 65-S			
r(microns)	% PV	2(% PV)	$\frac{2(\% PV)}{r}$, cm^{-1}
25	4.8	9.6	384.00
23	.4	.8	34.78
21	1.8	3.6	171.43
19	2.3	4.6	242.11
17	3.7	7.4	435.29
15	3.0	6.0	400.00
13	3.0	6.0	461.54
11	5.5	11.0	1,000.00
9.5	4.0	8.0	842.11
8.5	6.0	12.0	1,411.76
7.5	11.0	22.0	2,933.33
6.5	6.3	12.6	1,938.46
5.5	4.5	9.0	1,636.36
4.5	3.9	7.8	1,733.33
3.5	4.0	8.0	2,285.71
2.5	5.3	10.6	4,240.00
1.5	10.5	21.0	14,000.00
.5	20.0	40.0	80,000.00
			114,150.21

Surface Area = 114,150.21 cm^2/Unit Pore Vol.

Pore Vol. in 65-S-A = 12.7629 cm^3

Total Surface Area in 65-S-A = 1,456,886.57 cm^2

Total Surface Area/Unit Bulk Vol. = $\frac{1,456,886.57}{59.7728} = 24,373.7\ cm^{-1}$

APPENDIX B

EXPERIMENTAL DATA

TABLE 7

RESISTIVITY CHANGES DUE TO PRESSURE

Core Number 35-1

L = 5.15 cm
D = 3.92 cm
A = 12.065 cm^2

Net Pressure, Psi	r, ohms	T(°F)	Rw, Ω-m	Total Percent Decrease in Area, A	Ro, Ω-m	F	$\frac{F^P}{F}$
0	74.1	86.5	.0665		3.519	52.9293	
100	123.0	83.8	.0685	2.874	5.6746	82.8408	1.5651
200	128.0	83.0	.0690	4.215	5.8237	84.4014	1.5946
400	137.0	82.4	.0693	4.566	6.2104	89.6161	1.6931
800	142.0	82.1	.0694	4.764	6.4237	92.5605	1.7488
1,200	151.0	81.5	.0696	4.911	6.8203	97.9928	1.8514
1,900	162.0	81.2	.0697	5.097	7.3208	104.7747	1.9795
3,000	185.0	80.9	.0698	5.358	8.3167	119.1504	2.2511
4,000	190.0	80.3	.0701	5.566	8.5227	121.5791	2.2970
6,000	210.0	80.0	.0704	5.863	9.3902	133.3835	2.5200
8,000	230.0	79.8	.0708	6.124	10.2560	144.858	2.7358
10,000	248.0	79.3	.0716	6.331	11.0342	154.108	2.9116

TABLE 7--Continued

Core Number 48-A

L = 5.08 cm
D = 3.92 cm
A = 12.065 cm^2

Net Pressure, Psi	r, ohms	T(°F)	Rw, Ω-m	Total Percent Decrease in Area, A	Ro, Ω-m	F	$\frac{F^P}{F}$
0	44.1	73.5	.077		2.0948	27.205	
100	56.1	76.3	.0744	3.9581	2.5593	34.399	1.2644
200	58.0	77.7	.0735	4.9773	2.6179	35.618	1.3092
400	58.8	78.0	.0731	5.3262	2.6442	36.172	1.3296
800	59.8	80.0	.0704	5.5954	2.6811	38.084	1.4000
1,200	61.0	80.1	.0702	5.7897	2.7302	38.892	1.496
2,000	64.8	80.1	.0702	6.1088	2.8900	41.168	1.5133
3,000	69.9	80.0	.0704	6.4224	3.1070	44.134	1.6223
4,000	74.8	79.7	.0709	6.6572	3.3165	46.777	1.7194
6,000	83.9	79.3	.0716	7.0488	3.7043	51.736	1.9017
8,000	92.9	78.9	.0721	7.3596	4.0880	56.699	2.0841
10,000	101.0	78.7	.0724	7.6223	4.4318	61.213	2.2501

TABLE 7--Continued

Core Number 65-1

L = 4.80 cm
D = 3.89 cm
A = 11.8787 cm^2

Net Pressure, Psi	r, ohms	T(°F)	Rw, Ω-m	Total Percent Decrease in Area, A	Ro, Ω-m	F	$\frac{F^P}{F}$
0	52.3	74.7	.0758		2.4459	32.268	
100	68.0	75.1	.0754	3.0709	3.0825	40.8819	1.2669
200	86.8	75.5	.0749	5.6252	3.8183	50.9786	1.5799
400	105.0	75.6	.0748	6.7934	4.5769	61.1885	1.8963
800	111.0	75.8	.0747	6.9626	4.8296	64.6532	2.0036
1,200	113.0	76.0	.0745	7.1258	4.9081	65.8805	2.0417
2,000	118.0	76.0	.0745	7.3748	5.1115	68.6107	2.1263
3,000	121.0	76.2	.0744	7.6252	5.2273	70.2594	2.1774
4,000	128.0	76.2	.0744	7.7692	5.5211	74.2083	2.2997
6,000	138.0	76.3	.0744	8.0258	5.9358	79.7822	2.4725
8,000	150.0	76.4	.0743	8.2382	6.4372	86.6379	2.6849
10,000	163.0	76.4	.0743	8.4210	6.9811	93.9582	2.9118

TABLE 7--Continued

Core Number 48-3-A

L = 4.90 cm
D = 3.99 cm
A = 12.4972 cm^2

Net Pressure, Psi	r, ohms	T(°F)	Rw, Ω-m	Total Percent Decrease in Area, A	Ro, Ω-m	F	$\frac{F^P}{F}$
0	40.2	76.2	.0745		1.9779	26.5489	
100	55.2	79.2	.0717	4.1302	2.6037	36.3138	1.3678
200	57.9	80.0	.0704	5.3166	2.6973	38.3139	1.4431
400	61.0	80.0	.0704	5.7051	2.8301	40.2002	1.5142
800	66.0	80.1	.0703	6.0892	3.0496	43.3798	1.6340
1,200	69.0	80.1	.0703	6.2824	3.1816	45.2574	1.7047
2,000	76.2	80.0	.0704	6.5851	3.5023	49.7485	1.8738
3,000	84.5	80.0	.0704	6.8260	3.8737	55.0241	2.0726
4,000	91.1	80.0	.0704	7.0350	4.1670	59.1903	2.2295
6,000	105.0	80.0	.0704	7.3453	4.7867	67.9928	2.5610
8,000	118.0	80.0	.0704	7.6115	5.3639	76.1917	2.8699
10,000	130.0	80.0	.0704	7.8509	5.8940	83.7215	3.1534

TABLE 7--Continued

Core Number 65-3-A

L = 4.96 cm
D = 3.88 cm
A = 11.8174 cm^2

Net Pressure, Psi	r, ohms	T(°F)	Rw, Ω-m	Total Percent Decrease in Area, A	Ro, Ω-m	F	$\frac{F^P}{F}$
0	72.2	76.7	.0741		3.3591	45.3319	
100	94.9	78.1	.0728	3.8091	4.2470	58.3379	1.2869
200	103.0	78.2	.0727	5.0351	4.5508	62.5969	1.3809
400	110.0	78.2	.0727	5.3562	4.8437	66.6258	1.4697
800	119.0	78.5	.0722	5.6155	5.2256	72.3767	1.5966
1,200	127.0	78.6	.0721	5.7694	5.5478	77.2233	1.7035
2,000	138.0	78.6	.0721	6.0444	6.0324	83.6671	1.8457
3,000	150.0	78.8	.0719	6.3490	6.5357	90.8998	2.0052
4,000	160.0	78.9	.0718	6.6064	6.9522	96.8272	2.1360
6,000	181.0	79.1	.0717	7.0232	7.8296	109.1994	2.4089
8,000	210.0	79.0	.0717	7.3332	9.0538	126.2733	2.7855
10,000	231.0	78.9	.0718	7.6070	9.9298	138.2980	3.0508

TABLE 7--Continued

Core Number 200-2

L = 5.21 cm
D = 3.89 cm
A = 11.8786 cm^2

Net Pressure, Psi	r, ohms	T(°F)	Rw, Ω-m	Total Percent Decrease in Area, A	Ro, Ω-m	F	$\frac{F^P}{F}$
0	112	69.8	.0805		5.2378	65.0658	
100	160	72.5	.0780	4.3799	7.1549	91.7294	1.4098
200	180	73.7	.0768	5.7163	7.9367	103.3424	1.5883
400	205	75.4	.0750	6.1573	8.9967	119.9560	1.8436
800	249	75.9	.0747	6.4651	10.8919	145.8085	2.2409
1,200	290	76.9	.0740	6.6666	12.6580	171.0540	2.6289
2,000	360	77.0	.0740	6.9318	15.6688	211.7405	3.2543
3,000	438	77.0	.0740	7.2178	19.0050	256.8243	3.9471
4,000	509	77.9	.0732	7.4896	22.0211	300.8346	4.6235
6,000	621	78.7	.0720	7.8694	26.7563	371.6152	5.7114
8,000	730	78.9	.0719	8.1210	31.3668	436.2559	6.7048
10,000	841	78.9	.0719	8.3650	36.0402	501.2545	7.7038

TABLE 7--Continued

Core Number 200-A

L = 4.89 cm
D = 3.90 cm
A = 11.9399 cm^2

Net Pressure, Psi	r, ohms	T(°F)	Rw, Ω-m	Total Percent Decrease in Area, A	Ro, Ω-m	F	$\frac{F^P}{F}$
0	90.8	64.7	.0870		4.2683	49.0609	
100	124.0	66.2	.0850	5.3626	5.5163	64.8976	1.3228
200	150.0	67.3	.0840	8.1689	6.4751	77.0845	1.5712
400	161.0	68.1	.0828	10.0031	6.8111	82.2597	1.6767
800	186.0	68.8	.0815	10.5863	7.8178	95.9239	1.9552
1,200	217.0	69.2	.0811	10.7414	9.1049	112.2676	2.2883
2,000	280.0	69.8	.0805	10.9218	11.7246	145.6472	2.9687
3,000	351.0	69.8	.0805	11.0963	14.6688	182.2211	3.7142
4,000	411.0	69.9	.0803	11.2410	17.1482	213.5516	4.3528
6,000	505.0	70.9	.0796	11.4776	21.0141	263.9962	5.3810

TABLE 7--Continued

Core Number 65-S-A

L = 4.96 cm
D = 3.88 cm
A = 11.8174 cm^2

Net Pressure, Psi	r, ohms	T(°F)	Rw, Ω-m	Total Percent Decrease in Area, A	Ro, Ω-m	F	$\frac{F^P}{F}$
0	72.0	73.2	.0773		3.3498	43.3350	
100	109.0	75.6	.0749	3.8702	4.8749	65.0854	1.5019
200	122.0	76.1	.0746	7.1625	5.2695	70.6367	1.6300
400	138.0	77.3	.0737	7.4770	5.9403	80.6011	1.8602
800	160.0	77.3	.0737	7.8362	6.8607	93.0896	2.1481
1,200	176.0	77.1	.0739	8.0423	7.5299	101.8931	2.3513
2,000	209.0	76.3	.0744	8.4212	8.9048	119.6882	2.7619
3,000	258.0	76.3	.0744	8.8403	10.9423	147.0739	3.3939
4,000	299.0	76.0	.0746	9.1535	12.6377	169.4061	3.9092
6,000	378.0	75.3	.0751	9.6880	15.8826	211.4860	4.8803
8,000	457.0	73.8	.0767	10.1745	19.0986	249.0039	5.7460

TABLE 8

COMPRESSIBILITY DATA

Core Number 35-1			
Net Pressure, Psi	ΔPV, cc	PV, cc	Cp x 10^6, Psi^{-1}
0		7.8574	
	2.6188		
200		5.2386	1666
	.4321		
1,200		4.8065	82.48
	.1158		
1,900		4.6907	34.42
	.1625		
3,000		4.5282	31.49
	.1290		
4,000		4.3992	28.49
	.1844		
6,000		4.2148	20.96
	.1620		
8,000		4.0528	19.22
	.1291		
10,000		3.9237	15.93

Core Number 48-A			
Net Pressure, Psi	ΔPV, cc	PV, cc	Cp x 10^6, Psi^{-1}
0		9.0451	
	3.0506		
200		5.9945	1686
	.4979		
1,200		5.4966	83.06
	.1956		
2,000		5.3010	44.48
	.1922		
3,000		5.1088	36.26
	.1439		
4,000		4.9649	28.17
	.2400		
6,000		4.7249	24.17
	.1905		
8,000		4.5344	20.16
	.1610		
10,000		4.3744	17.75

TABLE 8--Continued

Net Pressure, Psi	ΔPV, cc	PV, cc	Cp x 10^6, Psi^{-1}
Core Number 65-1			
0		7.3983	
	3.2069		
200		4.1914	2167
	.8555		
1,200		3.3359	204.1
	.1420		
2,000		3.1939	53.21
	.1427		
3,000		3.0512	44.68
	.0821		
4,000		2.9691	26.91
	.1463		
6,000		2.8228	24.64
	.1211		
8,000		2.7017	21.45
	.1042		
10,000		2.5975	20.06
Core Number 48-3-A			
0		10.2260	
	3.2557		
200		6.9703	1592
	.5914		
1,200		6.3789	84.85
	.1854		
2,000		6.1935	36.33
	.1475		
3,000		6.0460	23.82
	.1280		
4,000		5.9180	21.17
	.1900		
6,000		5.7280	16.05
	.1630		
8,000		5.5650	14.23
	.1466		
10,000		5.4184	13.17

TABLE 8--Continued

Net Pressure, Psi	ΔPV, cc	PV, cc	Cp x 10^6, Psi^{-1}
	Core Number 65-3-A		
0		8.0225	
	2.9513		
200		5.0694	1839
	.4304		
1,200		4.6390	84.90
	.1612		
2,000		4.4778	43.44
	.1785		
3,000		4.2993	39.86
	.1509		
4,000		4.1484	35.10
	.2443		
6,000		3.9041	29.45
	.1817		
8,000		3.7224	23.27
	.1605		
10,000		3.5619	21.56
	Core Number 200-2		
Net Pressure, Psi	ΔPV, cc	PV, cc	Cp x 10^6, Psi^{-1}
0		8.3657	
	3.5377		
200		4.8280	2114
	.5881		
1,200		4.2399	121.81
	.1641		
2,000		4.0758	48.38
	.1770		
3,000		3.8988	43.43
	.1682		
4,000		3.7306	43.14
	.2351		
6,000		3.4955	31.51
	.1557		
8,000		3.3398	22.27
	.1510		
10,000		3.1888	22.60

TABLE 8--Continued

Net Pressure, Psi	ΔPV, cc	PV, cc	Cp x 10^6, Psi^{-1}
Core Number 200-A			
0		9.4128	
	4.7695		
200		4.6433	2533
	1.5020		
1,200		3.1413	323.48
	.1053		
2,000		3.0360	41.90
	.1019		
3,000		2.9341	33.56
	.0845		
4,000		2.8496	28.80
	.1381		
6,000		2.7115	24.23
Core Number 65-S-A			
0		12.7629	
	4.2812		
200		8.4817	1677
	.5259		
1,200		7.9558	62.00
	.2265		
2,000		7.7293	36.63
	.2505		
3,000		7.4788	33.49
	.1872		
4,000		7.2916	25.67
	.3195		
6,000		6.9721	22.91
	.2908		
8,000		6.6813	21.76

TABLE 9

CHANGE IN m ($F = \phi^{-m}$) WITH NET PRESSURE

Core Number 48-A

BV = 61.29 cc
ϕ = 14.7%
PV = 9.0451

Net Pressure, Psi	BV	PV	ϕ	log F	log ϕ	log ϕ	m	Δm
0	61.29	9.0451	14.70	1.43465	-1.16732	.83268-2	1.7229	0
200	58.2394	5.9945	10.2929	1.55167	-1.01257	.98743-2	1.5714	-.1515
1,200	57.7415	5.4966	9.5193	1.58986	-2.97860	1.02140-4	1.5565	-.1664
2,000	57.5459	5.3010	9.2118	1.61456	-2.96434	1.03566-4	1.5590	-.1639
3,000	57.3537	5.1088	8.9075	1.64477	-2.94976	1.05024-4	1.5661	-.1568
4,000	57.2098	4.9649	8.6784	1.67003	-2.93844	1.06156-4	1.5732	-.1497
6,000	56.9698	4.7249	8.2937	1.71379	-2.91875	1.08125-4	1.5850	-.1379
8,000	56.7793	4.5344	7.9860	1.75357	-2.90233	1.09767-4	1.5975	-.1254
10,000	56.6183	4.3744	7.7261	1.78684	-2.88796	1.11204-4	1.6068	-.1161

TABLE 9--Continued

Core Number 35-1

BV = 62.13
ϕ = 12.82%
PV = 7.8574

Net Pressure, Psi	BV	PV	ϕ	log F	log ϕ	log ϕ	m	Δm
0	62.13	7.8574	12.82	1.72369	-1.10789	.89211-2	1.9321	0
200	59.5112	5.2386	8.8027	1.92635	-2.94462	1.05538-4	1.8253	-.1068
1,200	59.0791	4.8065	8.1357	1.99119	-2.91040	1.08960-4	1.8275	-.1046
1,900	58.9633	4.6907	7.9553	2.02025	-2.90066	1.09934-4	1.8377	-.0944
3,000	58.8008	4.5282	7.7009	1.8645	-2.88654	1.11346-4	1.8645	-.0676
4,000	58.6718	4.3992	7.4980	2.08486	-2.87495	1.12505-4	1.8531	-.0790
6,000	58.4874	4.2148	7.2063	2.12509	-2.85771	1.14229-4	1.8604	-.0717
8,000	58.3254	4.0528	6.9486	2.16095	-2.84190	1.15810-4	1.8659	-.0662
10,000	58.1963	3.9237	6.7422	2.18783	-2.82880	1.17120-4	1.8680	-.0641

TABLE 9--Continued

Core Number 65-1

BV = 57.01 cm^3
ϕ = 14.90%
PV = 7.3983 cm^3

Net Pressure, Psi	BV	PV	ϕ	log F	log ϕ	log ϕ	m	Δm
0	57.01	7.3983	14.90	1.50867	-1.87319	.82681-2	1.8247	0
200	53.8031	4.1914	7.7903	1.70739	-2.89155	1.10845-4	1.5403	-.2884
1,200	52.9476	3.3359	6.3004	1.81875	-2.79937	1.20063-4	1.5148	-.3099
2,000	52.8056	3.1939	6.0484	1.83639	-2.78164	1.21836-4	1.5073	-.3174
3,000	52.6629	3.0512	5.7938	1.84671	-2.76296	1.23704-4	1.4928	-.3319
4,000	52.5808	2.9691	5.6467	1.87045	-2.75180	1.24820-4	1.4985	-.3262
6,000	52.4345	2.8228	5.3835	1.90190	-2.73107	1.26893-4	1.4988	-.3259
8,000	52.3134	2.7017	5.1645	1.93771	-2.71303	1.28697-4	1.5056	-.3191
10,000	52.2092	2.5975	4.9752	1.97293	-2.69681	1.30319-4	1.5139	-.3108

TABLE 9--Continued

Core Number 200-2

BV = 61.8875 cm^3
ϕ = 13.52%
PV = 8.3657 cm^3

Net Pressure, Psi	BV	PV	ϕ	log F	log ϕ	log ϕ	m	Δm
0	61.8875	8.3657	13.5176	1.81335	-1.13089	.86911	2.0864	0
200	58.3498	4.8280	8.2742	2.01428	-2.91773	1.08227-4	1.8612	-.2252
1,200	57.7617	4.2399	7.3403	2.23314	-2.86572	1.13428-4	1.9688	-.1176
2,000	57.5976	4.0758	7.0763	2.32580	-2.84980	1.15020-4	2.0221	-.0643
3,000	57.4206	3.8988	6.7899	2.40963	-2.83186	1.16814-4	2.0628	-.0236
4,000	57.2524	3.7306	6.5160	2.47833	-2.81398	1.18602-4	2.0896	+.0032
6,000	57.0173	3.4955	6.1306	2.57010	-2.78750	1.21250-4	2.1197	+.0333
8,000	56.8616	3.3398	5.8736	2.63975	-2.76890	1.23110-4	2.1442	+.0578
10,000	56.7106	3.1888	5.6229	2.70006	-2.74996	1.25004-4	2.1600	+.0736

TABLE 9--Continued

Core Number 48-3-A

BV = 61.2363 cm^3
ϕ = 16.70%
PV = 10.2260 cm^3

Net Pressure, Psi	BV	PV	ϕ	log F	log ϕ	log ϕ	m	Δm
0	61.2363	10.2260	16.70	1.42404	-1.22272	.77728-2	1.8321	0
200	57.9806	6.9703	12.0218	1.58336	-1.07997	.92003-2	1.7210	-.1111
1,200	57.3892	6.3789	11.1152	1.65569	-1.04591	.95402-2	1.7355	-.0966
2,000	57.2038	6.1935	10.8271	1.69678	-1.03451	.96549-2	1.7574	-.0747
3,000	57.0563	6.0460	10.5966	1.74055	-1.02516	.97484-2	1.7855	-.0466
4,000	56.9283	5.9180	10.3955	1.77225	-1.01684	.98316-2	1.8026	-.0295
6,000	56.7383	5.7280	10.0955	1.83247	-1.00413	.99587-2	1.8401	+.0080
8,000	56.5753	5.5650	9.8364	1.88191	-2.99284	1.00716-4	1.8685	+.0364
10,000	56.4287	5.4184	9.6022	1.92284	-2.98237	1.01763-4	1.8895	+.0574

TABLE 9--Continued

Core Number 65-3-A

BV = 58.6143 cm^3
ϕ = 13.6869%
PV = 8.0225 cm^3

Net Pressure, Psi	BV	PV	ϕ	log F	log ϕ	log ϕ	m	Δm
0	58.6143	8.0225	13.6869	1.65641	-1.13637	.86363-2	1.9180	0
200	55.6630	5.0694	9.1073	1.79655	-2.95939	1.04061-4	1.7264	-.1916
1,200	55.2326	4.6390	8.3990	1.88775	-2.94423	1.07577-4	1.7548	-.1632
2,000	55.0714	4.4778	8.1309	1.92256	-2.91013	1.08987-4	1.7640	-.1540
3,000	54.8929	4.2993	7.8322	1.95856	-2.89388	1.10612-4	1.7707	-.1473
4,000	54.7420	4.1484	7.5781	1.98600	-2.87956	1.12044-4	1.7725	-.1455
6,000	54.4977	3.9041	7.1638	2.03822	-2.85515	1.14485-4	1.7803	-.1377
8,000	54.3160	3.7224	6.8532	2.10130	-2.83589	1.16411-4	1.8051	-.1129
10,000	54.1555	3.5619	6.5772	2.14082	-2.81804	1.18196-4	1.8112	-.1068

TABLE 9--Continued

Core Number 200-A

BV = 58.3861 cm^3
ϕ = 16.1216
PV = 9.4128

Net Pressure, Psi	BV	PV	ϕ	log F	log ϕ	log ϕ	m	Δm
0	58.3861	9.4128	16.1216	1.69074	-1.20742	.79258-2	2.1332	0
200	53.6166	4.6433	8.6602	1.88697	-2.93753	1.06247-4	1.7760	-.3572
1,200	52.1146	3.1413	6.0277	2.05026	-2.78015	1.21985-4	1.6807	-.4525
2,000	52.0093	3.0360	5.8374	2.16330	-2.76622	1.23378-4	1.7534	-.3798
3,000	51.9074	2.9341	5.6526	2.26060	-2.75225	1.24775-4	1.8117	-.3215
4,000	51.8229	2.8496	5.4987	2.32950	-2.74026	1.25974-4	1.8492	-.2840
6,000	51.6848	2.7115	5.2462	2.42159	-2.71985	1.28015-4	1.8916	-.2416

TABLE 9--Continued

Core Number 65-S-A

BV = 59.7728
ϕ = 21.3523
PV = 12.7629

Net Pressure, Psi	BV	PV	ϕ	log F	log ϕ	log ϕ	m	Δm
0	59.7728	12.7629	21.3523	1.63684	-1.32944	.67056-2	2.4410	0
200	55.4916	8.4817	15.2847	1.84901	-1.18426	.81574-2	2.2667	-.1743
1,200	54.9657	7.9558	14.4741	2.00814	-1.16059	.83941-2	2.3923	-.0487
2,000	54.7392	7.7293	14.1202	2.07805	-1.14984	.85016-2	2.4443	+.0033
3,000	54.4887	7.4788	13.7254	2.16754	-1.13752	.86248-2	2.5131	+.0721
4,000	54.3015	7.2916	13.4280	2.22893	-1.12801	.87199-2	2.5561	+.1151
6,000	53.9820	6.9721	12.9156	2.32528	-1.11111	.88889-2	2.6159	+.1749
8,000	53.6912	6.6813	12.4439	2.39621	-1.09502	.90498-2	2.6478	+.2068

TABLE 10

CHANGE IN m ($\Delta m = m^P - m^{1200}$) WITH NET PRESSURE

Net Pressure, Psi	48-A	35-1	65-1	200-2	48-3-A	65-3-A	200-A	65-S-A
1,200	0	0	0	0	0	0	0	0
2,000	+.0025	+.0102	-.0075	+.0533	+.0219	+.0092	+.0727	+.0520
3,000	+.0096	+.0370	-.0220	+.0940	+.0500	+.0159	+.1310	+.1208
4,000	+.0167	+.0256	-.0163	+.1208	+.0671	+.0177	+.1685	+.1638
6,000	+.0285	+.0329	-.0160	+.1509	+.1046	+.0255	+.2109	+.2236
8,000	+.0410	+.0384	-.0092	+.1754	+.1330	+.0503		+.2555
10,000	+.0503	+.0405	-.0009	+.1912	+.1540	+.0564		

TABLE 11

RESISTIVITY CHANGES DUE TO TEMPERATURE

Core Number 35-1

Net Pressure, Psi	T, °F	r,	Rw, Ω-m	Re, Ω-m	F	$\frac{F^T}{F}$
2100-1100	73.7	95.7	.0768	4.5458	59.1901	
	106.1	70.2	.0545	3.3345	61.1834	1.03337
	148.7	53.4	.0380	2.5365	66.7500	1.1277
	198.7	42.2	.0269	2.0045	74.5167	1.2589
	238.2	36.6	.0219	1.7385	79.3835	1.3412
	277.4	30.6	.0181	1.4535	80.3038	1.3567
	317.6	29.2	.01495	1.3870	92.7759	1.5674

Core Number 48-A

Net Pressure, Psi	T, °F	r,	Rw, Ω-m	Re, Ω-m	F	$\frac{F^T}{F}$
2100-1100	69.0	54.6	.0815	2.5935	31.822	
	124.6	30.9	.0470	[illegible]	31.230	.9814
	175.0	26.6	.0320	[illegible]	[illegible].484	1.2408
	223.1	22.0	.0240	1.0450	43.541	1.3683
	272.9	17.4	.0183	.8265	45.164	1.4193
	320.0	15.8	.0149	.7505	50.369	1.5828
	376.8	15.5	.0120	.73625	61.354	1.9280

TABLE 11--Continued

Core Number 65-1

Net Pressure, Psi	T, °F	r,	Rw, Ω-m	Re, Ω-m	F	$\frac{F^T}{F}$
2100-1100	70.9	68.7	0.0800	3.2129	40.1612	
	105.1	47.9	0.0558	2.2401	40.1451	0.9996
	136.5	39.0	0.0420	1.8239	43.4261	1.0813
	160.5	34.4	0.0347	1.6088	46.3631	1.1544
	197.5	28.1	0.0271	1.3142	48.4944	1.2075
	239.7	24.8	0.0218	1.1598	53.2018	1.3247
	274.9	21.0	0.0181	0.9821	54.2597	1.3510
	311.7	20.3	0.0153	0.9494	62.0523	1.5451

Core Number 48-3A

Net Pressure, Psi	T, °F	r,	Rw, Ω-m	Re, Ω-m	F	$\frac{F^T}{F}$
2100-1100	68.0	70.0	0.0830	3.4441	41.4951	
	104.2	50.2	0.0558	2.4699	44.2634	1.0667
	139.3	40.0	0.0410	1.9681	48.0024	1.1568
	174.3	33.0	0.0315	1.6236	51.5428	1.2421
	203.2	29.1	0.0264	1.4318	54.2348	1.3070
	237.0	25.0	0.0220	1.2300	55.9090	1.3474
	273.5	21.0	0.0183	1.0332	56.4590	1.3606
	316.7	19.8	0.0150	0.9742	64.9467	1.5652

TABLE 11--Continued

Core Number 65-3-A

Net Pressure, Psi	T, °F	r,	Rw, Ω-m	Re, Ω-m	F	$\frac{F^T}{F}$
2100-1100	71.9	88.6	0.0785	4.1221	52.5108	
	108.7	63.6	0.0538	2.9590	55.0000	1.0474
	136.2	53.6	0.0421	2.4937	59.2327	1.1280
	167.2	45.0	0.0332	2.0936	63.0602	1.2007
	201.3	38.8	0.0265	1.8052	68.1207	1.2973
	236.5	32.8	0.0220	1.5260	69.3636	1.3209
	274.4	27.7	0.0182	1.2887	70.8076	1.3484
	319.2	27.1	0.0149	1.2608	84.6174	1.6114

Core Number 200-A

Net Pressure, Psi	T, °F	r,	Rw, Ω-m	Re, Ω-m	F	$\frac{F^T}{F}$
2100-1100	70	151.0	.0802	7.0981	88.5049	
	104	121.0	.0560	5.6879	101.5696	1.1476
	144	97.9	.0390	4.6020	118.0000	1.3333
	176.2	81.0	.0313	3.8076	121.6485	1.3745
	203.5	69.0	.0265	3.2435	122.3962	1.3829
	237.0	55.0	.0218	2.5854	118.5963	1.3400
	279.5	33.0	.0180	1.5512	86.1777	0.9737
	315.0	33.8	.0150	1.5889	105.9266	1.1968

TABLE 11--Continued

Core Number 200-2

Net Pressure, Psi	T, °F	r,	Rw, Ω-m	Re, Ω-m	F	$\frac{F^T}{F}$
2100-1100	72.0	239.0	0.0784	11.1771	142.565	
	104.1	191.0	0.0560	8.9323	159.505	1.1188
	141.3	161.0	0.0410	7.5293	183.641	1.2812
	172.5	139.0	0.0345	6.5005	188.420	1.3216
	197.5	113.0	0.0271	5.2846	195.004	1.3678
	241.1	89.0	0.0211	4.1622	197.261	1.3837

Core Number 65-S-A

Net Pressure, Psi	T, °F	r,	Rw, Ω-m	Re, Ω-m	F	$\frac{F^T}{F}$
2100-1100	70.4	140.0	0.0800	6.5135	81.4187	
	108.8	110.0	0.0537	5.1178	95.3035	1.1705
	140.1	92.1	0.0405	4.2850	105.8024	1.2995
	172.7	80.8	0.0320	3.7592	117.4750	1.4429
	200.7	74.0	0.0269	3.4429	127.9888	1.5720
	236.2	66.8	0.0222	3.1079	139.9954	1.7195
	272.8	55.8	0.0186	2.5961	139.5752	1.7143
	311.0	55.0	0.0152	2.5589	168.3486	2.0677

TABLE 12

"APPROXIMATE" PORE VOLUME CHANGE DUE TO TEMPERATURE

Core Number 48-3-A

ΔVw, cc	T, °F	FVF(w)	ΔFVF(w)	H_2O Expansion, cc	$\frac{\Delta PV, cc}{\Delta Vw\text{-}H_2O\ exp.}$	PV, cc	$\%\Delta V_T$
	68.0	.9975				10.2260	
.1213			.0065	.0665	.0548		17.89
	104.2	1.0040				10.1712	
.1930			.0085	.0865	.1065		34.77
	139.3	1.0125				10.0647	
.1740			.0110	.1107	.0633		20.67
	174.3	1.0235				10.0014	
.1670			.0115	.1150	.0520		16.98
	203.2	1.0350				9.9494	
.1650			.0136	.1353	.0297		9.70
	237.0	1.0486				9.9197	

TABLE 12--Continued

Core Number 200-A

ΔVw, cc	T, °F	FVF(w)	ΔFVF(w)	H_2O Expansion, cc	ΔPV, cc / ΔVw-H_2O exp.	PV, cc	$\%\Delta V_T$
	70	.9975				9.4128	
.1228			.0064	.0602	0.0626		14.52
	104	1.0039				9.3502	
.1985			.0101	.0944	0.1041		24.15
	144	1.0140				9.2461	
.1837			.0102	.0943	0.0894		20.74
	176.2	1.0242				9.1567	
.1812			.0108	.0987	0.0823		19.09
	203.5	1.0350				9.0744	
.2161			.0136	.1234	0.0927		21.50
	237.0	1.0486				8.9969	

TABLE 12--Continued

Core Number 65-S-A

ΔV_w, cc	T, °F	FVF(w)	ΔFVF(w)	H_2O Expansion, cc	$\frac{\Delta PV, cc}{\Delta V_w - H_2O\ exp.}$	PV, cc	$\%\Delta V_T$
	70.4	.9975				12.7629	
.1289			.0073	.0932	.0357		7.43
	108.8	1.0048				12.7272	
.2120			.0082	.1039	.1081		22.49
	140.1	1.0130				12.6191	
.2398			.0101	.1275	.1123		23.36
	172.7	1.0231				12.5068	
.2412			.0105	.1313	.1099		22.86
	200.7	1.0336				12.3969	
.2920			.0143	.1773	.1147		23.86
	236.2	1.0479				12.2826	

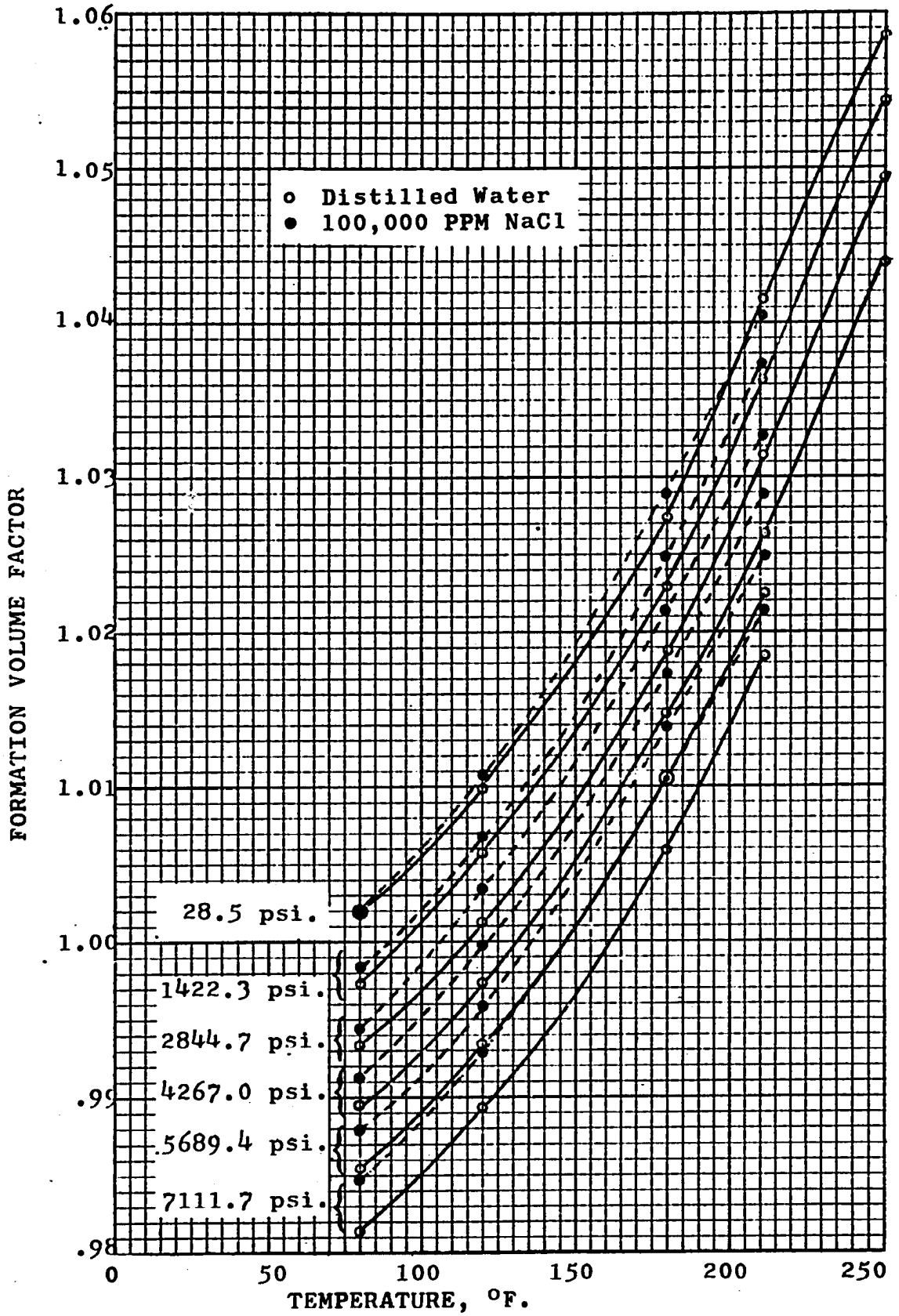

FIG. 43.--WATER FORMATION VOLUME FACTOR VS. PRESSURE AND TEMPERATURE (FROM REFERENCES 3 AND 23)

APPENDIX C

CALCULATED DATA ON NATURAL CORES

Studied by Hilchie[20]

TABLE 13

PORE SIZE DISTRIBUTION DATA

(From Hilchie[20])

	% PV				
R(microns)	Briar Hill	Berea	Bandera	Dean	Paradox
24	20.0	-	-	-	-
22	10.0	-	-	-	-
20	10.0	-	-	-	-
18	6.0	-	-	-	-
16	4.0	.5	-	-	-
14	4.0	1.5	-	-	-
12	3.0	6.5	-	-	-
10	2.0	23.0	-	-	-
9	2.0	10.0	-	-	-
8	2.0	10.0	-	-	-
7	1.0	8.0	-	-	-
6	1.0	6.0	-	-	-
5	2.0	4.0	.3	-	-
4	2.0	2.5	11.0	-	-
3	2.0	2.0	27.5	.2	-
2	2.0	3.0	12.0	.5	-
1	4.0	5.0	11.0	1.8	2.0
.6		3.0		2.1	.5
.5	5.0		6.0		
.4					
.3			6.0		
.2		5.0		0.9	
.1					7.5
0	18.0	10.0	26.0	94.5	90.0

TABLE 14

SURFACE AREA CALCULATIONS

r(microns)	Briar Hill %PV	2(%PV)	$\frac{2(\%PV)}{r}$, cm^{-1}
25	20.0	40.0	1,600.00
23	10.0	20.0	869.57
21	10.0	20.0	952.38
19	6.0	12.0	631.58
17	4.0	8.0	470.59
15	4.0	8.0	533.33
13	3.0	6.0	461.54
11	2.0	4.0	363.64
9.5	2.0	4.0	421.05
8.5	2.0	4.0	470.59
7.5	1.0	2.0	266.67
6.5	1.0	2.0	307.69
5.5	2.0	4.0	727.27
4.5	2.0	4.0	888.88
3.5	2.0	4.0	1,142.86
2.5	2.0	4.0	1,600.00
1.5	4.0	8.0	5,333.33
.5	23.0	46.0	92,000.00
			109,040.97

Surface Area = 109,040.97 cm^2/Unit Pore Vol.

Pore Vol. in Briar Hill "C" = 12.683 cm^3

Total Surface Area in Briar Hill "C" = 1,382,966.62 cm^2

Total Surface Area/Unit Bulk Vol. = $\frac{1,382,966.62}{59.631}$ = 23,192.0 cm^{-1}

TABLE 14--Continued

r(microns)	Berea %PV	Berea 2(%PV)	$\frac{2(\%PV)}{r}$, cm^{-1}
17	.5	1.0	53.82
15	1.5	3.0	200.00
13	6.5	13.0	1,000.00
11	23.0	46.0	4,181.82
9.5	10.0	20.0	2,105.26
8.5	10.0	20.0	2,352.94
7.5	8.0	16.0	2,133.33
6.5	6.0	12.0	1,846.62
5.5	4.0	8.0	1,454.55
4.5	2.5	5.0	1,111.11
3.5	2.0	4.0	1,142.86
2.5	3.0	6.0	2,400.00
1.5	5.0	10.0	6,666.67
.80	3.0	6.0	7,500.00
.40	5.0	10.0	25,000.00
.10	10.0	20.0	200,000.00
			259,153.98

Surface Area = 259,153.98 cm^2/Unit Pore Vol.

Pore Vol. in Berea "A" = 11.219 cm^3

Total Surface Area in Berea "A" = 2,907,448.50 cm^2

Total Surface Area/Unit Bulk Vol. = $\frac{2,907,448.50}{60.651}$ = 47,937.30 cm^{-1}

TABLE 14--Continued

Bandera			
r(microns)	%PV	2(%PV)	$\frac{2(\%PV)}{r}$, cm^{-1}
5.5	.3	.6	109.09
4.5	11.2	22.4	4,977.77
3.5	27.5	55.0	15,714.28
2.5	12.0	24.0	9,600.00
1.5	11.0	22.0	14,666.67
.75	6.0	12.0	16,000.00
.40	6.0	12.0	30,000.00
.15	26.0	52.0	346,667.00
			437,734.81

Surface Area = 437,734.81 cm^2/Unit Pore Vol.

Pore Vol. in Bandera "A" = 13.498 cm^3

Total Surface Area in Bandera "A" = 5,908,544.47 cm^2

Total Surface Area/Unit Bulk Vol. = $\frac{5,908,544.47}{60.545}$ = 97,589.3 cm^{-1}

TABLE 14--Continued

Dean

r(microns)	%PV	2(%PV)	$\frac{2(\%PV)}{r}$, cm^{-1}
3.5	.2	.4	114.29
2.5	.5	1.0	400.00
1.5	1.8	3.6	2,400.00
.75	2.1	4.2	5,600.00
.35	0.9	1.8	5,142.85
.10	94.5	189.0	1,890,000.00
			1,903,657.14

Surface Area = 1,903,657.14 cm^2/Unit Pore Vol.

Pore Vol. in Dean "C" = 4.507 cm^3

Total Surface Area in Dean "C" = 8,579,782.73 cm^2

Total Surface Area/Unit Bulk Vol. $= \frac{8,579,782.73}{60.824} = 141,059.1$ cm^{-1}

Paradox

r(microns)	%PV	2(%PV)	$\frac{2(\%PV)}{r}$, cm^{-1}
1.5	2.0	4.0	2,666.67
.75	.5	1.0	1,333.33
.30	7.5	15.0	50,000.00
.05	90.0	180.0	3,600,000.00
			3,654,000.00

Surface Area = 3,654,000.00 cm^2/Unit Pore Vol.

Pore Vol. in Paradox "B" = 1.712 cm^3

Total Surface Area in Paradox "B" = 6,255,648 cm^2

Total Surface Area/Unit Bulk Vol. $= \frac{6,255,648}{60.836} = 102,828.0$ cm^{-1}